Postsynaptic frequency filters shaped by the interplay of synaptic short-term plasticity and cellular time scales

Yugarshi Mondal [*1] [†], Guillermo Villanueva Benito [*2], Rodrigo F. O. Pena [*3], Horacio G. Rotstein [3] [‡§]

[1] Department of Mathematics and Statistics
Stony Brook University
[2] Department of Mathematics
Universitat Politécnica de Catalunya
[3] Federated Department of Biological Sciences
New Jersey Institute of Technology and Rutgers University

July 2, 2023

Abstract

Neuronal filters can be thought of as constituent building blocks underlying the ability of neuronal systems to process information, generate rhythms and perform computations. How neuronal filters are generated by the concerted activity of a multiplicity of process and interacting time scales within and across levels of neuronal organization is poorly understood. In this paper we address these issues in a feedforward network in the presence of synaptic short-term plasticity (STP, depression and facilitation). The network consists of a presynaptic spike-train, a postsynaptic passive cell, and an excitatory (AMPA) chemical synapse. The dynamics of each network components is controlled by one or more time scales. We use mathematical modeling, numerical simulations and analytical approximations of the network response to presynaptic spike trains. We explain the mechanisms by which the participating time scales shape the neuronal filters at the (i) synaptic update level (the target of the synaptic variable in response to presynaptic spikes), which is shaped by STP, (ii) the synaptic variable, and (iii) the postsynaptic membrane potential. We focus on two metrics giving rise to two types of profiles (curves of the corresponding metrics as a function of the spike-train input frequency or firing rate): (i) peak profiles and (ii) peak-to-trough amplitude profiles. The effects of STP are present at the synaptic update level and are communicated to the synaptic level where they interact with the synaptic decay time. STP band-pass filters (BPFs) are reflected in the synaptic BPFs with some modifications due primarily to the synaptic decay time. The postsynaptic filters result from the interaction between the synaptic variable and the biophysical properties of the postsynaptic cell. Postsynaptic BPFs can be inherited from the synaptic level or generated across levels of organization due to the interaction between (i) a synaptic low-pass filter and the postsynaptic summation filter (voltage peak BPF), and (ii) a synaptic high-pass filter and the postsynaptic summation filter (peak-to-trough amplitude BPF). These type of BPFs persist in response to jitter periodic spike trains and Poisson-distributed spike trains. The response variability depends on a number of factors including the spike train input frequency and are controlled by STP in a non-monotonic frequency manner. The lessons learned from the investigation of this relatively simple feedforward network will serve to construct a framework to analyze the mechanisms of generation of neuronal filters in networks with more complex architectures and a variety of interacting cellular, synaptic and plasticity time scales.

[*] Equal contribution
[†] Current address: Volen Center for Complex Systems, Brandeis University, Waltham, MA, USA
[‡] E-mail: horacio@njit.edu, corresponding author
[§] Graduate Faculty, Behavioral Neurosciences Program, Rutgers University; Corresponding Investigator, CONICET, Argentina.

Keywords: Preferred frequency responses, synaptic resonance, postsynaptic resonance, low-pass filters, band-pass filters, high-pass filters.

1 Introduction

Neuronal filters allow neuronal systems to select certain information or enhance the communication of specific information components over others [1–5]. As such, neuronal filters play important roles in neuronal information processing, rhythm generation and brain computations [3, 4, 6–17]. Band-pass frequency-filters are associated to the notion of resonance. Neuronal resonance refers to the ability of a neuronal system to exhibit a maximal response (e.g., subthreshold membrane potential, postsynaptic potential, firing rate) to periodic inputs at a preferred (resonant), non-zero frequency band. At the cellular level, frequency-filters reflect the time scales of the participating currents [1, 18, 19]. At the synaptic level, frequency-filters [20] reflect the synaptic raise and decay times. The observed postsynaptic responses reflect the combination of these and the time scales of the postsynaptic cell's participating currents [21]. The latter may give rise to additional filtering components resulting from the summation phenomenon [22]. In synaptic pairs with more complex synaptic dynamics, frequency-filters also reflect the time scales associated with synaptic short-term plasticity (STP) and may give rise to band-pass filters at the synaptic and postsynaptic levels [2, 3, 21, 23–25]. How does the concerted activity of this multiplicity of time scales shape neurona filters is poorly understood.

STP refers to the changes of the efficacy of synaptic transmission (synaptic conductance strength) in response to presynaptic spike trains (as the number spikes increases) with time scales ranging in the order of hundreds of milliseconds to seconds [23–25]. STP consists of the combination of two opposing processes with characteristic time scales: synaptic depression (efficacy decrease) and facilitation (efficacy increase). STP has been investigated in both vertebrates and invertebrates. It has been shown to be involved in a number of brain functions, including information filtering (temporal and frequency-dependent) [3, 8–10, 16, 22, 24, 26–43], adaptive filtering [9] and related phenomena (e.g., burst detection) [3, 33, 44–47], temporal coding and information processing [33, 34, 48–51], information flow [40, 52, 53] (given the presynaptic history-dependent nature of STP), gain control [54–56], the modulation of network responses to external inputs [57, 58], the prolongation of neural responses to transient inputs [15, 59, 60], direction selectivity [61], vision (e.g., microsacades) [62], sound localization and hearing [63, 64], the generation of cortical up and down states [65], attractor dynamics [55,66], navigation (e.g., place field sensing) [9,37], working memory [60,67], decision making [68] and neuronal computation [6, 53, 56, 69–71].

Neuronal resonance has been investigated both experimentally and theoretically at various levels of organization ranging from the cellular to the synaptic to the network levels [3, 4, 11, 17–19, 21, 46, 72–83]. However, the biophysical and dynamic mechanisms of generation of neuronal resonance beyond the single cell level are poorly understood. It is unclear how neuronal filters are shaped by the time scales of the participating building blocks at each level of organization. It is also unclear how the neuronal filtering properties are communicated across levels of organization and modified by the time scales and other biophysical properties as this communication proceeds.

In this paper we begin to systematically analyze and develop these ideas in a feedforward network (Fig. 1), which is arguably the elementary neuronal processing unit and involves a multiplicity of interacting time scales. The building blocks consist of a presynaptic spike-train (characteristic period Δ_{spk}), a postsynaptic passive cell (time constant τ), an excitatory (AMPA) chemical synapse (rise and decay time constants τ_{rse} and τ_{dec}, respectively), and synaptic short-term plasticity (STP) [23–25] (characteristic time constants τ_{dep} and τ_{fac}). We focus on the stationary postsynaptic (subthreshold) membrane potential response to presynaptic spike trains. We use both periodic spike-trains with frequencies within some range and Poisson-distributed spike-trains with mean frequencies within the same range. We consider two types of response profiles: (i) peak vs. input frequency, and (ii) peak-to-trough amplitude versus input frequency. The latter metrics are an analogous to the impedance profile for the computation of the standard subthreshold filters. The former metrics are relevant for the transition from subthreshold to suprathreshold responses. We use mathematical modeling, numerical simulations and analytical approximations of the network response to presynaptic spike trains at the STP, synaptic and postsynaptic levels.

In spite of its simplicity, the feedforward network we use is dynamically rich. Passive cells produce subthreshold (membrane potential) low-pass filters in response to sinusoidal inputs currents (the voltage amplitude response as a function of the input frequency is monotonically decreasing), but they may produce subthreshold high-pass filters in response to presynaptic periodic spike-train inputs due to the effects of summation. Synaptic depression and facilitation produce low- and high-pass filters, respectively in response to presynaptic spike inputs [3]. The cellular filtering properties are primarily the result of feedback effects, while STP filtering properties are primarily a history-dependent process. Filters may be generated and interact within and across levels of organization [4,44] as the result of the interplay of the biophysical building blocks that give rise to them. The lessons learned from this study will serve to construct a framework to analyze the mechanisms of generation of neuronal filters in networks with more complex cells and architecture.

In previous work [44], we thoroughly investigated the temporal (transient) responses and the associated temporal filters in the same feedforward network (Fig. 1). One important result of this study was the description of the link between the STP time constants governing the dynamics of the single events (in response to each presynaptic spikes; τ_{dep} and τ_{fac}) and the corresponding global, emergent time scales describing the long-term dynamics of the (low-, high- and band-pass) temporal filters. A second important result was the discovery of a third global time scale for temporal band-pass filters involving a combination of both τ_{dep} and τ_{fac}, highlighting the complexity of the non-trivial interaction between depression and facilitation. A third important result was the finding that the postsynaptic temporal filters are not proportional to the synaptic temporal filters as assumed in some simplified models, [46], thus demonstrating that the synaptic temporal filters are not directly communicated to the postsynaptic cell level, but rather modified by the postsynaptic intrinsic properties. While temporal filters are not predictive of frequency-filters and both types of filters are generated by different mechanisms, the type of complexity described above is present in the frequency-filters and informs our study.

2 Methods

2.1 Models

2.1.1 Postsynaptic cell

The current-balance equation for the post-synaptic cell is given by

$$C\,\frac{dV}{dt} = -G_L\,(V - E_L) + I_{app} - I_{syn} + I_{noise}, \tag{1}$$

where t is time (ms), V represents the voltage (mV), C is the specific capacitance (μF/cm^2), G_L is the leak conductance (mS/cm^2), I_{app} is the tonic (DC) current (μA/cm^2), $I_{noise} = \sqrt{2\,D}\,\eta(t)$ represents white noise (delta correlated with zero mean) with variance D, and I_{syn} is an excitatory synaptic current of the form

$$I_{syn} = G_{syn}\,S\,(V - E_{syn}). \tag{2}$$

In eq. (2), G_{syn} is the maximal synaptic conductance (mS/cm^2), E_{syn} is the reversal potential and S is the synaptic variable.

2.1.2 Synaptic dynamics

The synaptic variables S obey a kinetic equation of the form

$$\frac{dS}{dt} = N(V_{pre})\,\frac{(\Delta S - S)}{\tau_{rse}} - \frac{S}{\tau_{dec}}, \tag{3}$$

where V_{pre} is the membrane potential of the presynaptic spike, $N(V)$ denotes the sigmoid function

$$N(V) = \frac{1 + \tanh(V/4)}{2} \tag{4}$$

τ_{rse} and τ_{dec} are the rise and decay time constants respectively (msec), and ΔS is a target value for S. For AMPA excitation (E-cells, $G_{syn} = G_{ex}$), we used $E_{syn} = E_{ex} = 0$, $\tau_{rse} = 0.1$ and $\tau_{dec} = 3.0$ [84]. In the absence of synaptic short-term dynamics (depression and facilitation), $\Delta S = 1$. Otherwise, ΔS, interpreted as the magnitude ΔS of the synaptic release per presynaptic spike, is determined as described below (Sections 2.1.4 and 2.1.6).

We refer the reader to [85–87] for additional details on biophysical (conductance-based) models.

2.1.3 Presynaptic spike-trains

We model the spiking activity of the presynaptic cell as a spike train with presynaptic spike times $t_1, t_2, \ldots, t_N$. We consider three types of input spike-trains. Periodic inputs are characterized by the interspike interval (ISI) of length Δ_{spk} (msec) or, alternatively, by the spiking frequency (Hz)

$$f_{spk} = \frac{1000}{\Delta_{spk}}. \tag{5}$$

Jittered-periodic presynaptic spike trains consist of perturbations of periodic presynaptic spiking patterns of the form

$$\Delta_{spk,n} = \Delta_{spk} + \delta_{spk,n} \tag{6}$$

where Δ_{spk} is constant (n-independent) and $\delta_p = \{\delta_{spk,n}\}_{n=1}^{N_{spk}}$ is a sequence of real numbers. We take δ_p to be normally distributed with zero mean and variance σ^2. Poisson distributed (homogeneous) presynaptic spike trains are characterized by the mean spiking rate (and the associated exponential distribution of ISIs).

2.1.4 The DA (Dayan-Abbott) model for short-term dynamics: synaptic depression and facilitation

This phenomenological model is presented in [86] and attributed to Dayan and Abbott (and collaborators). The magnitude ΔS of the synaptic release per presynaptic spike is assumed to be the product of the depression (x) and facilitation (z) variables

$$\Delta S = x^- \, z^+ \tag{7}$$

where

$$\frac{dx}{dt} = \frac{x_\infty - x}{\tau_{dep}} - a_d \, x \, \delta(t - t_{spk}), \tag{8}$$

and

$$\frac{dz}{dt} = \frac{z_\infty - z}{\tau_{fac}} + a_f \, (1 - z) \, \delta(t - t_{spk}). \tag{9}$$

Each time a presynaptic spike arrives ($t = t_{spk}$), the depressing variable x is decreased by an amount $a_d \, x$ (the release probability is reduced) and the facilitating variable z is increased by an amount $a_f \, (1 - z)$ (the release probability is augmented). During the presynaptic ISIs both x and z decay exponentially to their saturation values x_∞ and z_∞ respectively. The rate at which this occurs is controlled by the parameters τ_{dep} and τ_{fac}. Following others we use $x_\infty = 1$ and $z_\infty = 0$. The superscripts "$\pm$" in the variables x and z indicate that the update is carried out by taking the values of these variables prior ($^-$) or after ($^+$) the arrival of the presynaptic spike.

Figs. 2-A1 and -B1 illustrates the x-, z-traces (curves of x and z as a function of time) in response to a periodic presynaptic input train for representative parameter values. The updated of the variable S at the arrival of presynaptic spikes is given by $\Delta S = x^- z^+$. The sequence of peaks for ΔS is defined by $\Delta S_n = X_n Z_n$ where X_n and Z_n are the sequence of peaks for the variables x and z, respectively (see also [44]).

2.1.5 DA model in response to presynaptic inputs

Peak dynamics and temporal filters

By solving the differential equations (8)-(9) during the presynaptic ISIs and appropriately updating the solutions at $t = t_n$ (occurrence of each presynaptic spike), one arrives at the following recurrent formula for the peak sequences in terms of the model parameters

$$X_{n+1} = x_\infty + [\,(1-a_d)X_n - x_\infty\,]\,e^{-\Delta_{spk,n}/\tau_{dep}} \tag{10}$$

and

$$Z_{n+1} = a_f + (1-a_f)\,[\,z_\infty + (Z_n - z_\infty)e^{-\Delta_{spk,n}/\tau_{fac}}\,] \tag{11}$$

where $\{\Delta_{spk,n}\}_{n=1}^{Nspk}$ represents the lengths of the presynaptic ISIs.

The temporal filtering properties of the DA model in response to periodic and Poisson-distributed presynaptic inputs was studied in [44].

Steady-state frequency-dependent filters in response to periodic presynaptic inputs

For periodic inputs, $\Delta_{spk,n} = \Delta_{spk}$, independent of n, eqs. (10)-(11) are linear 1D difference equations. Therefore both the sequences X and Z obey linear discrete dynamics (e.g., see [88]), decaying to their steady state values

$$\bar{X} = \frac{(\,1 - e^{-\Delta_{spk}/\tau_{dep}}\,)\,x_\infty}{1-(1-a_d)\,e^{-\Delta_{spk}/\tau_{dep}}} \tag{12}$$

and

$$\bar{Z} = \frac{(\,1 - e^{-\Delta_{spk}/\tau_{fac}}\,)\,(1-a_f)\,z_\infty + a_f}{1-(1-a_f)\,e^{-\Delta_{spk}/\tau_{fac}}}. \tag{13}$$

For the reminder of this paper we use $x_\infty = 1$ and $z_\infty = 0$.

2.1.6 The MT (Markram-Tsodkys) model for short-term dynamics: synaptic depression and facilitation

This phenomenological model was introduced in [46] as a simplification of earlier models [23, 49, 89]. It is slightly more complex and widely used than the DA model described above [3, 90]. As for the DA model, the magnitude ΔS of the synaptic release per presynaptic spike is assumed to be the product of the depressing and facilitating variables

$$\Delta S = R^-\,u^+ \tag{14}$$

where, in its more general formulation,

$$\frac{dR}{dt} = \frac{1-R}{\tau_{dep}} - R^- u^+\,\delta(t-t_{spk}), \tag{15}$$

and

$$\frac{du}{dt} = \frac{\hat{U}-u}{\tau_{fac}} + U\,(1-u^-)\,\delta(t-t_{spk}). \tag{16}$$

Each time a presynaptic spike arrives ($t = t_{spk}$), the depressing variable R is decreased by R^-u^+ and the facilitating variable u is increased by $U\,(1-u^-)$. As before, the superscripts "$\pm$" in the variables R and u indicate that the update is carried out by taking the values of these variables prior ($^-$) or after ($^+$) the arrival of the presynaptic spike. In contrast to the DA model, the update of the depression variable R is affected by the value of the facilitation variable u^+. Simplified versions of this model include making $\hat{U} = 0$ [2, 28, 46, 47, 91, 92] and $\hat{U} = U$ [3].

2.1.7 MT model in response to presynaptic inputs

Peak dynamics and temporal filters

By solving the differential equations (15)-(16) during the presynaptic ISIs and appropriately updating the solutions at $t = t_n$ (occurrence of each presynaptic spike), one arrives at the following recurrent formula for the peak sequences in terms of the model parameters

$$R_{n+1} = R_n(1 - u_{n+1})e^{-\Delta_{spk}/\tau_{dep}} + 1 - e^{-\Delta_{spk,n}/\tau_{dep}} \tag{17}$$

and

$$u_{n+1} = \hat{U} + U - \hat{U}U + u_n(1 - U)e^{-\Delta_{spk,n}/\tau_{fac}} - \hat{U}(1 - U)e^{-\Delta_{spk,n}/\tau_{fac}}. \tag{18}$$

The temporal filtering properties of the DA model in response to periodic presynaptic inputs was studied in [44].

Steady-state frequency-dependent filters

As before, for periodic presynaptic inputs $\Delta_{spk,n} = \Delta_{spk}$, independent of n, these equations represent a system of two 1D difference equations. The steady-state values are given by

$$\bar{R} = \frac{1 - e^{-\Delta_{spk}/\tau_{dep}}}{1 - (1 - \bar{u})\, e^{-\Delta_{spk}/\tau_{dep}}} \tag{19}$$

and

$$\bar{u} = \frac{\hat{U} + U - \hat{U}U - \hat{U}\,(1 - U)e^{-\Delta_{spk}/\tau_{fac}}}{1 - (1 - U)\, e^{-\Delta_{spk}/\tau_{fac}}}. \tag{20}$$

For the reminder of this paper we will use $\hat{U} = 0$ and $U = 0.1$.

2.2 Postsynaptic potential (PSP) peak sequences: Analytical approximation of the membrane potential response of passive cells to presynaptic spikes

In order to analyze the PSP peak and amplitude responses of passive cells to presynaptic spikes we derive an analytical approximation of the solution to the model (1)-(4). The process consists of creating a hybrid model by substituting the conductance-based synaptic current in I_{syn} (2) by a presynaptic ISI-dependent current-based input where the synaptic input coefficient is updated every cycle to account for the changes in V relative to E_{syn} across cycles.

Eq. (1) is linear, but the conductance-based synaptic input in I_{syn} (2) is multiplicative. Previous work showed that the subthreshold rhythmic properties of cells in response to conductance- and current-based synaptic inputs may qualitatively differ [93, 94], and therefore the additive, current-based synaptic inputs, which would eliminate the multiplicative nature of I_{syn} by substituting the factor $V - E_{syn}$ by a constant, will not produce good enough approximations to the responses of conductance-based synaptic inputs (e.g., Figs. S3 and S4). In the hybrid approach we develop here, we approximate $V - E_{syn}$ by a constant, which we update at the end of each presynaptic ISI to account for the changing value of $V - E_{syn}$ across cycles. We present here the main ideas and results. The detailed calculations are provided in the Appendix A. We intend this hybrid model and the resulting approximation to be an analytical tool to analyze the PSP peak and amplitude filters, which can be thought of as a simplified model that captures the dynamics of the model (1)-(4), rather than a uniformly accurate approximation to the solution to this model.

We first approximate eq. (1) as follows

$$\tau \frac{dV}{dt} = -V + \alpha_n\, S_a(t) \tag{21}$$

for $n = 1, \ldots, N$ where

$$\tau = \frac{C}{G_L}, \qquad \alpha = \frac{G_{syn}\,(E_{syn} - \bar{V})}{G_L} \qquad \text{and} \qquad \alpha_n = \alpha\,(1 - \sigma_n). \tag{22}$$

The variable V in eq. (21) represents $V - E_L - I_{app}/G_L$ in eq. (1) and $\bar{V} = E_L + I_{app}/G_L$. The right hand second term in eq. (21) is a current input approximation to the conductance input in the synaptic current eq. (1). To account for this, we introduce a correction factor $1 - \sigma_n$ where σ_n is updated at the beginning of each ISI proportionally to the distance between the PSP response and E_{syn} and $\sigma_1 = 0$. The function $S_a(t)$ is an approximation to the variable S whose dynamics are described by eq. (3) with $S(0) = 0$, under the assumption of instantaneous raise to a value ΔS_n ($n = 1, \ldots, N$) at the arrival of each presynaptic spike. The assumption $S(0) = 0$ implies that $S(t) = 0$ for $0 \le t \le t_1$. For the duration of each presynaptic spike ($t_n < t < t_n + T_{sw}$), we approximate $S(t)$ by the synaptic update value ΔS_n (constant). For the remainder of the presynaptic interspike interval ($t_n + T_{sw} \le t < t_{n+1}$), $S_a(t)$ decreases according to the second term in (3). The approximate solution is given by

$$S_a(t) = \begin{cases} \sigma_s\,\Delta S_n & t_n < t < t_n + T_{sw} \\ \\ \sigma_s\,\Delta S_n\,e^{-(t - t_n - T_{sw})/\tau_{dec}} & t_n + T_{sw} \le t < t_{n+1} \end{cases} \tag{23}$$

for $n = 1, \ldots, N$. In our computations we take $T_{sw} = 1$ and $\sigma_s = \tau_{dec}/(\tau_{dec}+\tau_{rse})\,(1 - exp(-(\tau_{dec}+\tau_{rse})/(\tau_{dec}\tau_{rse})))$, which is the solution of eq. (3) computed at $t = T_{sw} = 1$. For $\tau_{rse} = 0.1$ and $\tau_{dec} = 10$, $\sigma_s = 0.9901$, while for $\tau_{rse} = 0.1$ and $\tau_{dec} = 3$, $\sigma_s = 0.9677$. The approximation error is $\tau_{dec}/(\tau_{dec} + \tau_{rse})\,\Delta S\,\tau_{rse}\tau_{dec}/(\tau_{rse} + \tau_{dec}) - (1 + \tau_{rse}\tau_{dec}/(\tau_{rse} + \tau_{dec}))\,exp(-(\tau_{dec} + \tau_{rse})/(\tau_{dec}\tau_{rse}))$. For $\tau_{dec} = 10$, the error is equal to 0.0098 ($0.098\,\Delta S$) and for $\tau_{dec} = 3$, the error is equal to 0.0094 ($0.094\,\Delta S$).

For each input frequency f_{spk}, we compute the PSP peak sequence $V_{peak,n}$ ($n = 1, 2, \ldots$) until $|\,V_{peak,n} - V_{peak,n-1}\,| < \delta = 0.0001$. This tolerance δ is a conservative number that allows for the transient responses (temporal filters, see [44]) to wear off. We approximate the stationary value of $\bar{V}_{peak}$ by $V_{peak,n}$ (the last value in the resulting vector), V_{trough} by $V_{trough,n}$, $t_{V,peak}$ by the time at which $V_{peak,n}$ occurs, and we use the corresponding value of t_{spk}, $t_{spk,n}$ (immediately preceding $V_{peak,n}$) for the computation of the PSP phase response in eq. (66).

The PSP sequences are given by

PSP peak sequences for $\tau_{dec} \neq \tau$

$$V_{peak,n} = \frac{\alpha_n\,\tau_{dec}\,\Delta S_n}{\tau_{dec} - \tau}\,e^{Tsw/\tau_{dec}}\,e^{-(t_{peak,n} - t_n)/\tau_{dec}} + \left[\beta_n - \frac{\alpha_n\,\tau_{dec}\,\Delta S_n}{\tau_{dec} - \tau}\right]\,e^{T_{sw}/\tau}\,e^{-(t_{peak,n} - t_n)/\tau} \tag{24}$$

where

$$t_{peak,n} = t_n + \frac{\tau_{dec}\,\tau}{\tau_{dec} - \tau}\,\ln\left(-\frac{b_n\,\tau_{dec}}{a_n\,\tau}\right), \qquad a_n = \frac{\alpha_n\,\tau_{dec}\,\Delta S_n}{\tau_{dec} - \tau}\,e^{T_{sw}/\tau_{dec}} \qquad b_n = \left[\beta_n - \frac{\alpha_n\,\tau_{dec}\,\Delta S_n}{\tau_{dec} - \tau}\right]\,e^{T_{sw}/\tau}, \tag{25}$$

$$\alpha_n = \alpha\,(1 - \sigma_n), \qquad \text{and} \qquad \sigma_{n+1} = \frac{\eta\,V_{peak,n}}{(E_{syn} - E_L)} \qquad \text{with} \qquad \sigma_1 = 0, \tag{26}$$

$$\beta_n = \alpha_n\,\Delta S_n + (V_{o,n} - \alpha_n\,\Delta S_n)\,e^{-T_{sw}/\tau}, \tag{27}$$

and

$$V_{0,n+1} = \frac{\alpha_n\,\tau_{dec}\,\Delta S_n}{\tau_{dec} - \tau}\,e^{T_{sw}/\tau_{dec}}\,e^{-\Delta_{spk,n}/\tau_{dec}} + \left[\beta_n - \frac{\alpha_n\,\tau_{dec}\,\Delta S_n}{\tau_{dec} - \tau}\right]\,e^{T_{sw}/\tau}\,e^{-\Delta_{spk,n}/\tau} \qquad \text{with} \qquad V_{0,1} = 0. \tag{28}$$

Eq. (24) is obtained from eq. (83) in the Appendix A. Note that $V_{trough,n} = V_{0,n+1}$.

PSP peak sequences for $\tau_{dec} = \tau$

$$V_{peak,n} = \frac{\alpha_n \, \Delta S_n}{\tau} \, e^{(t_n + T_{sw})/\tau_{dec}} \, t_{peak,n} \, e^{-t_{peak,n}/\tau} + \left[\beta_n - \frac{\alpha_n \, \Delta S_n}{\tau} \, (t_n + T_{sw}) \right] \, e^{(t_n + T_{sw})/\tau_{dec}} \, e^{-t_{peak,n}/\tau} \quad (29)$$

where

$$t_{peak,n} = t_n + \tau - \frac{b_n}{a_n} \qquad a_n = \frac{\alpha_n \, \Delta S_n}{\tau} \, e^{T_{sw}/\tau_{dec}} \qquad \text{and} \qquad b_n = \left[\beta_n - \frac{\alpha_n \, \Delta S_n}{\tau} \, T_{sw} \right] \, e^{T_{sw}/\tau_{dec}}. \quad (30)$$

$$V_{0,n+1} = \frac{\alpha_n \, \Delta S_n}{\tau} \, e^{T_{sw}/\tau_{dec}} \, t_{n+1} \, e^{-\Delta_{spk,n}/\tau} + \left[\beta_n - \frac{\alpha_n \, \Delta S_n}{\tau} \, (t_n + T_{sw}) \right] \, e^{T_{sw}/\tau_{dec}} \, e^{-\Delta_{spk,n}/\tau}. \quad (31)$$

and α_n, σ_n and β_n are given by eqs. (26) and (27). Eq. (90) is obtained from eq. (83) in the Appendix A. In both cases we use $\eta = 1$. Note that $V_{trough,n} = V_{0,n+1}$.

Figs. S1 and S2 compare the numerical solutions to the model (1)-(4) and the analytical approximation using eqs. (21)-(23) together with eqs. (80) and (83) in the Appendix A for representative parameter values. The analytical approximation tracks the numerical solution with relatively high accuracy. Figs. S3 and S4 show the error between the numerical and analytical approximations to the stationary peaks (V_{peak}), troughs (V_{trough}) and peak times (t_{peak}) of the membrane potential responses of passive cells to presynaptic spikes for representative parameter values. For V_{peak} and V_{trough} (left and middle columns), the error is significantly higher for $\eta = 0$ (green curves) than for values of $\eta = 1$ (blue curves) or around this value (red and light blue curves). Setting $\eta = 0$ is equivalent to the current-based synaptic input approximation, while setting $\eta = 1$ (or around this value), corrects for the driving force, which varies as V varies. In contrast, the error for t_{peak} (right columns) is largely independent of η.

2.3 Impedance amplitude and phase profiles: cellular membrane potential response to sinusoidal input currents

2.3.1 General formulation

The impedance of a neuronal system receiving an input current $I_{in}(t)$ is defined as the ratio of the output (voltage) $V_{out}(t)$ and input (current) Fourier transforms

$$Z(f) = \frac{\mathcal{F}[V(t)]}{\mathcal{F}[I(t)]} \quad (32)$$

where f is frequency. The impedance $Z(f)$ is a complex quantity with amplitude and phase. For simplicity, here we used the notation $Z(f)$ for the impedance amplitude and Φ_Z for the impedance phase. In practice, for nonlinear cells, we use the Fast Fourier Transform algorithm (FFT) to compute $\mathcal{F}[x(t)]$.

2.3.2 Impedance and phase profiles for the passive cell

The steady-state voltage response of a linear system receiving sinusoidal current inputs of the form

$$I_{in}(t) = A_{in} \, sin(\omega \, t) \qquad \text{with} \qquad \omega = \frac{2\pi f}{1000}, \quad (33)$$

where f is the input frequency (Hz), is given by

$$V_{out}(t) = A_{out}(f) \, \sin\left(\omega \, t - \phi(f)\right) \quad (34)$$

where $\phi(f)$ is the phase offset (time difference between the peaks of the input current and the output voltage normalized by $2\,\pi$). The impedance amplitude is given by

$$Z(f) = \frac{A_{out}}{A_{in}}. \tag{35}$$

For the passive cell, standard calculations show that

$$Z(\omega) = \frac{\tau}{C}\,\frac{1}{\sqrt{1+\tau^2\,\omega^2}} \tag{36}$$

and

$$\Phi(\omega) = \tan^{-1}(\tau\,\omega). \tag{37}$$

2.4 Numerical simulations

The numerical solutions were computed using the modified Euler method (Runge-Kutta, order 2) [95] with a time step $\Delta t = 0.01$ ms (or smaller values of Δt when necessary) in MATLAB (The Mathworks, Natick, MA). The codes are available at \https://github.com/BioDatanamics-Lab/Frequency_Filters_STP_21_06.

Figure 1: **Feedforward network diagram in the presence of short-term synaptic plasticity.** The presynaptic cell is modeled as a spike train either periodic (period Δ_{spk}) or Poisson distributed (mean interspike interval $< \Delta_{spk} >$). The postsynaptic cell is modeled as a passive cell (capacitive and leak currents) with a membrane time constant τ. The excitatory synaptic function S raises and decays with time constants τ_{rse} and τ_{dec}, respectively. The synaptic depression and facilitation time constants are τ_{dep} and τ_{fac}, respectively.

3 Results

The question we ask in this paper is how the postsynaptic cell's membrane potential frequency-filters (or -profiles), which are curves of the appropriate metrics (for each level of organization) as a function of the input frequency (f_{spk}; e.g., Fig. 2-C), depend on the properties of the participating building blocks: the presynaptic spike trains, the synaptic raise and decay dynamics, the synaptic short-term plasticity (STP) and the intrinsic properties of the postsynaptic cells (Fig. 1, left).

Specifically, we conduct a systematic study of the steady-state postsynaptic cell response to periodic presynaptic inputs over a range of frequencies $f_{spk} = 1000/\Delta_{spk}$ (Fig. 1, left) that capture the postsynaptic membrane potential filtering properties. We then extend our study to include jittered periodic inputs with mean frequency $f_{spk} = 1000/\Delta_{spk}$ and Poisson-distributed presynaptic inputs with mean rate $r_{spk} = 1000/ < \Delta_{spk} >$ (Fig. 1, right).

We divide our study in three steps: (i) the response profiles of the synaptic update ΔS to the presynaptic spike trains, (ii) the response profiles of the synaptic variable S to ΔS, and (iii) the response profiles of the postsynaptic

membrane potential V to S. Synaptic short-term plasticity (STP) operates at the ΔS level. The interactions between depression and facilitation (time constants τ_{dep} and τ_{fac}, respectively) create the synaptic update sequences $\Delta S_n = X_n Z_n$ (Fig. 2, left column, blue dots) where X_n and Z_n are the sequence of peaks for the depression and facilitation variables x and z, respectively. These sequences are the target for the synaptic variables S during the raise phase after the arrival of each presynaptic spike. In the absence of STP, ΔS_n is constant (typically set up to one). The interplay of ΔS_n and the synaptic dynamics (raise and decay time constants τ_{rse} and τ_{dec}, respectively) create the response synaptic (S) patterns (Fig. 2, middle column). The synaptic variable S is the input to the current-balance equation (1) where the synaptic patterns interact with the postsynaptic biophysical properties (membrane time constants τ_m and ionic, resonant time constants τ_{res}) to generate the postsynaptic (V) response patterns (Fig. 2, right column).

Here we focus on the frequency filtering properties of the steady-state responses for ΔS_n, S and V. We characterize them by using the $\bar{\Delta S}$, $\bar{S}$ and $\bar{V}$ peak profiles (Fig. 2-C, blue), defined as the curves of the stationary peaks for the corresponding quantities as a function of the input frequency f_{spk}, and the stationary peak-to-trough amplitude profiles (Fig. 2-C, light blue), consisting of the peak-to-trough amplitude curves as a function of f_{spk}, for the latter two quantities. The temporal filtering properties (transient responses to spike-spike trains) of these feedforward networks were systematically investigated in [44].

3.1 $\bar{\Delta S}$ band-pass filters: interplay of low-pass (depression) and high-pass (facilitation) filters

From eqs. (12), (13) and (5), $\bar{X}$ is monotonically decreasing (low-pass filter; LPF), transitioning from $\bar{X} = 1$ ($f_{spk} = 0$) to $\bar{X} = 0$ ($f_{spk} \to \infty$), and $\bar{Z}$ is monotonically increasing (high-pass filter; HPF), transitioning from $\bar{Z} = a_f$ ($f_{spk} = 0$) to $\bar{Z} = 1$ ($f_{spk} \to \infty$). This is illustrated in Fig. 3 (red and green) for representative parameter values. The interplay of depression and facilitation $\bar{\Delta S} = \bar{X}\bar{Z}$ produces LPFs, BPFs or more complex patterns depending on the relative values of τ_{dep} and τ_{fac} (Fig. 3, blue), for fixed values of the remaining parameters.

To simplify the mechanistic analysis, we define

$$\hat{\Delta}_{spk} = \frac{\Delta_{spk}}{\tau_{dep}} \qquad \text{and} \qquad \eta_{stp} = \frac{\tau_{dep}}{\tau_{fac}}. \tag{38}$$

Substitution into eqs. (12) and (13) (with $x_\infty = 1$ and $z_\infty = 0$) yields

$$\hat{X} = \frac{1 - e^{-\hat{\Delta}_{spk}}}{1 - (1 - a_d)\, e^{-\hat{\Delta}_{spk}}} \qquad \text{and} \qquad \hat{Z} = \frac{a_f}{1 - (1 - a_f)\, e^{-\hat{\Delta}_{spk}/\eta_{stp}}}. \tag{39}$$

Clearly, the rescaling does not affect the shapes of $\bar{X}$ and $\bar{Z}$ ($\hat{X}$ and $\hat{Z}$), but it affects the dependence of their rates of change with Δ_{spk} ($\hat{\Delta}_{spk}$). Specifically, $\hat{X}$ decreases with increasing values of $\hat{\Delta}_{spk}$ in a η_{stp}-independent manner, while the rate of increase of $\hat{Z}$ with $\hat{\Delta}_{spk}$ depends on the ratio η_{stp} of τ_{dep} and τ_{fac}. This rescaling allows us to investigate the mechanisms of generation of $\bar{\Delta S}$ band-pass filters (BPFs) as a function of a single parameter (η_{stp}). The shapes of the $\bar{\Delta S}$ filters for all values of τ_{dep} and τ_{fac} unfold from the shapes of the corresponding $\hat{\Delta S}$ filters by reversing the rescaling.

For large enough values of η_{stp}, the increase of $\hat{Z}$ with increasing values of f_{spk} is much slower than the decrease of $\hat{X}$ (in the limiting case $\eta \to \infty$, $\hat{Z} \sim a_f$, a constant). Therefore, $\hat{\Delta S}$ is a LPF (e.g., Fig. 3-A and -B, blue). For small enough values of η_{stp}, $\hat{Z}$ increases very fast with increasing values of f_{spk} as compared to $\hat{X}$ (in the limiting case $\eta_{spk} \to 0$, $\hat{Z}$ increases instantaneously and is approximately a constant, $\hat{Z} \sim 1$). Therefore, $\hat{\Delta S}$ is also a LPF. The transition between these two LPFs as η_{stp} changes occurs via the development BPFs (e.g., Fig. 3-D to -F, blue). Within some range of values of η_{stp} in between the LPFs and BPFs, the $\bar{\Delta S}$ patterns develop a local minimum preceding the local maximum (e.g., Fig. 3-C, blue).

The shapes of the $\bar{X}$ LPFs and $\bar{Z}$ HPFs, and therefore the $\bar{\Delta S}$ BPFs, are controlled by the single-event time constants τ_{dep} and τ_{fac} governing the depression and facilitation dynamics, respectively, in response to each presynaptic

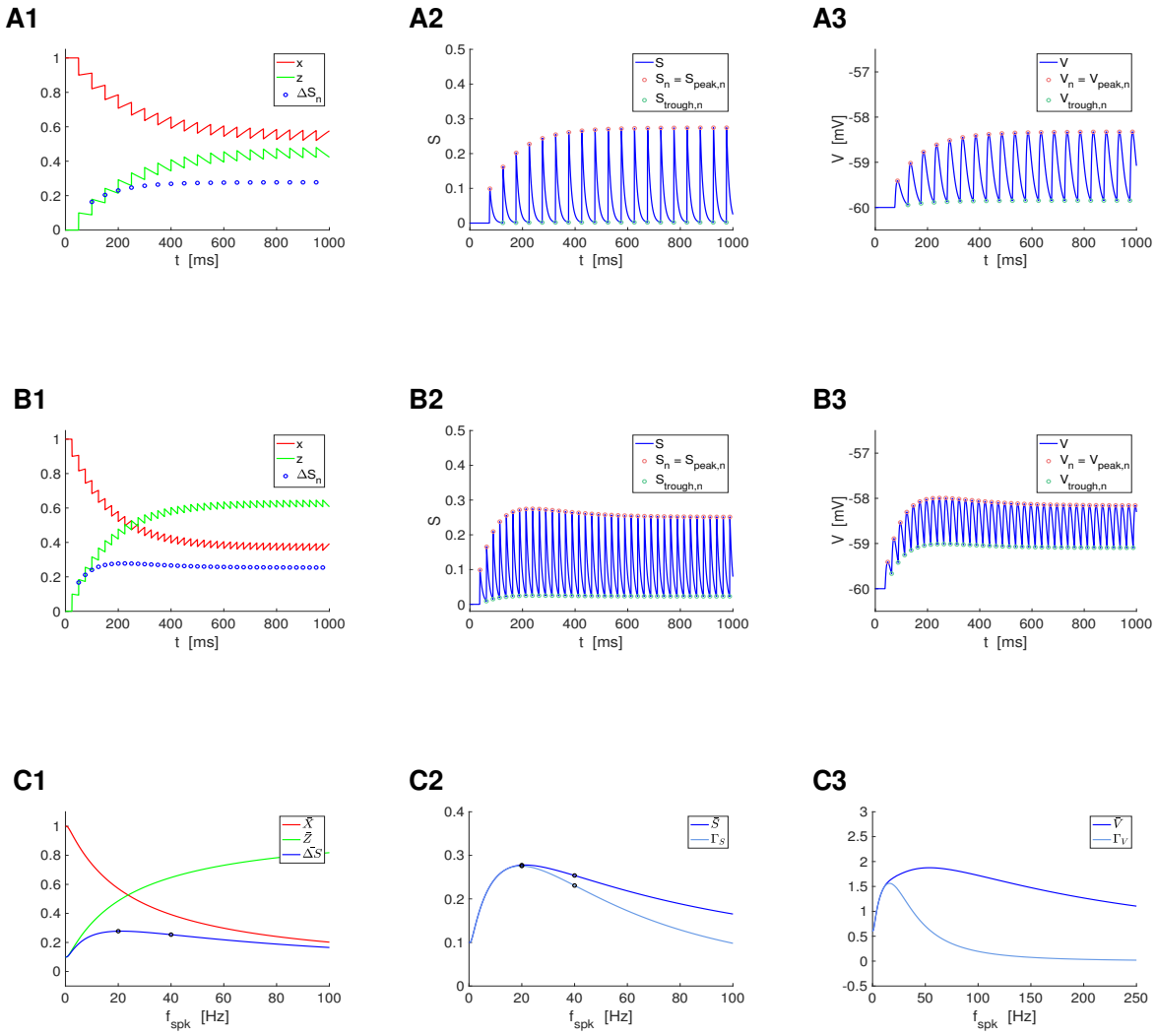

Figure 2: **Representative temporal patterns for the synaptic update ΔS, the synaptic variable S, and the postsynaptic membrane potential V in the presence of short-term dynamics (STD).** We used the model for the postsynaptic cell described by eqs. (1)-(4) with STD described by the DA model (7)-(9), and periodic presynaptic spike trains with frequency f_{spk} (see schematic Fig. 1, left). **Left column.** Short-term dynamics. The peak sequence ΔS_n ($n = 1, \dots, N_{spk}$) is the synaptic update to the synaptic variable S upon the arrival of each presynaptic spike, and results from the combined effect of the depression (x) and facilitation (z) variables. The stationary value of the ΔS_n sequences is referred to as $\bar{\Delta S}$. **Middle column.** Synaptic dynamics. The amplitude $\Gamma_S = \bar{S}_{peak,n} - \bar{S}_{trough,n}$, where $\bar{S} = \bar{S}_{peak}$ and $\bar{S}_{trough}$ are the stationary values of the sequenes $S_{peak,n}$ and $S_{trough,n}$, respectively. **Right column.** Membrane potential dynamics. The amplitude $\Gamma_V = \bar{V}_{peak,n} - \bar{V}_{trough,n}$, where $\bar{V} = \bar{V}_{peak}$ and $\bar{V}_{trough}$ are the stationary values of the sequenes $V_{peak,n}$ and $V_{trough,n}$, respectively. **A.** $f_{spk} = 20Hz$. **B.** $f_{spk} = 40Hz$. **C.** Frequency profiles of the stationary peaks $\bar{\Delta S}$ (left, blue), $\bar{S}$ (middle, blue) and $\bar{V}$ (right, blue) for the peak sequences ΔS_n, S_n and V_n, respectively, and stationary peak-to-trough amplitude profiles Γ_S (middle, light blue) and Γ_V (right, light blue) for S and V, respectively. The black dots correspond to the presynaptic input frequencies in A and B. We used the following additional parameter values: $a_d = 0.1$, $a_f = 0.1$, $x_\infty = 1$, $z_\infty = 0$, $\tau_{dep} = 400$, $\tau_{fac} = 400$, $\tau_{rse} = 0.1$, $\tau_{dec} = 10$, $C = 1$, $E_L = -60$, $G_L = 0.1$, $I_{app} = 0$, $G_{syn} = 0.025$, $E_{syn} = 0$.

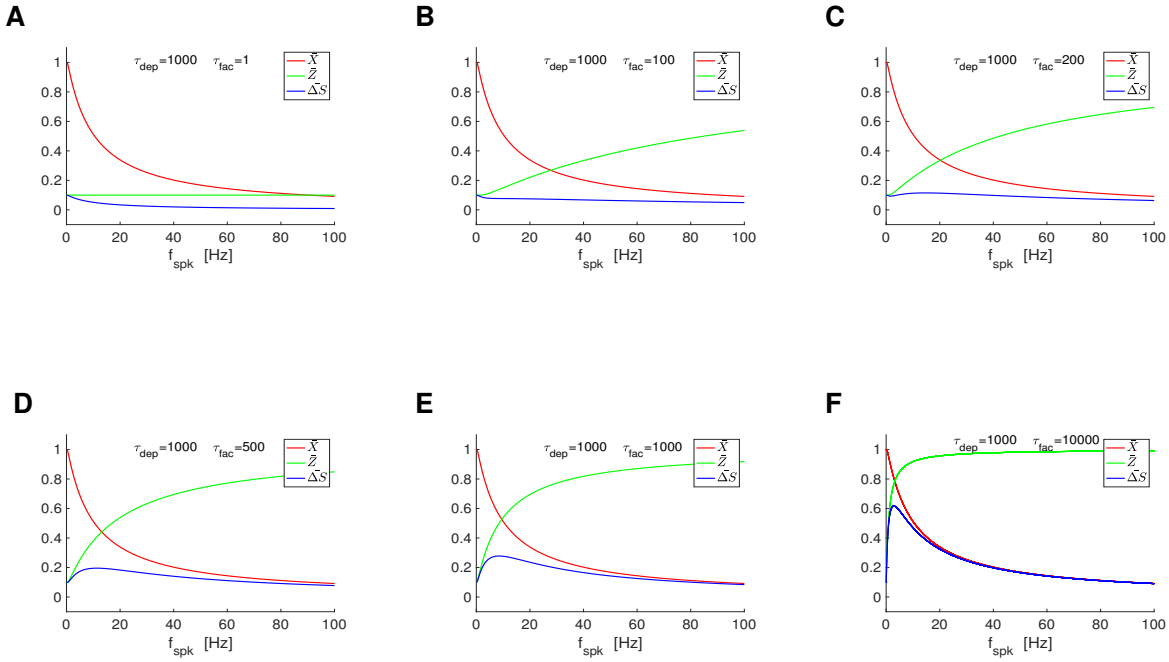

Figure 3: $\bar{\Delta S}$ **filters in response to periodic presynaptic spike inputs (frequency f_{spk}) for the DA model: representative examples.** We used eqs. (12) and (13). **A.** $\tau_{fac} = 1$. **B.** $\tau_{fac} = 100$. **C.** $\tau_{fac} = 200$. **D.** $\tau_{fac} = 500$. **E.** $\tau_{fac} = 1000$. **F.** $\tau_{fac} = 10000$. We used the following additional parameter values: $a_d = 0.1$, $a_f = 0.1$, $x_\infty = 1$, $z_\infty = 0$ and $\tau_{dep} = 1000$.

spike. However, the dependencies of these filters with τ_{dep} and τ_{fac} are non-trivial, similarly to what was found for temporal filters [44].

We characterize the properties of the $\bar{X}$ and $\bar{Z}$ filters in terms of the characteristic frequencies σ_{dep} and σ_{fac}, respectively (Fig. 4-A2). These are defined as the frequencies for which the filters reached 63% of the gap between their values at $f_{spk} = 0$ and $f_{spk} \to \infty$ (black dots in Figs. 4-A1 and -A2). For the characterization of the $\bar{\Delta S}$ BPFs we use four attributes (Fig. 4-A3): the characteristic frequencies κ_{rse} and κ_{dec}, the $\bar{\Delta S}$ resonant frequency $f_{\bar{\Delta S},res}$ and the peak frequency $\bar{\Delta S}_{max}$. The characteristic frequencies were computed as the frequency difference between the peak and the frequency value at which $\bar{\Delta S}$ reached 63% of the gap between the peak and the value at $f_{spk} = 0$ (κ_{rse}) and $f_{spk} \to \infty$ (κ_{dec}).

Fig. 4-B shows the dependence of the characteristic frequencies for the $\bar{X}$ and $\bar{Z}$ filters with the parameters defining the depression and facilitation processes at the single event level, in particular the corresponding time constants τ_{dep} and τ_{fac}, respectively. Specifically, σ_{dep} and σ_{fac} are decreasing functions of τ_{dep} and τ_{fac}, respectively, and decreasing functions of a_d and a_f, respectively. In other words, the larger the time constants, the more pronounced the decrease and increase of the corresponding filters with f_{spk}. The difference $\Delta\kappa = \kappa_{dec} - \kappa_{rse}$ is a measure of the spread of the BPFs.

Fig. 4-C shows the dependence of the attributes for the $\bar{\Delta S}$ BPFs with the time constants of the interacting depression and facilitation processes. We fixed the value of $\tau_{dep} = 1000$ (Fig. 4-C, blue) so the range of resonant frequencies $f_{\bar{\Delta S},res}$ is relatively low. Using this information one can obtain the dependences for other values of τ_{dep} by reversing the rescaling (38). For comparison, we also present the results for $\tau_{dep} = 250$ (Fig. 4-C, red). Specifically, the resonant frequency decreases with increasing values of τ_{fac} and τ_{dep}, the $\bar{\Delta S}$ peak increases with increasing values of τ_{fac} and decreases with increasing values of τ_{dep} and the peak becomes sharper ($\Delta\kappa$ decreases) as τ_{fac} or τ_{dep} increase. Fig. 4-D shows the same results as a function of the characteristic frequency σ_{fac}.

3.2 Interplay of $\bar{\Delta S}$ and $\bar{S}$ filters: inherited and cross-level mechanisms of generation of $\bar{S}$ BPFs

The dynamics of the synaptic variable S is determined by eq. (3). For the parameter values consistent with AMPA excitation (and $GABA_A$ inhibition), the synaptic raise time τ_{rse} is very fast as compared to the synaptic decay time τ_{dec} and other times scales present in the model. Therefore, as a first step, one can approximate the dynamics of S by

$$\frac{dS}{dt} = -\frac{S}{\tau_{dec}} \, [+] \, \Delta S_n \, \delta(t - t_{spk,n}) \tag{40}$$

where the sign $[+]$ indicates that each presynaptic spike (e.g., at time t_n) instantaneously raises S "to" ΔS_n. We refer to this model as the "to-ΔS" model in contrast to the scenario where each presynaptic spike instantaneously raises S "by" some value ΔS_n, which is discussed in the next section.

For generality, it is instructive to explore how the results obtained for the above models are affected by the presence of a non-zero synaptic raise time at the arrival of the presynaptic spikes. The extended to-ΔS model reads

$$\frac{dS}{dt} = \hat{H}(t_{spk,n}, t_{spk,n} + T_{sw}) \, \frac{\Delta S_n - S}{\tau_{rse}} - \hat{H}(t_{spk,n} + T_{sw}, t_{spk,n+1}) \, \frac{S}{\tau_{dec}}, \tag{41}$$

where T_{sw} is the spike width, $t_{spk,n+1} = t_{spk,n} + \Delta_{spk,n}$ and $\hat{H}(t_1, t_2)$ is a square pulse defined by the appropriate product of Heaviside functions $H(t)$, $\hat{H}(t_1, t_2) = H(t - t_1) \, H(t_2 - t)$. From the arrival of each spike and for the duration of this spike, S evolves according the first term in eq. (41). For the remaining of the presynaptic period, S evolves according to the second term in eq. (41).

We characterize the response of S to periodic presynaptic inputs by considering two attributes: the steady-state value $\bar{S}$ ($= \bar{S}_{peak}$) of the peak sequence S_n ($= S_{peak,n}$) (Fig. 2, middle column, coral dots) and the peak-to-trough steady-state amplitude

$$\Gamma_S = \bar{S}_{peak,n} - \bar{S}_{trough,n} \tag{42}$$

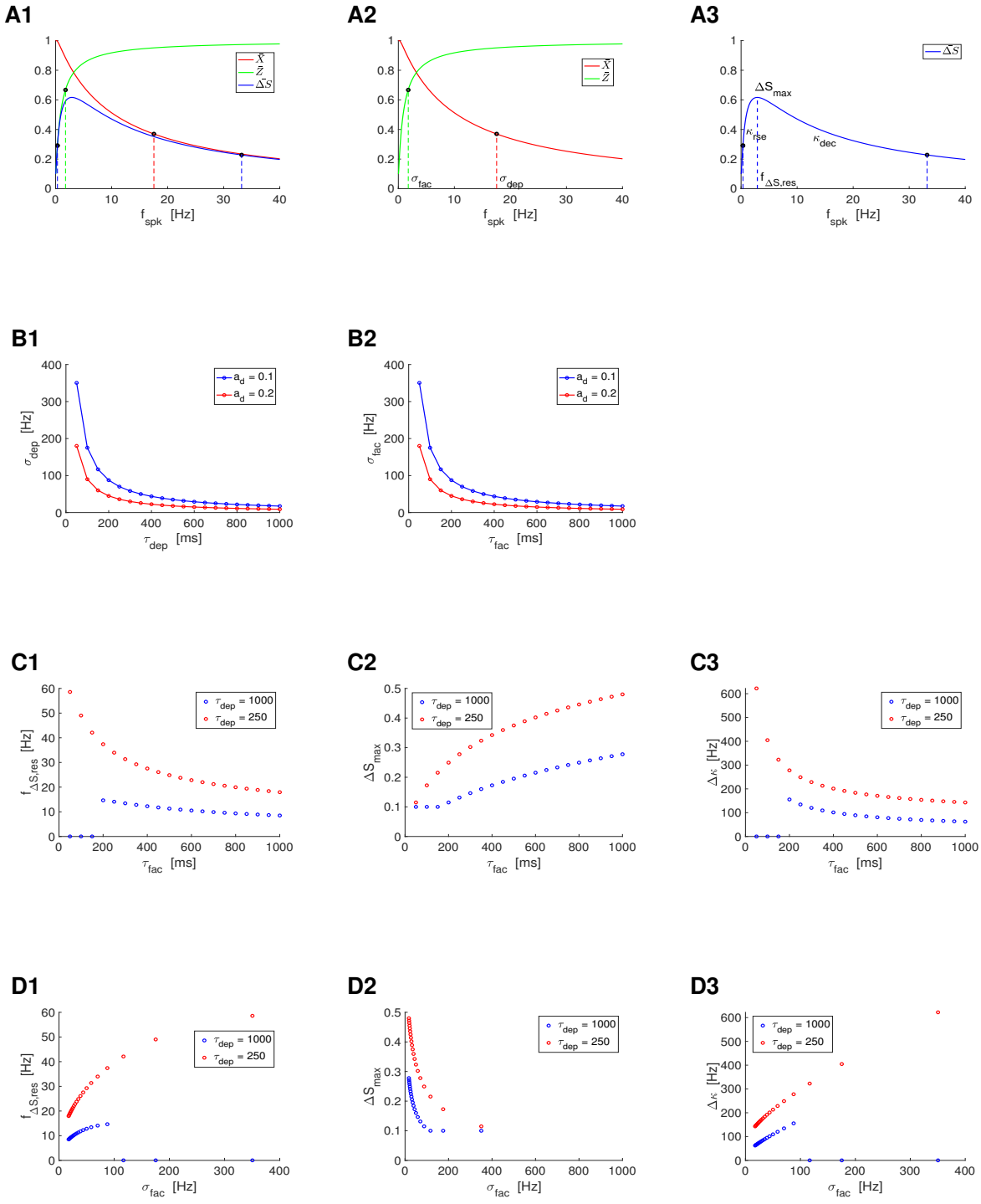

Figure 4: $\bar{\Delta S}$ **filters in response to periodic presynaptic spike inputs (frequency** f_{spk}**) for the DA model: frequency attributes. A.** The black dots on the $\bar{X}$, $\bar{Z}$ and $\bar{\Delta S}$ filters indicate the characteristic frequencies (projections on the f_{spk} axis) defined as the change in the corresponding quantities by 63 % of the gap between their final and initial values (σ_{dep} and σ_{fac}) and between their maximum and minimum values (κ_{rse} and κ_{dec}). The $\bar{\Delta S}$ resonant frequency $f_{\Delta S,res}$ is the peak frequency and ΔS_{max} is the peak value. **B.** Dependence of the $\bar{X}$ and $\bar{Z}$ attributes (characteristic frequencies σ_{dep} and σ_{fac}) with the depression and facilitation time constants τ_{dep} and τ_{fac}, respectively. **C.** Dependence of the $\bar{\Delta S}$ attributes with τ_{fac} for representative values of τ_{dep}. **D.** Dependence of the $\bar{\Delta S}$ attributes with σ_{fac} for representative values of τ_{dep}. For $\tau_{dep} = 1000$, $\sigma_{dep} \sim 17.6$, and for $\tau_{dep} = 250$, $\sigma_{dep} \sim 70.1$.

where $\bar{S}_{trough}$ is the steady-state value of the trough sequence $S_{trough,n}$ (Fig. 2, middle column, acquamarine dots). Fig. 2 (middle column) illustrates that both $\bar{S}$ and Γ_S vary with the input frequency f_{spk}. The temporal filtering properties of these responses were investigated in [44].

3.2.1 The to-$\bar{\Delta S}$ update model with instantaneous S raise

By solving the differential equation (40) for a constant value of $\Delta S_{spk,n} = \Delta S_{spk}$ during the presynaptic ISIs and updating the solution at the occurrence of each presynaptic spike at $t = t_{spk,n}$ ($n = 1, \ldots, N_{spk}$), one arrives to the following discrete linear difference equation for the peak sequences

$$S_{n+1} = e^{-\Delta_{spk}/\tau_{dec}}\, \Delta S_n. \tag{43}$$

By construction, the steady state value $\bar{S}$ is given by

$$\bar{S} = \bar{\Delta S} \tag{44}$$

for all input frequencies f_{spk} where $\bar{\Delta S}$ is the steady-state profile of the sequence ΔS_n. In other words, the peak envelope profiles $\bar{S}$ are identical to the $\bar{\Delta S}$ profiles.

The peak-to-trough envelope amplitude profile Γ_S is given by

$$\Gamma_S = \bar{\Delta S}\,(\,1 - e^{-\Delta_{spk}/\tau_{dec}}\,). \tag{45}$$

where the second term is the trough envelope profile for the stationary solution to eq. (43).

This expression is the product of two frequency-dependent processes: $\bar{\Delta S}$ and

$$Q_A = 1 - e^{-\Delta_{spk}/\tau_{dec}}, \tag{46}$$

which is a LPF. As f_{spk} increases, the Γ_S profiles transition from $\Gamma_S = \bar{\Delta S}$ ($f_{spk} \to 0$) to $\Gamma_S = 0$ ($f_{spk} \to \infty$) (Fig. 5). For fixed values of f_{spk}, the Γ_S profiles transition from $\Gamma_S = \bar{\Delta S}$ ($\tau_{dec} \to 0$) to $\Gamma_S = 0$ ($\tau_{dec} \to \infty$) as τ_{dec} increases. In other words, for small enough values of τ_{dec}, the Γ_S profiles reproduce the $\bar{\Delta S}$ profiles (Fig. 5-A1 to A3), but for larger values of τ_{dec}, the Γ_S and $\bar{\Delta S}$ profiles are different. These differences increase as f_{spk} and τ_{dec} increase (Fig. 5). For generality, in Fig. 5 we included values of τ_{dec} beyond the biophysically plausible regime for AMPA excitation.

When $\bar{\Delta S}$ is constant (frequency-independent, no STP) or is an LPF, Γ_S is a LPF (Fig. 5-A2 and A3). These LPFs become more pronounced as τ_{dec} increases. When $\bar{\Delta S}$ is a BPF, the Γ_S BPFs evoked by $\bar{\Delta S}$ become sharper as τ_{dec} increases (Fig. 5-A1).

These Γ_S filters are inherited from the $\bar{\Delta S}$ ones and modulated by τ_{dec}. In contrast, when $\bar{\Delta S}$ is a HPF, Γ_S BPFs emerge as the product of a HPF and a LPF (Fig. 5-A4). As τ_{dec} increases, the Q_A LPF is more pronounced as a function of f_{spk} and therefore the Γ_S BPF is sharper and peaks at a smaller value (Fig. 5-A5 and -A6).

3.2.2 The to-$\bar{\Delta S}$ update model with non instantaneous S raise

The solution to the first and second terms in (41) are given by

$$S = \Delta S + [\,S(t_{spk,n}) - \Delta S\,]\, e^{-(t-t_{spk,n})/\tau_{rse}} \tag{47}$$

and

$$S = [\,\Delta S + (\,S(t_{spk,n}) - \Delta S\,)\, e^{-(T_{sw}/\tau_{rse})}\,]\, e^{-(t-t_{spk,n}-T_{sw})/\tau_{dec}}, \tag{48}$$

respectively. Using this, one can compute the difference equation governing the evolution of the sequence of peaks

$$S_{n+1} = \Delta S \left(1 - e^{-T_{sw}/\tau_{rse}}\right) + S_n\, e^{-(\Delta_{spk,n}-T_{sw})/\tau_{dec}}\, e^{-T_{sw}/\tau_{rse}}. \tag{49}$$

By assuming a constant $\Delta_{spk,n} = \Delta_{spk}$, one obtains

$$\bar{S} = \bar{\Delta S}\,\frac{1 - e^{-T_{sw}/\tau_{rse}}}{1 - e^{-T_{sw}/\tau_{rse}}\,e^{-(\Delta_{spk}-T_{sw})/\tau_{dec}}} \tag{50}$$

and

$$\Gamma_S = \bar{S}\,\left[1 - e^{-(\Delta_{spk}-T_{sw})/\tau_{dec}}\right]. \tag{51}$$

Both expressions are the products of frequency-dependent filters and reduce to eqs. (44) and (45) for $\tau_{rse} \to 0$ and $T_{sw} \to 0$ with $\tau_{rse}/T_{sw} \ll 1$.

For $\tau_{rse} \to 0$, the second factor in eq. (50)

$$Q_C = \frac{1 - e^{-T_{sw}/\tau_{rse}}}{1 - e^{-T_{sw}/\tau_{rse}}\,e^{-(\Delta_{spk}-T_{sw})/\tau_{dec}}} \tag{52}$$

is $Q_C = 1$, independent of f_{spk}. For $\tau_{rse} > 0$, Q_C is a HPF, changing from $Q_{C,0} = 1 - e^{-T_{sw}/\tau_{rse}} < 1$ (for $f_{spk} = 0$) to $Q_{C,\infty} = (1 - e^{-T_{sw}/\tau_{rse}})/(1 - e^{-T_{sw}(1/\tau_{rse}-1/\tau_{dec})}) > 1$ (as $f_{spk} \to \infty$). $Q_C = 1$ for $f_{spk} = 1000/T_{sw}$, independently of τ_{dec} and τ_{rse}. As τ_{rse} increases (all other parameters fixed), within some bounds, $Q_{C,0}$ decreases and $Q_{C,\infty}$ increases, causing an increase in the HPF amplitude of Q_C. As τ_{dec} increases (all other parameters fixed), also within some bounds, Q_C increases for $0 < f_{spk} < 1000/T_{sw}$ and decreases for $f_{spk} > 1000/T_{sw}$. Therefore, for $f_{spk} < 1000/T_{sw}$, increasing values of τ_{rse} cause an attenuation of the $\bar{S}$ profiles (Fig. 6-A1 to -A3), and this attenuation is less pronounced the larger τ_{dec} (not shown). For $f_{spk} > 1000/T_{sw}$, increasing values of τ_{rse} cause an amplification of the $\bar{S}$ profiles (Fig. 6-A3), which is less pronounced the larger τ_{dec} (not shown). However, for $T_{sw} = 1$, the latter range is well beyond the frequencies we are interested in this paper.

The bounds mentioned above are set by the requirement that the denominator of Q_C is positive, which in turn requires that $\Delta_{spk} > T_{sw}(\tau_{rse} - \tau_{dec})/\tau_{rse}$. This is satisfied for all values of Δ_{spk} if $\tau_{rse} < \tau_{dec}$. (For larger values of τ_{res}, this imposes a bound on Δ_{spk} for which $Q_C > 0$.) The realistic values of τ_{rse} and τ_{dec} we use here satisfy this condition. Moreover, for these values of τ_{rse} and τ_{dec}, Q_C is a HPF, converging asymptotically to $Q_{C,\infty}$.

Because Q_C has HPF properties, the question arises whether a $\bar{S}$ BPF can be created by the interplay of a $\bar{\Delta S}$ LPF and Q_C for nonzero values of τ_{rse}. This is not possible for the model with instantaneous raise since $\bar{S} = \bar{\Delta S}$ (see Section 3.2.1). Figs. 6-A4 to -A7 illustrates that this is indeed possible $\tau_{rse} > 0$. The generation of a $\bar{S}$ band-pass filter requires that the $Q_C(0)$ is low enough, which is achieved by increasing τ_{rse} above some threshold value (Fig. 6-A5). This band-pass filter can be amplified by making the increase of Q_C sharper for low values of f_{spk}, which can be achieved by increasing τ_{dec} (Fig. 6-A6). The band-pass filter in Fig. 6-A5 is attenuated by further increasing τ_{rse} since this causes the intersection between the constituents low- and high-pass filters to move down (Fig. 6-A7). An increase in the values of τ_{dep} (Fig. 6-A7) causes the $\bar{\Delta S}$ low-pass filter to decrease sharper as compared to Fig. 6-A5, decreasing the intersection between the $\bar{\Delta S}$ low-pass filter and the Q_C high-pass filter. The resulting attenuation produces a $\bar{S}$ low-pass filter (Fig. 6-A7).

The second factor in eq. (51),

$$Q_D = 1 - e^{-(\Delta_{spk}-T_{sw})/\tau_{dec}}, \tag{53}$$

is a low-pass filter, provided Δ_{spk} is large enough as compared to T_{sw}, and is independent of τ_{rse}. Therefore, the effect of τ_{rse} on the Γ_S filters is inherited from the effect of τ_{rse} on $\bar{S}$ filters. The Γ_S filters are further attenuated by the Q_D filter. The Γ_S BPFs, in addition, become wider and the Γ_S resonant frequency is displaced (Fig. S14-A1, -A3). The attenuation is more pronounced for the larger frequencies as τ_{dec} increases, therefore the BPFs become sharper and the Γ_S resonant frequency is displaced as τ_{dec} increases (not shown).

3.3 Interplay of $\bar{\Delta S}$ and summation PSP filters

The synaptic variable S determined by eq. (3) is the input to the current balance equation (1) for the postsynaptic voltage response V. In the absence of STP ($\Delta S = 1$), summation effects give rise to postsynaptic (PSP) high-pass filters whose properties depend on the membrane potential properties, particularly the membrane time constant (τ_m).

In the presence of STP, the PSP filters reflect the interaction of the $\bar{\Delta S}$ filters and the summation filters. For small enough values of τ_m, the PSP filters are well approximated by the $\bar{\Delta S}$ filters. Previous work has considered PSP and $\bar{\Delta S}$ filters to be proportional (e.g., [28, 46, 92], but see [21]). However, for larger values of τ_m, the PSP filters are expected to depart from the weak modulation of the $\bar{\Delta S}$ filters.

As an intermediate step for the investigation of the interaction between $\bar{\Delta S}$ and PSP summation filters, we use an alternative formulation for the reduced synaptic dynamics described above given by

$$\frac{dS}{dt} = -\frac{S}{\tau_{dec}} + \Delta S_n \, \delta(t - t_{spk,n}), \tag{54}$$

where S is interpreted as the PSP response. Each presynaptic spike instantaneously raises S "by" some value ΔS_n, which, as before, varies depending on the properties of the STP (depression and/or facilitation). We refer to this model as the "by-ΔS" model.

The extended by-ΔS model (54) including the description of the raise phase reads

$$\frac{dS}{dt} = \hat{H}(t_{spk,n}, t_{spk,n} + T_{sw}) \, \frac{\hat{\Delta S}_n - S}{\tau_{rse}} - \hat{H}(t_{spk,n} + T_{sw}, t_{spk,n+1}) \, \frac{S}{\tau_{dec}}, \tag{55}$$

where $\hat{\Delta S}_n$ is the sum of ΔS_n and the value of S preceding the arrival of each presynaptic spike, and the other components are as for eq. (41) above.

The advantage of this formulation as compared to the conductance-based formulation described in Section 2 is that is amenable for analytical calculations, which help obtaining a better insight into the interplay of the STP time constants (τ_{dep} and τ_{fac}) and the synaptic time constants (τ_{dec} and τ_{rse}) in controlling the PSP filtering properties. We investigate the response of conductance-based models to periodic presynaptic inputs in the presence of STP in the next Section.

3.3.1 The by-$\bar{\Delta S}$ update model with instantaneous S raise

By solving the differential equation (54) for a constant value of $\Delta S_n = \Delta S$ during the presynaptic ISIs and updating the solution at each occurrence of the presynaptic spikes at $t = t_n$, $n = 1, \ldots, N_{spk}$, one arrives to the following discrete linear differential equation for the peak sequences in terms of the model parameters

$$S_{n+1} = e^{-\Delta_{spk}/\tau_{dec}} \, S_n + \Delta S. \tag{56}$$

The steady state values of (56) are given by

$$\bar{S} = \frac{\bar{\Delta} S}{1 - e^{-\Delta_{spk}/\tau_{dec}}}. \tag{57}$$

By construction,

$$\Gamma_S = \bar{\Delta S}. \tag{58}$$

In other words, the Γ_S filtering properties are inherited from the $\bar{\Delta S}$ profiles.

Eq. (57) is the product of two frequency-dependent processes. The factor

$$Q_B = \frac{1}{1 - e^{-\Delta_{spk}/\tau_{dec}}} \tag{59}$$

is a HPF transitioning from $Q_B = 1$ (for $f_{spk} = 0$) to $Q_B \to \infty$ (for $f_{spk} \to \infty$), and increasing faster the larger τ_{dec}. From eq. (57), for small enough values of f_{spk}, $\bar{S} \sim \bar{\Delta S}$. In the limit $f_{spk} \to 0$, $\bar{S} = \bar{\Delta S}$. As f_{spk} increases, Q_B increases and therefore the difference between $\bar{S}$ and $\bar{\Delta S}$ also increases.

In the absence of STP, $\bar{\Delta S}$ is constant and therefore $\bar{S}$ increases unboundedly as $f_{spk} \to \infty$ (Fig. 5-B3). Similarly unbounded $\bar{S}$ profiles are also obtained for $\bar{\Delta S}$ HPFs. Under certain circumstances, the presence of STP puts a bound on the increase of $\bar{S}$, particularly for large values of τ_{dec} and the resulting filters remain bounded. Specifically,

BPFs (Fig. 5-B1) and LPFs (Fig. 5-B2) may remain so for low enough values of τ_{dec} and transition to (bounded) HPFs for larger values of τ_{dec}. However, these HPFs may raise to saturation values that are too high to be realistic. This together with the presence of unbounded profiles (e.g., Fig. 5-B3) suggests that more complex biophysical models we investigate below include mechanism that cause the summation effects to be realistically saturated. In some cases (e.g., Fig. 5-B2), the transition to a HPF involves the generation of a trough in the $\bar{S}$ profiles for large enough values of τ_{dec} (synaptic antiresonance).

3.3.2 The by-$\bar{\Delta S}$ update model with non-instantaneous S raise

The solution to the first and second terms in (55) are given by eqs. (47) and (48), respectively, with ΔS substituted by $\hat{\Delta S}$. Using this, one can compute the difference equation governing the evolution of the sequence of peaks

$$S_{n+1} = \Delta S \left(1 - e^{-T_{sw}/\tau_{rse}}\right) + S_n \, e^{-(\Delta_{spk,n} - T_{sw})/\tau_{dec}}. \tag{60}$$

By assuming a constant $\Delta_{spk,n} = \Delta_{spk}$, one obtains

$$\bar{S} = \bar{\Delta S} \, \frac{1 - e^{-T_{sw}/\tau_{rse}}}{1 - e^{-(\Delta_{spk} - T_{sw})/\tau_{dec}}} \tag{61}$$

and

$$\Gamma_S = \bar{S} \left(1 - e^{-(\Delta_{spk,n} - T_{sw})/\tau_{dec}}\right) = \bar{\Delta S} \left(1 - e^{-T_{sw}/\tau_{rse}}\right). \tag{62}$$

Eq. (61) is the product of frequency-dependent processes. The second factor

$$Q_E = \frac{1 - e^{-T_{sw}/\tau_{rse}}}{1 - e^{-(\Delta_{spk} - T_{sw})/\tau_{dec}}} \tag{63}$$

reduces to Q_B in eq. (46) for $\tau_{rse} \to 0$ and $T_{sw} \to 0$ with $\tau_{rse}/T_{sw} \ll 1$. This case was discussed in Section 3.3.1 and serves as a reference here.

The presence of T_{sw} in Q_E (for $\tau_{rse} > 0$) causes a decrease in the initial values of $Q_E(f_{spk} = 0)$ and shrinks the range of values of f_{spk} for which the denominator of Q_E is positive to finite values: $f_{spk} < 1000/T_{sw}$. As $f_{spk} \to 1000/T_{sw}$, Q_E increases unboundedly. This in turn causes $\bar{S}$ to increase unboundedly. However, this behavior is not alway monotonic. For low enough frequencies, but large enough to be within the range of realistic values we consider in this paper, LPFs and BPFs emerge (Fig. 6-B1 and -B2). Within this range of frequencies, increasing values of τ_{rse} cause an attenuation of the $\bar{S}$ profiles. Away from this range of frequencies, the $\bar{S}$ profiles for $\tau_{rse} > 0$ increase above the $\bar{S}$ profile of $\tau_{rse} \to 0$ as they grow unboundedly. Increasing values of τ_{dec} amplify the grow of the $\bar{S}$ profiles consistent with the results of $\tau_{rse} \to 0$.

The second factor in eq. (62) is independent of f_{spk} and therefore increasing values of τ_{rse} attenuate the Γ_S filters without affecting their types (Fig. S15).

3.4 Interplay of synaptic STP and PSP summation frequency filters for postsynaptic passive cells: PSP peak, amplitude and phase profiles

Here we focus on the stationary membrane potential fluctuations of passive postsynaptic cells in response to periodic presynaptic inputs in the presence of STP (Fig. 1-A) for relatively fast synaptic raise and decay times (see Methods), consistent with AMPA excitation and GABA$_A$ inhibition.

The passive postsynaptic cell is described by

$$C \, \frac{dV}{dt} = -G_L \, V + I_{in}(t) - I_{syn}(t), \tag{64}$$

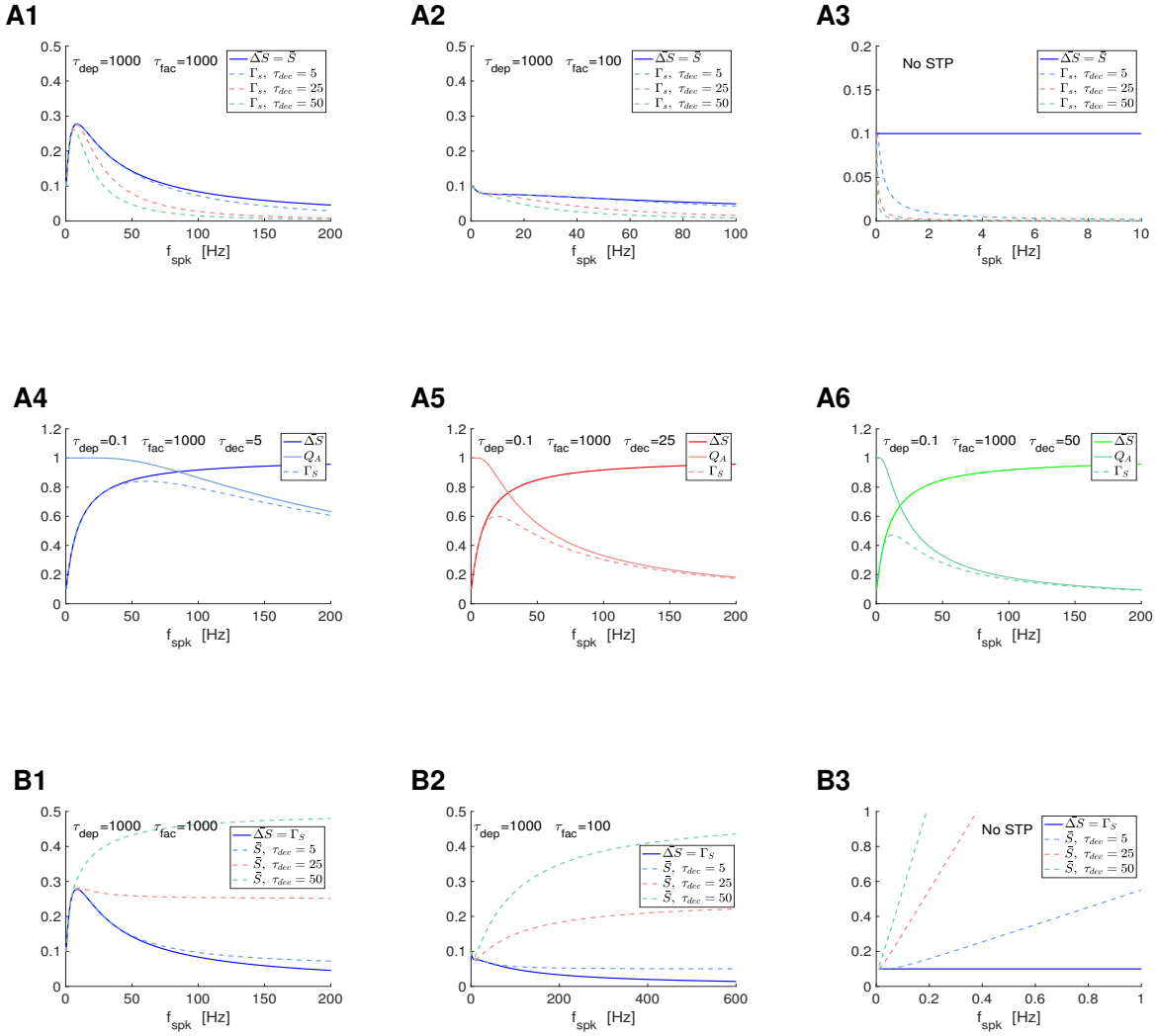

Figure 5: S **and** Γ_S **filters in response to periodic presynaptic spike inputs (frequency** f_{spk}**) for the to- and by-**ΔS **update models with instantaneous raise: representative examples.** We used eqs. (12) and (13) (DA model) for $\bar{\Delta S}$. **A.** To-ΔS model (synaptic update to ΔS). We used eq. (45) for Γ_S and eq. (46) for Q_A. **A1.** $\bar{\Delta S}$ and Γ_S are band-pass filters. **A2.** $\bar{\Delta S}$ and Γ_S are low-pass filters. **A3.** No STP. $\bar{\Delta S}$ is constant and Γ_S are low-pass filters. **A4 to A6.** Γ_S band-pass filters generated from $\bar{\Delta S}$ high-pass filters and Q_A low-pass filters. **B.** Synaptic update by ΔS. We used eq. (57) for $\bar{S}$. **B1.** $\bar{\Delta S}$ is a band-pass filter, while $\bar{S}$ transitions form band- to high-pass filters as τ_{dec} increases. **B2.** $\bar{\Delta S}$ is primarily a low-pass filter, while $\bar{S}$ transitions form low- to high-pass filters as τ_{dec} increases. **B3.** No STP. $\bar{\Delta S}$ is constant, while $\bar{S}$ are high-pass filters. We used the following additional parameter values: $a_d = 0.1$, $a_f = 0.1$, $x_\infty = 1$ and $z_\infty = 0$.

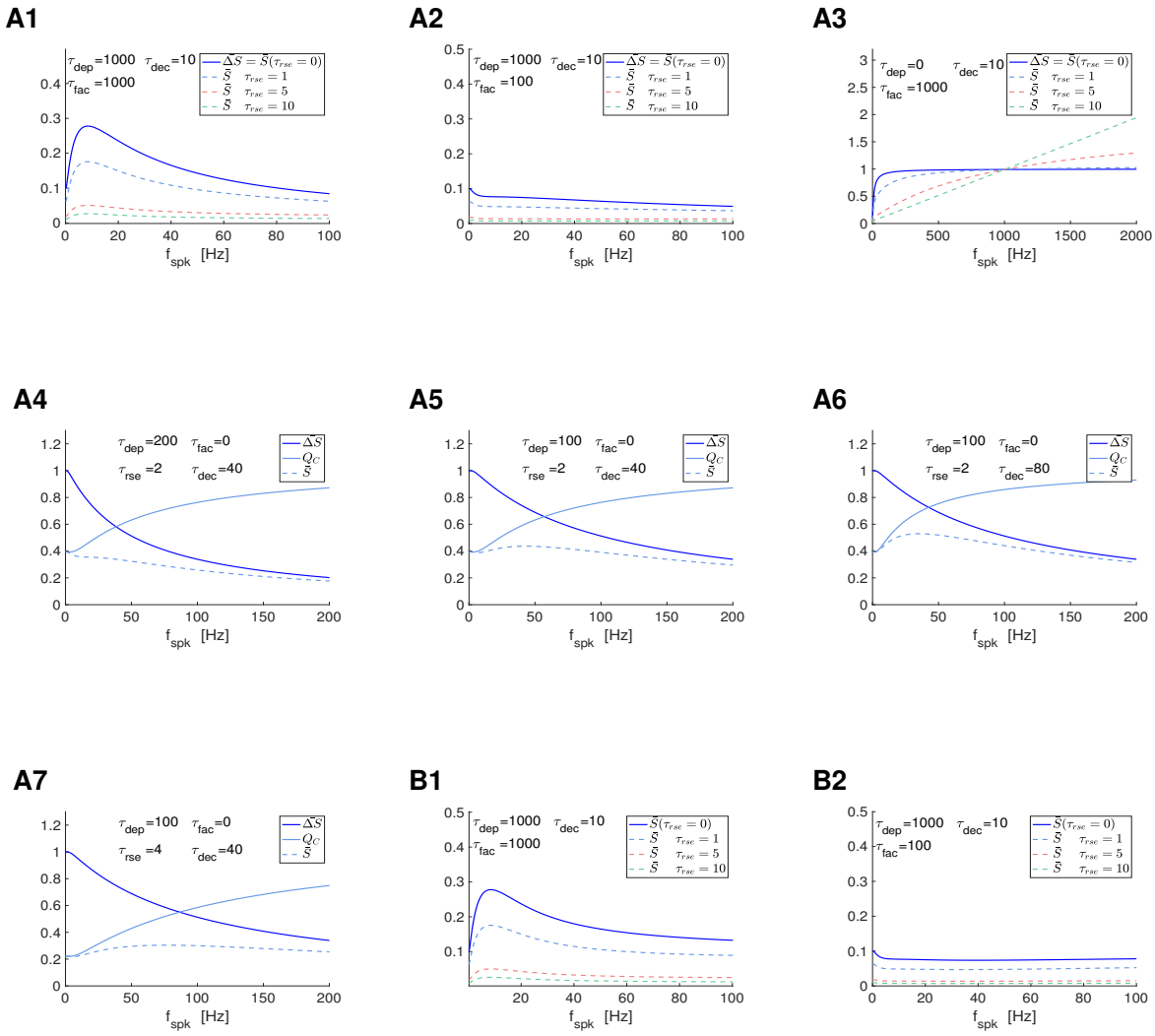

Figure 6: $\bar{S}$ **and** Γ_S **filters in response to periodic presynaptic spike inputs (frequency** f_{spk}**) for the to- and by-**ΔS **update models with non-instantaneous raise: representative examples.** We used eqs. (12) and (13) (DA model) for $\bar{\Delta S}$ **A.** To-ΔS model (synaptic update to ΔS). The S and Γ_S filters were computed using eqs. (50) and (51), respectively, with Q_C and Q_D given by (52) and (53), respectively. **A1 to A3.** Effects of τ_{rse}. **A1.** $\bar{S}$ BPFs attenuated by increasing values of τ_{rse}. **A2.** $\bar{S}$ LPFs attenuated by increasing values of τ_{rse}. **A3.** $\bar{S}$ HPFs filters attenuated (amplified) by increasing values of τ_{rse} for lower (higher) values of f_{spk}. **A4.** $\bar{S}$ low-pass filters created by the interplay of a $\bar{\Delta S}$ low-pass filter and a Q_C high-pass filter. **A5, A6, A7.** $\bar{S}$ band-pass filters created by the interplay of $\bar{\Delta S}$ low-pass filters and Q_C high-pass filters. **B.** By-ΔS model (synaptic update by ΔS). The S and Γ_S filters were computed using eqs. (61) and (62), respectively, with Q_E given by (63). We used the following additional parameter values: $a_d = 0.1$, $a_f = 0.1$, $x_\infty = 1$, $z_\infty = 0$ and $T_{sw} = 1$.

where the variable V in eq. (64) represents $V - V_{eq}$ in eq. (1) with $V_{eq} = E_L - I_{app}/G_L$ and I_{syn} is described by eqs. (2)-(4) appropriately adapted (to account for the interpretation of V as membrane potential fluctuations around the equilibrium). We use the analytical approximations described in Section 2.2 (see also Appendix A).

We distinguish between the filtering properties of passive cells in response to direct current injection (I_{in}) and presynaptic activation (I_{syn}). We also distinguish between the cell's membrane potential (peak-to-trough) amplitude and peak response profiles.

A cell's response frequency content can be measured by using the impedance amplitude (Z) and phase (Φ_Z) profiles (see Section 2.3.1; Fig. 8-A, green). For direct sinusoidal current activation of cells with linear subthreshold dynamics, the cell's response (peak-to-trough) amplitude and peak profiles coincide and are described by the Z profiles (Fig. 8-A1, green). (For certain types of cells with nonlinear subthreshold dynamics, the Z profiles provide a good approximation to these quantities or the Z profiles can be adapted to capture these quantities [77, 78, 96, 97].) For presynaptic activation of cells, in contrast, the PSP (peak-to-trough) amplitude and peak profiles do not generally coincide [94] (see discussion in Section 3.3; Fig. 8-A1, blue and light blue).

We therefore consider three metrics for the PSP response to periodic presynaptic inputs : (i) the PSP peak profiles V_{peak} (curves of the stead-state peak values of V as a function of the input frequency f_{spk}) (Fig. 8-A1, blue), (ii) the peak-to-trough PSP amplitude profiles Γ_V, defined as

$$\Gamma_V(f_{spk}) = V_{peak}(f_{spk}) - V_{trough}(f_{spk}) \tag{65}$$

where V_{trough} are the PSP trough profile (curves of the steady-state trough values of V as a function of the input frequency f_{spk}) (Fig. 8-A1, light blue), and (iii) the PSP phase profiles Φ_V, defined as

$$\Phi_V = \frac{t_{peak,V} - t_{spk}}{\Delta_{spk}/\pi}, \tag{66}$$

expressed in radians, where $t_{peak,V}$ is V_{peak} time and t_{spk} is the presynaptic spike time immediately preceding the occurrence of this peak (Fig. 8-A2, blue). The V_{peak} and Φ_V profiles are analogous metrics to the Z and Φ_Z profiles. The V_{peak} profiles capture the postsynaptic cell's ability to preferentially produce spikes within certain presynaptic frequency ranges, and is therefore relevant for the frequency-dependent communication of information to the postsynaptic spiking regime.

The PSP filtering properties, captured by the V_{peak}, Γ_V and Φ_V profiles, depend on the filtering properties of the participating building blocks and are controlled by the time constants operating at each level (Fig. 1): τ_{dep} and τ_{fac} (STP), τ_{dec} (synaptic) and τ (postsynaptic). From our results in Section 3.2 (see also Section 2.2), the steady-state S peak profiles S_{peak} (or $\bar{S}$) depend at most mildly on τ_{rse} for the type fast synaptic raise times we consider here.

In the next sections we first discuss the PSP summation HPFs in passive cells (controlled by τ and modulated by τ_{dec}) in the absence of STP, and their link to the passive cells' LPFs (captured by Z, also controlled by τ). We then discuss the PSP filtering properties of passive cells in response to periodic presynaptic inputs in the presence of either depression (LPF) or facilitation (HPF).

3.5 Digression: PSP response of passive cells to presynaptic spikes for individual input frequencies

We analyze here the properties of the PSP response of passive cells to presynaptic spikes from the arrival of a presynaptic spike ($t = t_n$) to the arrival of the next presynaptic spike ($t = t_{n+1} = \Delta_{spk,n}$). By construction (see Section 2.2 and Appendix A.2), the analytical approximation to $V(t)$, namely $V_I(t)$ (80) for the duration of the presynaptic spike ($t_n < t < t_n + T_{sw}$) followed by $V_{II}(t)$ (83 or 90) for the reminder of the presynaptic ISI ($t_n + T_{sw} < t < t_n + \Delta_{spk,n}$), depends on the model parameters both explicitly and implicitly through the initial condition $V_{0,n}$ for each presynaptic ISI and the update parameter α_n. The implicit dependence is inherited from the previous presynaptic ISI. We assume here the PSP response is in the steady-state regime and therefore we focus our analysis on the explicit dependence of $V(t)$ on the model parameters.

From eq. (80) for $V_I(t)$ ($t_n < t < t_n + T_{sw}$), the larger τ, the larger $\beta_n = V_I(t_n + T_{sw}) = V_I I(t_n + T_{sw})$ (81). This dependence is affected by the presynaptic ISI $\Delta_{spk,n}$ through $V_{0,n} = V_{II}(t_{n-1})$ (from the previous presynaptic ISI). For the remainder of the presynaptic ISI ($t_n + T_{sw} < t < t_{n+1}$), from eqs. (83) and (90), respectively,

$$V_{II}(t) = \frac{\alpha_n\ \Delta S_n}{1-\eta}\, e^{-(t-t_n-T_{sw})\,\eta/\tau} + \left[\beta_n - \frac{\alpha_n\ \Delta S_n}{1-\eta}\right] e^{-(t-t_n-T_{sw})/\tau} \qquad \text{if} \quad \tau_{dec} \neq \tau \tag{67}$$

with

$$\eta = \frac{\tau}{\tau_{dec}}, \tag{68}$$

and

$$V_{II}(t) = \left[\frac{\alpha_n\, \Delta S_n}{\tau}\,(t - t_n - T_{sw}) + \beta_n\right] e^{-(t-t_n-T_{sw})/\tau} \qquad \text{if} \quad \tau_{dec} = \tau. \tag{69}$$

The PSP response to presynaptic inputs $V(t)$ is shaped by a balance among τ_{dec}, τ and $\Delta_{spk,n}$ (Fig. 7), and is modulated by G_{syn} (constant) and the STP time constants (τ_{dep} and τ_{fac}) through ΔS_n (frequency-dependent). The latter determines the target for the peak of the synaptic function S. In Fig. 7, ΔS_n is independent of f_{spk}. The properties of the PSP response for frequency-dependent ΔS_n profiles are investigated in the next Sections.

If $\tau_{dec} \ll \tau$, $\eta \gg 1$ in eq. (67) and $V_{II}(t)$ is dominated by the second term. In the limiting cases $\eta \to \infty$ ($\tau_{dec} \to 0$ or $\tau \to \infty$), $V_{II}(t)$ begins to decrease at $t_n + T_{sw}$. As η decreases, $V_{II}(t)$ continues to increase passed $t_n + T_{sw}$ in response to $S_a(t) > 0$. The larger τ_{dec} for fixed values of τ , the larger $V_{II}(t)$ over the presynaptic ISI (Fig. 7-B) and the larger the peak time $t_{peak,n}$. Similarly, the larger τ for fixed values of τ_{dec}, the larger $V_{II}(t)$ over the presynaptic ISI (Fig. 7-A) and the larger the peak time $t_{peak,n}$. If $\tau_{dec} \gg \tau$, $\eta \ll 1$ in eq. (67) and $V_{II}(t)$ is dominated by the first term. In the limit $\eta \to 0$ ($\tau_{dec} \to \infty$ or $\tau \to 0$), $V_{II}(t)$ only increases over the presynaptic ISI. If $\tau_{dec} = \tau_{fac}$, $V_{II}(t)$ has the form of an alpha function. The larger τ, the larger $V_{II}(t)$ over the presynaptic ISI. Increasing values of G_{syn} also cause an increase in $V_{II}(t)$ over the presynaptic ISI (Fig. 7-C) with at most a mild effect on the peak times. This suggests that while increasing values of τ_{dec} and G_{syn} increase the total input current to the postsynaptic cell, their effect on the properties of the PSP filters may differ.

Comparison between the left ($f_{spk} = 10$) and right ($f_{spk} = 40$) columns in Fig. 7 illustrates that effects of summation. One of them is the increase in the PSP peak response as f_{spk} increases and the other one is the decrease in the peak-to-trough amplitude as f_{spk} increases.

3.6 Response of passive cells to periodic presynaptic inputs in the absence of STP: summation (SUM) filters

3.6.1 PSP peak (LPFs), amplitude (LPFs) and phase (delay) profiles in response to direct activation of oscillatory inputs (revisited)

Passive cells are LPFs in response to direct activation of sinusoidal input currents and always exhibit a delayed response (see Section 2.3.2). The Z profile (36) is a decreasing function of the input frequency f (Fig. 8-A1, green) and the Φ_Z profile (37) is an increasing function of f, converging to $\pi/2$ (Fig. 8-A2, green). These profiles are affected by the membrane time constant $\tau = C/G_L$. Increasing values of τ cause (i) an increase in $Z_{max} = Z(0)$ (compare Figs. 8-A1 and B1, green), (ii) a sharper decrease of the Z profile (compare Figs. 8-A1 and B1, green), and (iii) a sharper increase of the Φ_Z profile (compare Figs. 8-A2 and B2, green).

3.6.2 PSP peak (HPFs), amplitude (LPFs) and phase (delay) profiles in response to periodic presynaptic inputs

In response to periodic presynaptic inputs (with no STP), passive cells are Γ_V LPFs (Fig. 8, left column, light blue), but V_{peak} HPFs (Fig. 8, left column, blue), while always exhibit a delayed response (Fig. 8, right column, blue)

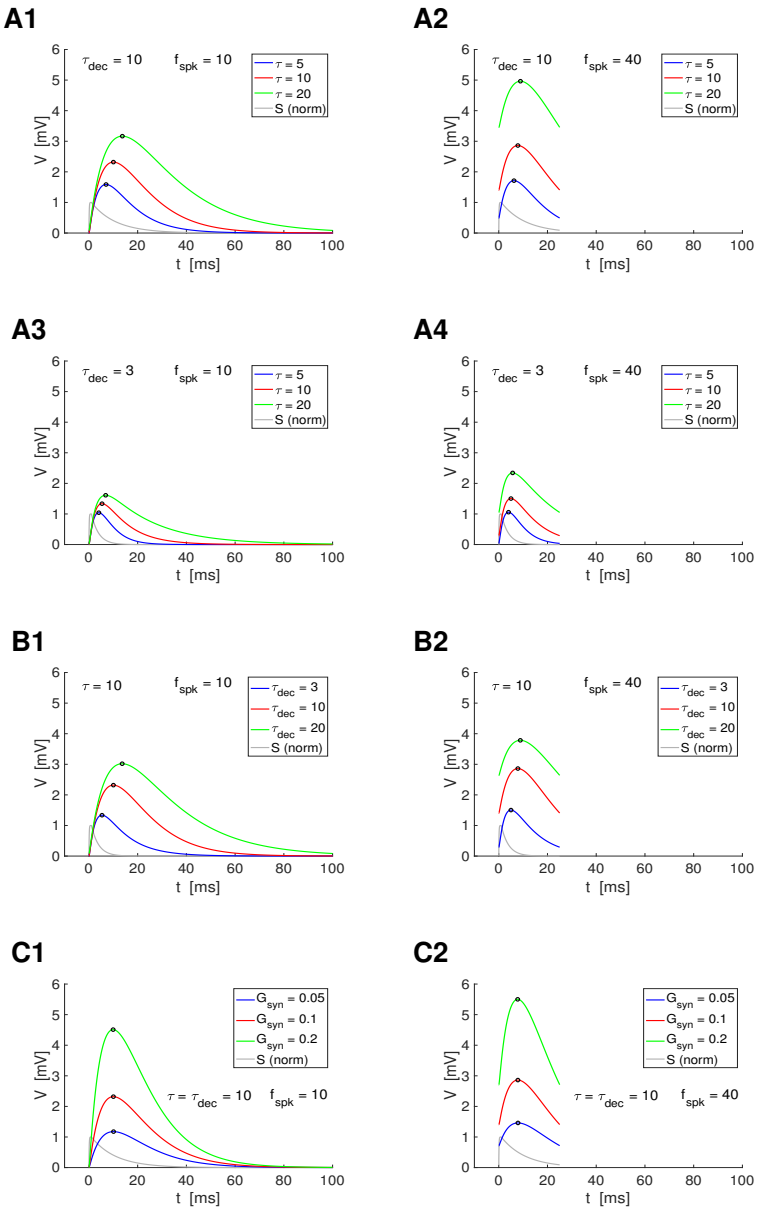

Figure 7: **Properties of the membrane potential response of passive cells to periodic presynaptic spikes for representative parameter values.** For the numerical approximations we used the model for a passive cell receiving presynaptic spike-train input (1)-(4). For STP we used the DA model (7)-(9). The graphs correspond to the steady-state solutions (translated to $t = 0$). The summation effect is observed in panels B. The synaptic function S was normalized by its maximum in the presynaptic interspike interval. **A.** $G_{syn} = 0.1$ **Top row:** $\tau_{dec} = 10$. **Bottom row:** $\tau_{dec} = 3$. **Left column.** $f_{spk} = 10$. **Right column.** $f_{spk} = 40$. $G_{syn} = 0.1$. **B.** $G_{syn} = 0.1$ and $\tau = 10$ **B1.** $f_{spk} = 10$. **B2.** $f_{spk} = 40$. **C.** $\tau = 10$, $\tau_{dec} = 10$ **C1.** $f_{spk} = 10$. **C2.** $f_{spk} = 40$. We used the following additional parameter values: $a_d = 0.1$, $a_f = 0.1$, $x_\infty = 1$, $z_\infty = 0$, $\tau_{rse} = 0.1$, $C = 1$, $E_L = -60$, $I_{app} = 0$, $E_{syn} = -60$, $\tau_{dep} = \tau_{fac} = 0.1$.

similarly to Φ_Z. The V_{peak} HPFs result from the summation phenomenon. These profiles are affected by both τ (membrane time constant) and τ_{dec} (synaptic decay time).

Increasing values of τ, amplify and sharpen the V_{eq} and Γ_V profiles (Fig. 8-A1 and -B1), and sharpen the Φ_V profiles (peak responses are more delayed) (Fig. 8-A2 and -B2). Increasing values of τ_{dec}, also amplify and sharpen the V_{eq} and Γ_V profiles (Fig. 8-C1), and sharpen the Φ_V profiles (peak responses are more delayed) (Fig. 8-C2). More specifically, increasing values of τ cause cause (i) an amplification of the V_{peak} profiles (compare Figs. 8-A1 and B1, blue), (ii) a sharper increase of the V_{peak} profile with f_{spk} (compare Figs. 8-A1 and B1, blue), (iii) an amplification of the Γ_V profiles, which is more pronounced for the lower values of f_{spk} (compare Figs. 8-A1 and B1, light blue), (iv) a sharper decrease in the Γ_V profile with increasing values of f_{spk} (compare Figs. 8-A1 and B1, green), and (v) a sharper increase in the Φ_V profile with increasing values of f_{spk} (compare Figs. 8-A2 and B2, blue). Increasing values of τ_{dec} cause (i) an amplification of both the V_{peak} and Γ_V profiles (Fig. 8-C1, blue and light blue), (ii) a sharper decrease of the Γ_V profiles with increasing values of f_{spk} (Fig. 8-C1, light blue), and (iii) a sharper increase of the Φ_V profiles with increasing values of f_{spk} (Fig. 8-C2, blue).

3.6.3 Summation: heuristic explanation

By approximating S by ΔS_n for the duration of the presynaptic spike ($t_n \leq t \leq t_n + T_{sw}$), the passive membrane equation receiving presynaptic inputs equation is approximated by

$$\tau \frac{dV}{dt} = -V + \gamma_{syn}\, \Delta S_n\, \tau\, (V - E_{syn}) \tag{70}$$

where the variable V has the same interpretation as in eq. (21), $V(0) = 0$ and

$$\gamma_{syn} = \frac{G_{syn}}{C}. \tag{71}$$

The solution to eq. (70) is given by

$$V(t) = V_\infty + [\, V(t_n) - V_\infty \,]\, e^{-(1/\tau + \gamma_{syn}\, \Delta S_n)\, (t - t_n)} \tag{72}$$

where

$$V_\infty = \frac{\gamma_{syn}\, \Delta S_n\, \tau}{1 + \gamma_{syn}\, \Delta S_n\, \tau}\, E_{syn}. \tag{73}$$

$V(t)$ increases and approaches its steady-state value V_∞, which increases from $V_\infty = 0$ ($\tau = 0$) to $V_\infty = E_{syn}$ ($\tau \to \infty$). $V(t)$ reaches its peak value

$$\tilde{V}_{peak,n} = V(t_n + T_{sw}) = V_\infty\, [\, 1 - e^{-(1/\tau + \gamma_{syn}\, \Delta S_n)\, T_{sw}} \,] + V(t_n)\, e^{-(1/\tau + \gamma_{syn}\, \Delta S_n)\, T_{sw}} < V_\infty \tag{74}$$

during the presynaptic ISI. For the remaining of the presynaptic ISI ($t_n + T_{sw} < t < t_{n+1}$), $V(t)$ decays exponentially to some value $\tilde{V}_{trough,n} = V(t_{n+1}) > 0$, which depends on the presynaptic ISI $\Delta_{spk,n}$.

The peak value $\tilde{V}_{peak,n}$ increases from $\tilde{V}_{peak,n} = 0$ ($\tau = 0$) to $\tilde{V}_{peak,n} = E_{syn} + [\, V(t_n) - E_{syn} \,]\, e^{-\gamma_{syn}\, \Delta S_n\, T_{sw}}$ ($\tau \to \infty$), and is an increasing function of $V(t_n)$ whose value is inherited from the previous presynaptic ISI.

For periodic presynaptic inputs and synaptic update values ΔS_n independent of n, the V_{peak} and Γ_V summation are originated in the temporal domain (as n increases) and are frequency-dependent. For each value of f_{spk}, $V(t_2) = V_{trough,1} > V(t_1) = 0$ and therefore, $V_{peak,2} > V_{peak,1}$. This causes $V_{trough,2} = V_{trough,1}$. Following this process for increasing values of n, leads to two monotonically non-decreasing sequences converging to V_{peak} and V_{trough}. As f_{spk} increases, $V_{troough,n}$ also increase for fixed values of n, since there is less time for V to decay, and therefore $V_{peak,n}$ also increase.

Therefore, V_{peak} and V_{trough} are increasing functions of f_{spk}. If the V_{peak} profile increases slower than V_{trough} profile, then the Γ_V profile is a LPF (Fig. 8, column 1). For $\tau \to 0$, the V_{peak} profile is proportional to S_{peak} and $V_{peak} \to 0$. As τ increases, both the V_{peak} and Γ_V profiles are amplified.

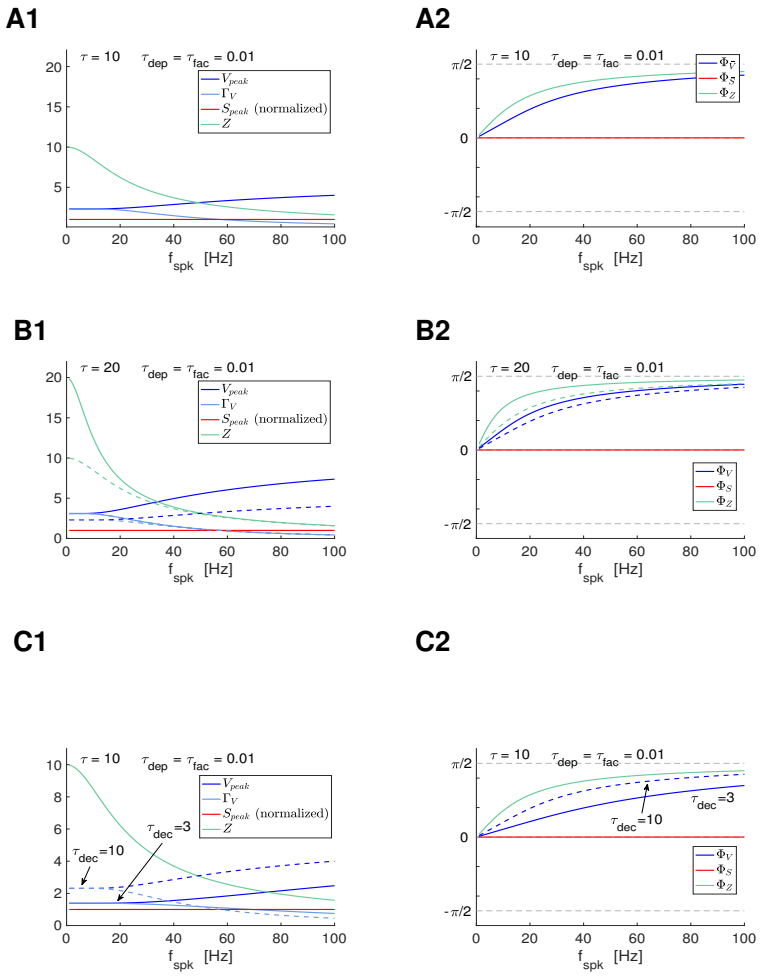

Figure 8: **Postsynaptic filters in response to periodic presynaptic spike inputs for the passive (postsynaptic) cell in the absence of STP.** We used eq. (64) for the PSP V with I_{syn} described by eqs. (2)-(4) appropriately adapted to account for the translation of V to the equilibrium point. We used eqs. (12) and (13) (DA model) with very values of τ_{dep} and τ_{fac} in the no STP regime. The impedance amplitude (Z) and phase (Φ_Z) were computed using eqs. (36) and (37). The analytical approximations for the PSP peak sequence response of passive cells to presynaptic inputs are described in Section 2.2 (see also Appendix A). The approximation of $V_{peak,n}$, $V_{trough,n}$ and $t_{V,peak}$ were computed as described in Section 3.4. The PSP amplitude Γ_V was computed by using eq. (65) and the PSP phase Φ_V was computed using eq. (66). The synaptic (S) peak (S_{peak}) and phase (Φ_S) profiles were computed similarly to these for V. **A.** $\tau = 10$ ($G_L = 0.1$), $\tau_{dec} = 10$. **B.** $\tau = 20$ ($G_L = 0.05$), $\tau_{dec} = 10$. The dashed curves correspond to panels B ($\tau = 10$) and are presented for comparison purposes. **C.** $\tau = 10$ ($G_L = 0.1$), $\tau_{dec} = 3$. The dashed curves correspond to panels B ($\tau_{dec} = 10$) and are presented for comparison purposes. We used the following additional parameter values: $C = 1$, $E_L = -60$, $I_{app} = 0$, $G_{syn} = 0.1$, $E_{syn} = 0$, $a_d = 0.1$, $a_f = 0.1$, $x_\infty = 1$, $z_\infty = 0$ and $T_{sw} = 1$.

3.7 PSP V_{peak} and Γ_V profiles: Inherited and cross level BPFs (resonances)

The V_{peak}, Γ_V and Φ_V profiles are shaped by the feedforward interaction among the participating filters. For small enough values of τ_{dec} and τ, the V_{peak} profile is almost proportional to the S_{peak} profile, the V_{trough} profile is almost zero, and therefore the Γ_V profile is almost equal to the V_{peak} profile. In the limit of $\tau \to 0$ and $\tau_{dec} \to 0$ these relationships are strictly valid. In this sense, the PSP V_{peak} and Γ_V profiles (and filtering properties) are inherited from the synaptic level S_{peak} profile. If τ_{dec} increases ($\tau \ll 1$), then the V_{peak} profile remains almost proportional to S_{peak} profile, but the V_{trough} profile increases with f_{spk} and therefore the Γ_V profile is lower than the V_{peak} profile. If, on the other hand, τ increases ($\tau_{dec} \ll 1$), the V_{peak} profile is no longer proportional to the S_{peak} profile and the V_{trough} profile is an increasing function of f_{spk}, and therefore the Γ_V and V_{peak} profiles are different. This remains true when both τ and τ_{dec} increase. In these cases, the V_{peak} and Γ_V profiles are either modulated versions of the S_{peak} profiles or exhibit a qualitatively different shape from the S_{peak} profiles.

Similarly to the generation of the STP-mediated $\bar{\Delta S}$ BPFs discussed above, under certain balance conditions, synaptic and postsynaptic filters with opposite monotonic dependencies with f_{spk} are expected to produce BPFs, while synaptic and postsynaptic filters with the same monotonic dependencies with f_{spk} are expected to reinforce each other.

The interplay of synaptic depression (LPF) and V_{peak} summation (HPF) is able to generate V_{peak} BPFs (Fig. 9-A1, solid blue), but not Γ_V BPFs (Fig. 9-A, solid light blue) since both the S_{peak} and the Γ_V summation profiles are LPFs. In contrast, the interplay of synaptic facilitation (HPF) and Γ_V summation (LPF) is able to generated Γ_V BPFs (Fig. 9-B, solid light blue), but not V_{peak} BPFs since both the S_{peak} and V_{peak} summation profiles are HPFs (Fig. 9-B, solid blue). In the presence of both synaptic depression (LPF) and facilitation (HPF), the S_{peak} profiles are BPFs (Fig. 9-C, solid red). These are communicated to the postsynaptic level where they interact with the postsynaptic membrane potential properties. In certain parameter regimes, these modulations produce PSP V_{peak} and Γ_V BPFs (Fig. 9-C, solid blue). We analyzed the various possible scenarios and mechanisms in the next sections.

3.8 Interplay of synaptic depression (LPFs) and PSP summation filters: V_{peak} BPFs and Γ_V LPFs

The presence of short-term depression generates S_{peak} LPFs that become sharper and more attenuated as τ_{dep} increases (Fig. 10-A3) and are independent of τ, τ_{dec} and G_{syn} (Fig. 10-B3 to -D3)

3.8.1 Emergence of V_{peak} resonance (BPFs): interplay of a depression LPF and a PSP summation HPF

The interaction between these filters and the PSP summation HPF (Fig. 8-A1, blue) produces V_{peak} BPFs for values of τ_{dep} within some range (Fig. 10-A1, blue and red). We refer to this preferred frequency PSP peak response to periodic presynaptic inputs as (PSP) V_{peak} resonance. This maximal amplification of the V_{peak} response is often preceded by a relatively small trough. V_{peak} resonance reflects balances between the two participating filters. As τ_{dep} increases (sharper decrease of the S_{peak} profile), the V_{peak} profiles are dominated by depression and therefore they are attenuated as they transition to LPFs for larger values of τ_{dep} (Fig. 10-A1, blue to light blue). This is accompanied by a decrease in the V_{peak} resonant frequency. As τ increases, the V_{peak} profiles are dominated by summation and therefore they are amplified (Fig. 10-A2). This is accompanied by an increase in the V_{peak} resonant frequency. Changes in τ_{dec} and G_{syn} do not affect the S_{peak} profiles, but they affect the V response to presynaptic spikes in a frequency-dependent manner (Fig. 7-C). Consistently with that, increasing values of τ_{dec} and G_{syn} amplify the V_{peak} response with lesser effects on their shapes than changes in τ_{dep} and τ (Fig. 10-C1 and -D1). This is more prominent for G_{syn}, which has almost a multiplicative effect on the V_{peak} profiles, than for τ_{dec}, consistently with the different ways in which they control the synaptic currents.

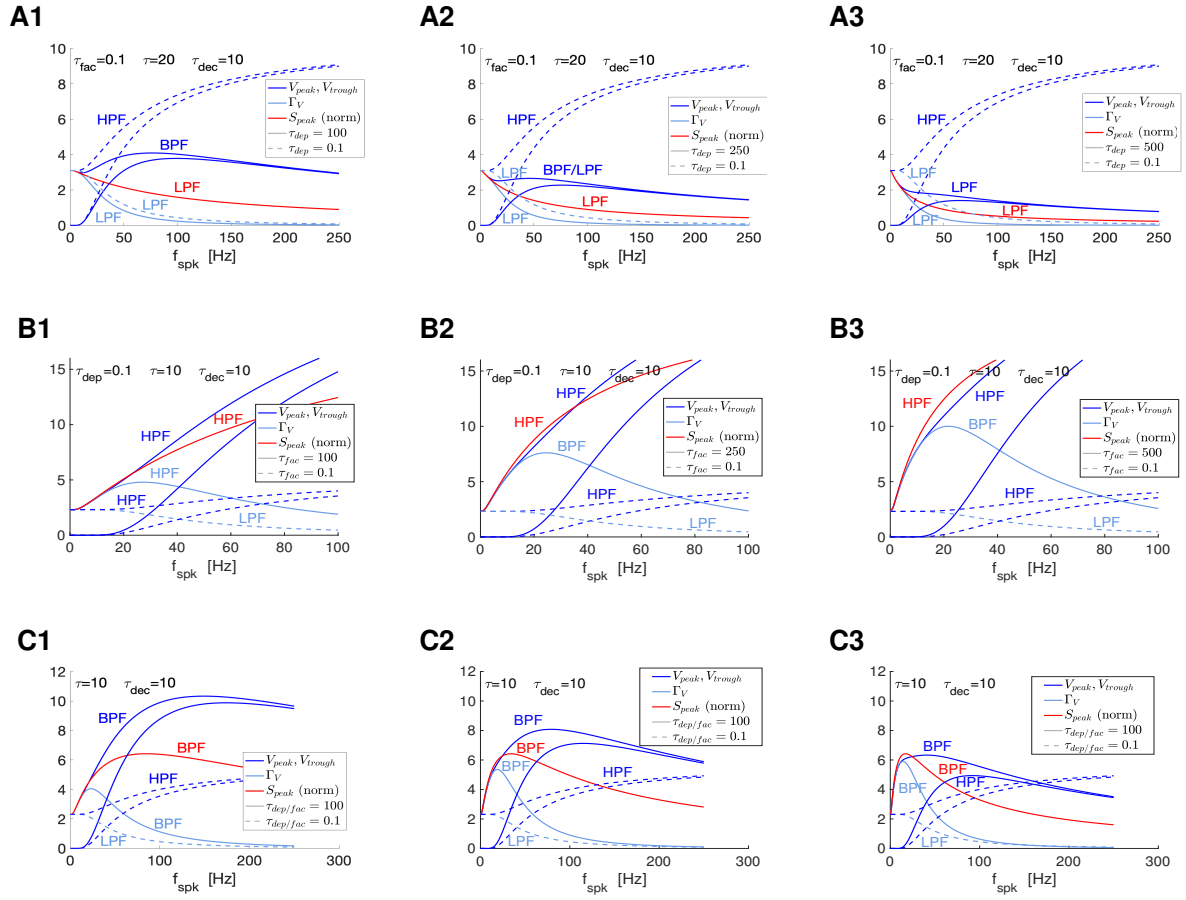

Figure 9: **Postsynaptic BPFs filters in response to periodic presynaptic spike inputs emerging from the interplay of short-term depression (LPF), short-term facilitation (HPF) and postsynaptic summation (HPF).** Each panel shows the superimposed V_{peak}, V_{trough} and Γ_V profiles in response to presynaptic inputs in the presence (solid) and absence (dashed) of STP. The S_{peak} profiles are normalized to coincide with the V_{peak} profiles for the lowest value of f_{spk} ($f_{spk} = 0.1$ in the simulations). The summation HPFs are generated in response to presynaptic inputs in the absence of STP ($\tau_{dep} = 0.1$, $\tau_{fac} = 0.1$ or $\tau_{dep} = \tau_{fac} = 0.1$ in the simulations). The S_{peak} profiles in the absence of STP are horizontal lines (not shown). **A.** V_{peak} BFPs (solid blue) generated by the interplay of S_{peak} LPFs (red) and V_{peak} summation HPFs (dashed blue) in the presence of synaptic depression only. The interplay of the Γ_V summation LPF (dashed light blue) and the S_{peak} LPF (red) produces a Γ_V LPF (solid light blue). **B.** Γ_V BFPs (light blue) generated by the interplay of S_{peak} HPFs (red) and Γ_V summation LPFs (dashed blue) in the presence of synaptic facilitation only. The interplay of of the V_{peak} summation HPF (dashed blue) and the S_{peak} HPF (red) produces a V_{peak} HPF (solid blue). **C.** V_{peak} BPFs (solid blue) and Γ_V BPFs (solid light blue) generated by the interplay of the inherited S_{peak} BFPs (red) and modulated by the V_{peak} summation HPFs (dashed blue) and the $Gamma_V$ summation LPFs (dashed light blue). We used eq. (64) for the PSP V with I_{syn} described by eqs. (2)-(4) appropriately adapted to account for the translation of V to the equilibrium point, and STP described by eqs. (12) and (13) (DA model). The impedance amplitude (Z) and phase (Φ_Z) were computed using eqs. (36) and (37). The analytical approximations for the PSP peak sequence response of passive cells to presynaptic inputs are described in Section2.2 (see also Appendix A). The approximation of $V_{peak,n}$ and $V_{trough,n}$ were computed as described in Section 3.4. The PSP amplitude Γ_V was computed by using eq. (65) and the PSP phase Φ_V was computed using eq. (66). The synaptic (S) peak (S_{peak}) and phase (Φ_S) profiles were computed similarly to these for V. We used the following additional parameter values: $C = 1$, $E_L = -60$, $I_{app} = 0$, $G_{syn} = 0.1$, $E_{syn} = 0$, $a_d = 0.1$, $a_f = 0.1$, $x_\infty = 1$, $z_\infty = 0$ and $T_{sw} = 1$.

3.8.2 Modulation of Γ_V LPFs: interplay of depression and PSP amplitude LPFs

In the absence of STP, the Γ_V LPF is controlled by the membrane time constant τ (Fig. 8-B1) and the synaptic decay time constant τ_{dec} (Fig. 8-C1). Here we focus on the effects of synaptic depression (τ_{dep}) and the interplay between the three time constants in the modulation of Γ_V. Increasing values of τ_{dep} sharpen Γ_V without affecting $\Gamma_V(0)$ (Fig. 10-A2). The magnitude of the modulation depend on the other parameter values (Fig. S5, column 2). Increasing values of τ and τ_{dec} sharpen Γ_V and increase $\Gamma_V(0)$ (Fig. 10-B2 and -C2). This is at most mildly affected by τ_{dep} (Fig. S7, column 2) and τ_{dec} (Fig. S8, column 2). Increasing values of G_{syn} have a multiplicative effect on Γ_V (Fig. 10-D2).

3.8.3 Modulation of the Φ_V

In the absence of STP, the Φ_V profile is controlled by τ and τ_{dec} (Fig. 8). Changes in τ_{dep} do not affect Φ_V (Fig. 10-A4 and S5). Changes in τ and τ_{dec} affect Φ_V in the same direction as in the absence of STP (Figs. 10-B4, -A4, S6 and S7). Consistently with the previous findings, changes in G_{syn} do not affect Φ_V.

Figs. S5-S7 extend our results for additional parameter combinations. Figs. S5-S7 (left column), in particular, illustrate how the balances between the depression LPFs and peak summation HPFs shape the V_{peak} profiles for additional parameter regimes.

3.9 Interplay of synaptic facilitation (HPFs) and PSP summation filters: V_{peak} LPFs and Γ_V BPFs

The presence of short-term facilitation generates S_{peak} HPFs that become sharper and more amplified as τ_{fac} increases (Fig. 11-A3) and are independent of τ, τ_{dec} and G_{syn} (Fig. 11-B3 to -D3)

3.9.1 Modulation of V_{peak} HPFs: interplay of facilitation and PSP summation HPFs

In the absence of STP, the V_{peak} HPF is controlled by the membrane time constant τ (Fig. 8-B1) and the synaptic decay time constant τ_{dec} (Fig. 8-C1). Here we focus on the effects of synaptic facilitation (τ_{fac}) and the interplay between the three time constants in the modulation of V_{peak}. Increasing values of τ_{fac} cause an amplification of the S_{peak} profiles (Fig. 11-A3) and therefore an amplification of the V_{peak} profiles (Fig. 11-A1). Increasing values of τ_{dec} and G_{syn} increase I_{syn} in a frequency-dependent manner, and therefore they also amplify the V_{peak} profiles (Fig. 11-C1 and -D1). Finally, consistently with our findings in Fig. 7-A, increasing values of τ also amplify the V_{peak} profiles.

3.9.2 Emergence of Γ_V resonance (BPFs): interplay of a facilitation HPF and a PSP amplitude LPF

The presence of short-term facilitation generates S_{peak} HPFs that become sharper and more amplified as τ_{fac} increases (Fig. 11-A3). The interaction between these filters and the PSP amplitude LPFs (Fig. 8-A1, light-blue) produces BPFs (Fig. 10-A2). We refer to this preferred frequency PSP amplitude response to periodic presynaptic inputs as (PSP) Γ_V resonance. Similarly to other resonances, Γ_V resonance reflects balances between the two participating process. As τ_{fac} increases, the Γ_V profiles are more dominated by facilitation and therefore the Γ_V profiles are amplified as the Γ_V resonant frequency decreases (Fig. 11-A2).

As τ increases, the STP-independent Γ_V LPFs are amplified and sharpened (Fig. 8-B1). Therefore, increasing values of τ amplify the Γ_V BPFs and shift the resonant frequency to lower values (Fig. 10-B2). Similarly, increasing values of τ_{dec}, which sharpen the STP-independent Γ_V LPFs (Fig. 8-C1), shift the facilitation-induced Γ_V resonant frequency to lower values and amplifies the Γ_V BPFs within certain range of values of τ (Fig. 11-C2). Increasing values of G_{syn} in contrast amplify the Γ_V profile with a much lesser effect on the Γ_V resonant frequency (Fig. 11-D2)

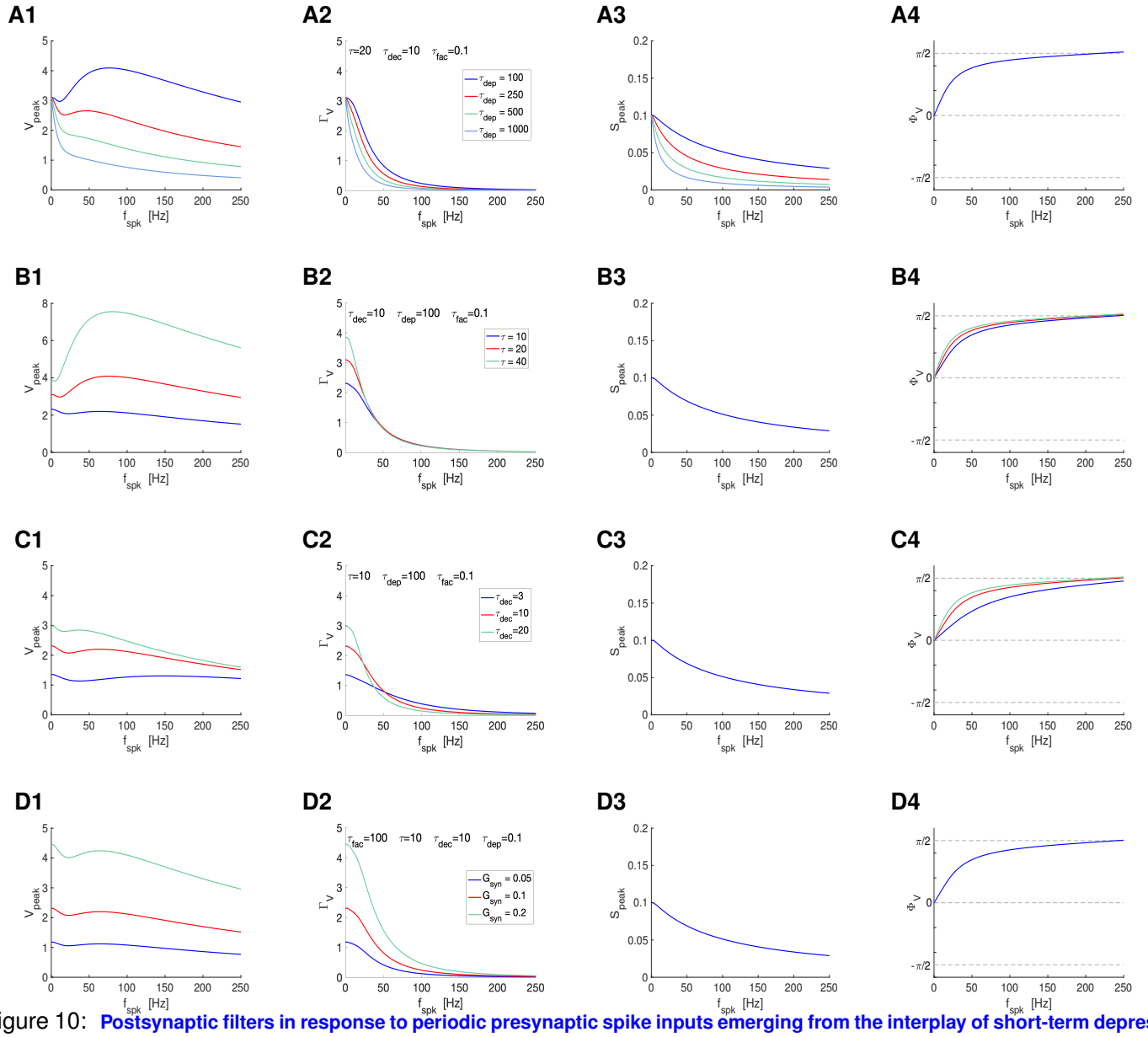

Figure 10: **Postsynaptic filters in response to periodic presynaptic spike inputs emerging from the interplay of short-term depression and postsynaptic summation. A.** Superimposed filters for various values of the short-term depression time constant τ_{dep} and representative parameter values: $\tau = 10$, $\tau_{dec} = 10$ and $\tau_{fac} = 0.1$. Fig. S5 extends these results for additional values of τ. The Φ_V profiles are independent of τ_{dep}. **B.** Superimposed filters for various values of the postsynaptic membrane time constant τ and representative parameter values: $\tau_{dec} = 10$, $\tau_{dep} = 100$ and $\tau_{fac} = 0.1$. Fig. S6 extends these results for additional values of τ_{dep}. The S_{peak} profiles are independent of τ_{dep}. **C.** Superimposed filters for various values of the synaptic decay time τ_{dec} and representative parameter values: $\tau = 10$, $\tau_{dep} = 100$ and $\tau_{fac} = 0.1$. The S_{peak} profiles are independent of τ_{dep}. Fig. S7 extends these results for additional values of τ_{dep}. **D.** Superimposed filters for representative values of the synaptic decay time constant G_{syn} and representative parameer values: $\tau_{fac} = 100$, $\tau = 10$, $\tau_{dec} = 10$ and $\tau_{dep} = 0.1$. Fig. S10 extends these results for additional values of τ_{fac}. The S_{peak} and Φ_V profiles are independent of G_{syn}. **Left column.** V peak profiles. **Middle-left column.** V peak-to-trough amplitude profiles. **Middle-right column.** S peak profiles. **Right column.** V phase profiles. We used eq. (64) for the PSP V with I_{syn} described by eqs. (2)-(4) appropriately adapted to account for the translation of V to the equilibrium point, and STP described by eqs. (12) and (13) (DA model). The impedance amplitude (Z) and phase (Φ_Z) were computed using eqs. (36) and (37). The analytical approximations for the PSP peak sequence response of passive cells to presynaptic inputs are described in Section2.2 (see also Appendix A). The approximation of $V_{peak,n}$, $V_{trough,n}$ and $t_{V,peak}$ were computed as described in Section 3.4. The PSP amplitude Γ_V was computed by using eq. (65) and the PSP phase Φ_V was computed using eq. (66). The synaptic (S) peak (S_{peak}) and phase (Φ_S) profiles were computed similarly to these for V. We used the following additional parameter values: $C = 1$, $E_L = -60$, $I_{app} = 0$, $G_{syn} = 0.1$, $E_{syn} = 0$, $a_d = 0.1$, $a_f = 0.1$, $x_\infty = 1$, $z_\infty = 0$ and $T_{sw} = 1$.

3.9.3 Modulation of the Φ_V

In the absence of STP, the Φ_V profile is controlled by τ and τ_{dec} (Fig. 8). Similarly to our findings in the previous section, changes in τ_{fac} do not affect Φ_V (Fig. 11-A4 and S8). Changes in τ and τ_{dec} affect Φ_V in the same direction as in the absence of STP (Figs. 11-B4, -A4, S9 and S10). Consistently with the previous findings, changes in G_{syn} do not affect Φ_V (Fig. 11-D4).

Figs. S8-S10 extend our results for additional parameter combinations. Figs. S8-S10 (middle-left column), in particular, illustrate how the balances between the facilitation HPFs and amplitude LPFs shape the Γ_V profiles for additional parameter regimes.

3.10 Interplay of synaptic depression (LPFs), synaptic facilitation (HPFs) and PSP summation filters: V_{peak} and Γ_V BPFs

The presence of short-term depression and facilitation generates S_{peak} BPFs (synaptic resonance) that become sharper as τ_{dep} and τ_{fac} increase (Fig. 12-A3). This is accompanied by a decrease in the synaptic resonance frequency. The S_{peak} BPFs are independent of τ, τ_{dec} and G_{syn} (Fig. 12-B3 to -D3). As discussed above, for small enough values of τ_{dec} and τ, the S_{peak} profiles are inherited to the postsynaptic level and therefore the PSP V_{peak} and Γ_V profiles are almost identical, and are almost proportional to the S_{peak} profiles (not shown). For larger values of τ_{dec} and τ, the PSP V_{peak} and Γ_V profiles are modulated by the PSP membrane properties and the summation HPF.

3.10.1 Modulation of V_{peak} BPFs

Earlier studies modeled the PSP response of cells to periodic presynaptic spike inputs (V_{peak} profiles) in the presence of STP to be proportional to the S_{peak} profiles [28, 46, 92]. For larger, more realistic values of τ and τ_{dec} the V_{peak} profiles are wider than the S_{peak} profiles (compare Figs. 12-A1 and -A3) and the V_{peak} resonant frequency is larger than the S_{peak} resonant frequency. The V_{peak} profiles are amplified by decreasing values of τ_{dep} and τ_{fac}. The amplification is stronger as τ increases (Fig. S11, column 1). The V_{peak} amplification is accompanied by an increase in the V_{peak} resonant frequency as τ_{dep} and τ_{fac} decrease. The V_{peak} profiles are also amplified by increasing values of τ, τ_{dec} and G_{syn} (Figs. 12, column 1). Increasing values of τ and τ_{dec} cause an increase in the V_{peak} resonant frequency (Figs. 12-B1 and -C1, see also Figs. S12 and S13, column 1), but the V_{peak} resonant frequency is at most slightly affected by increasing values of G_{syn} (Figs. 12-D1).

3.10.2 Modulation of Γ_V BPFs

The Γ_V profiles are amplified and sharpened by increasing values of τ_{dep} and τ_{fac} (Fig. 12-A2). This is more pronounced as τ increases (Fig. S11, column 2). This is accompanied by a decrease in the Γ_V resonant frequency. The Γ_V profiles are also amplified by increasing values of τ, τ_{dec} and G_{syn}. In the former two cases they are also sharpened.

3.10.3 Modulation of the Φ_V

In the absence of STP, the Φ_V profile is controlled by τ and τ_{dec} (Fig. 8). Consistent with our findings in the previous two sections, changes in τ_{dep} and τ_{fac} do not affect Φ_V (Fig. 12-A4 and S11). Changes in τ and τ_{dec} affect Φ_V in the same direction as in the absence of STP (Figs. 12-B4, -A4, S11 and S12). Consistent with the previous findings, changes in G_{syn} do not affect Φ_V (Figs. 12-D4)

Figs. S11-S13 extend our results for additional parameter combinations.

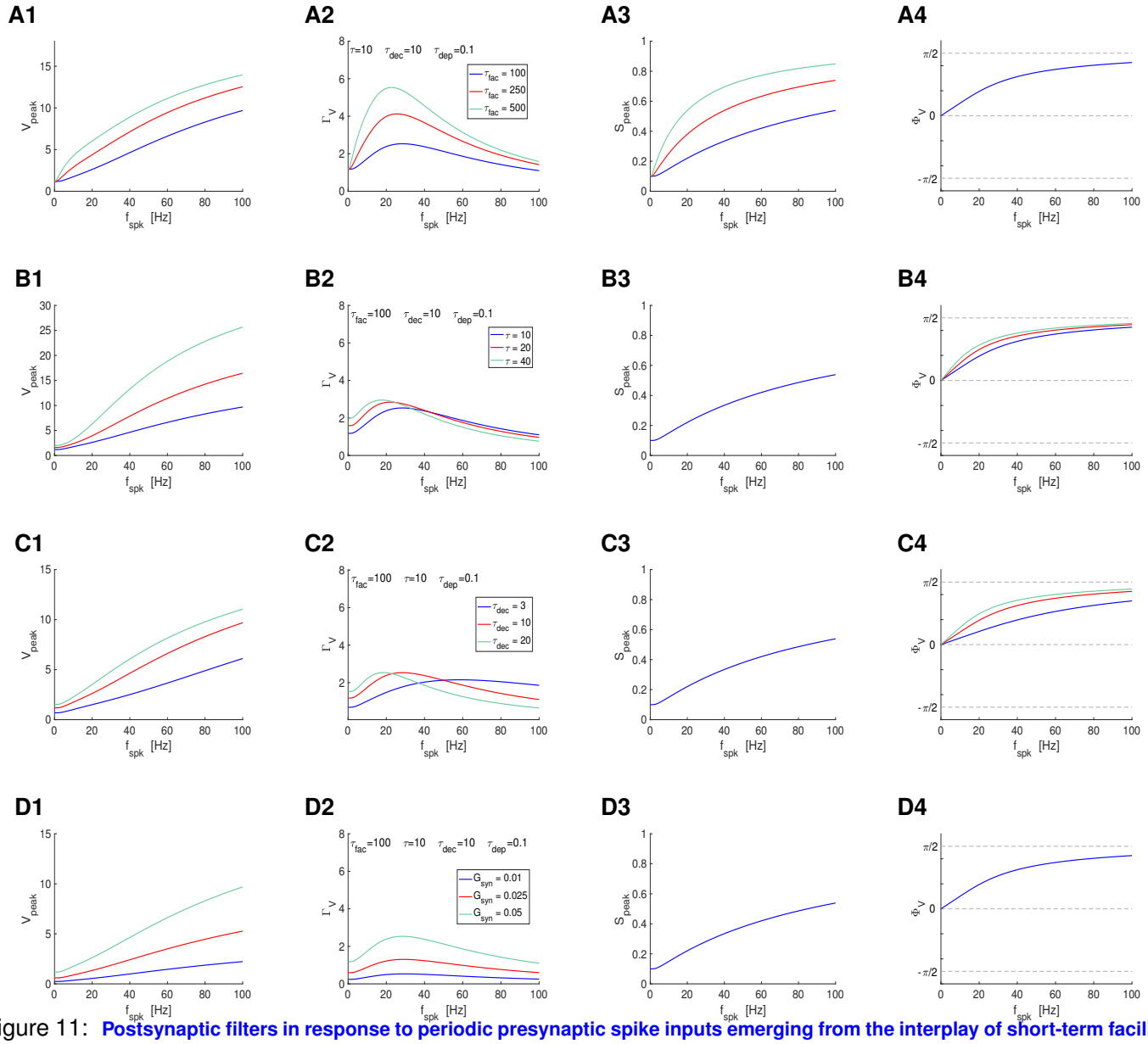

Figure 11: **Postsynaptic filters in response to periodic presynaptic spike inputs emerging from the interplay of short-term facilitation and postsynaptic summation. A.** Superimposed filters for various values of the short-term depression time constant τ_{fac} and representative parameter values: $\tau = 10$, $\tau_{dec} = 10$ and $\tau_{dep} = 0.1$. Fig. S8 extends these results for additional values of τ. The Φ_V profiles are independent of τ_{fac}. **B.** Superimposed filters for various values of the membrane time constant τ and representative parameter values: $\tau_{fac} = 100$, $\tau_{dec} = 10$ and $\tau_{dep} = 0.1$. Fig. S9 extends these results for additional values of τ_{fac}. The S_{peak} profiles are independent of τ. **C.** Superimposed filters for representative values of the synaptic decay time constant τ_{dec} and representative parameer values: $\tau_{fac} = 100$, $\tau = 10$ and $\tau_{dep} = 0.1$. Fig. S10 extends these results for additional values of τ_{fac}. The S_{peak} profiles are independent of τ_{dec}. **D.** Superimposed filters for representative values of the synaptic decay time constant G_{syn} and representative parameer values: $\tau_{fac} = 100$, $\tau = 10$, $\tau_{dec} = 10$ and $\tau_{dep} = 0.1$. Fig. S10 extends these results for additional values of τ_{fac}. The S_{peak} and Φ_V profiles are independent of G_{syn}. **Left column.** V peak profiles. **Middle-left column.** V peak-to-trough amplitude profiles. **Middle-right column.** S peak profiles. **Right column.** V phase profiles. We used eq. (64) for the PSP V with I_{syn} described by eqs. (2)-(4) appropriately adapted to account for the translation of V to the equilibrium point, and STP described by eqs. (12) and (13) (DA model). The impedance amplitude (Z) and phase (Φ_Z) were computed using eqs. (36) and (37). The analytical approximations for the PSP peak sequence response of passive cells to presynaptic inputs are described in Section2.2 (see also Appendix A). The approximation of $V_{peak,n}$, $V_{trough,n}$ and $t_{V,peak}$ were computed as described in Section 3.4. The PSP amplitude Γ_V was computed by using eq. (65) and the PSP phase Φ_V was computed using eq. (66). The synaptic (S) peak (S_{peak}) and phase (Φ_S) profiles were computed similarly to these for V. We used the following additional parameter values: $C = 1$, $E_L = -60$, $I_{app} = 0$, $G_{syn} = 0.05$, $E_{syn} = 0$, $a_d = 0.1$, $a_f = 0.1$, $x_\infty = 1$, $z_\infty = 0$ and $T_{sw} = 1$.

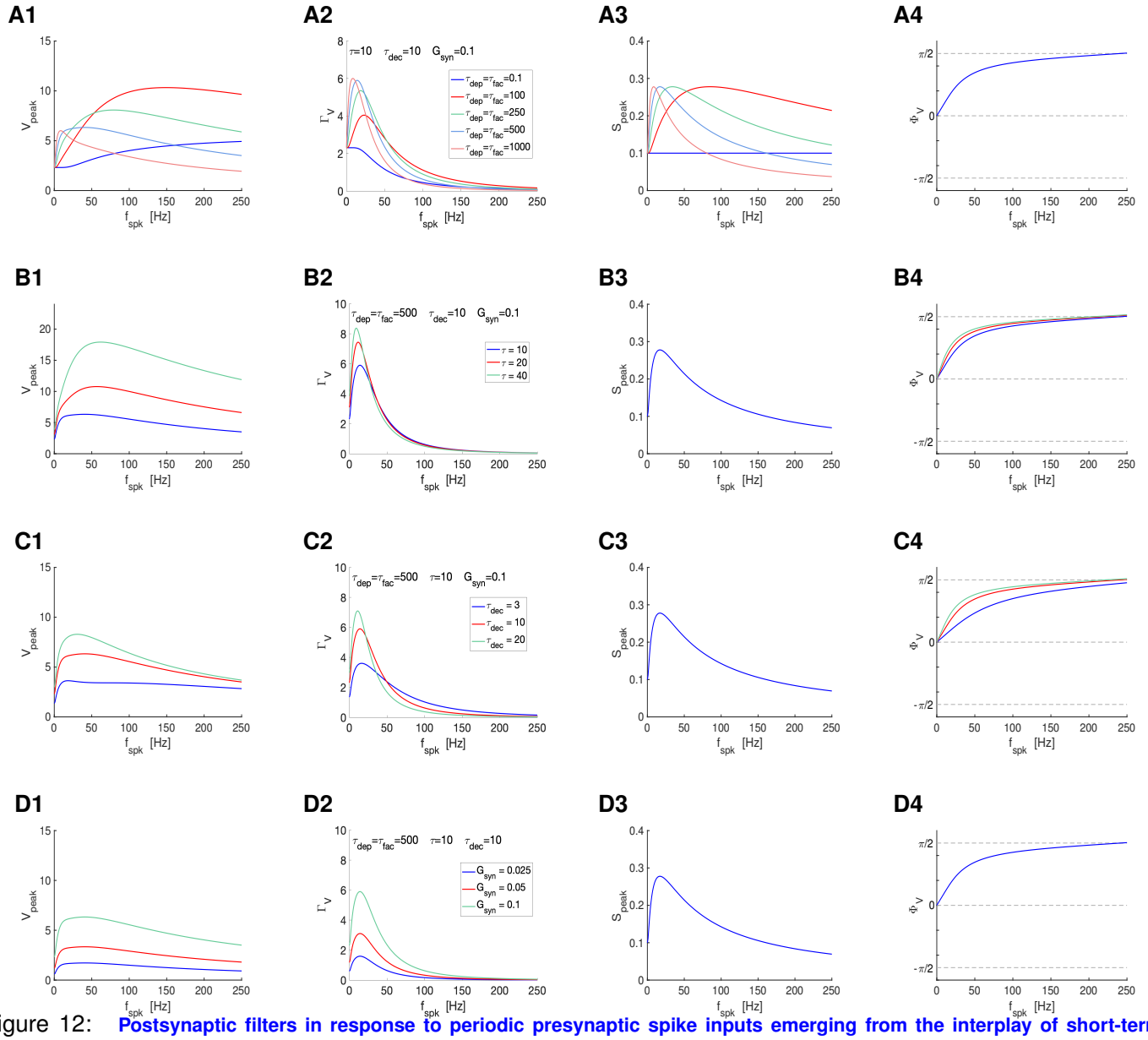

Figure 12: **Postsynaptic filters in response to periodic presynaptic spike inputs emerging from the interplay of short-term depression, facilitation and postsynaptic summation. A.** Superimposed filters for representative values of the depression and facilitation time constants τ_{dep} and τ_{fac}, respectively, and representative parameter values: $\tau = 10$, $\tau_{dec} = 10$ and $G_{syn} = 0.1$. Fig. S11 extends these results for additional values of τ. The Φ_V profiles are independent of τ_{dep} and τ_{fac}. **B.** Superimposed filters for representative values of the depression membrane time constant τ and representative parameter values: $\tau_{dep} = 500$, $\tau_{fac} = 500$, $\tau_{dec} = 10$ and $G_{syn} = 0.1$. Fig. S12 extends these results for additional values of τ. The S_{peak} profiles are independent of τ. **C.** Superimposed filters for representative values of the depression synaptic decay time τ_{dec} and representative parameter values: $\tau_{dep} = 500$, $\tau_{fac} = 500$, $\tau = 10$ and $G_{syn} = 0.1$. Fig. S13 extends these results for additional values of τ. The S_{peak} profiles are independent of τ. **D.** Superimposed filters for representative values of the synaptic decay time constant G_{syn} and representative parameer values: $\tau_{dep} = \tau_{fac} = 500$, $\tau = 10$, $\tau_{dec} = 10$. Fig. S10 extends these results fo **Left column.** V peak profiles. **Middle-left column.** V peak-to-trough amplitude profiles. **Middle-right column.** S peak profiles. **Right column.** V phase profiles. We used eq. (64) for the PSP V with I_{syn} described by eqs. (2)-(4) appropriately adapted to account for the translation of V to the equilibrium point, and STP described by eqs. (12) and (13) (DA model). The impedance amplitude (Z) and phase (Φ_Z) were computed using eqs. (36) and (37). The analytical approximations for the PSP peak sequence response of passive cells to presynaptic inputs are described in Section 2.2 (see also Appendix A). The approximation of $V_{peak,n}$, $V_{trough,n}$ and $t_{V,peak}$ were computed as described in Section 3.4. The PSP amplitude Γ_V was computed by using eq. (65) and the PSP phase Φ_V was computed using eq. (66). The synaptic (S) peak (S_{peak}) and phase (Φ_S) profiles were computed similarly to these for V. We used the following additional parameter values: $C = 1$, $E_L = -60$, $I_{app} = 0$, $E_{syn} = 0$, $a_d = 0.1$, $a_f = 0.1$, $x_\infty = 1$, $z_\infty = 0$ and $T_{sw} = 1$.

3.11 Persistence and modulation of STP-mediated PSP V_{peak} and Γ_V BPFs in response to randomly-distributed spike trains

In the previous sections we used periodic presynaptic inputs over a range of spiking frequencies to describe a number of mechanisms of generation of STP-mediated PSP V_{peak} and Γ_V BPFs both inherited from S level of organization (S_{peak} BPFs) and generated across levels of organization.The question arises whether PSP V_{peak} and Γ_V filters emerge in more general scenarios, in response to more realistic presynaptic spike trains having some frequency content, what are their properties, and how they are affected by the input variability (how they are related to the classical filters in response to periodic inputs). We address these questions by using two types of presynaptic spike inputs: jittered-periodic spike trains [44] and Poisson-distributed spike trains [85, 98].

3.11.1 PSP V_{peak} and Γ_V BPFs persist in response to randomly perturbed periodic spike trains

Following [44], we consider perturbations of periodic presynaptic spiking patterns with ISIs of the form 75 for $n = 1, \ldots, N_{spk}$, where Δ_{spk} is constant (n-independent) and $\delta_p = \{\delta_{spk,n}\}_{n=1}^{N_{spk}}$ is a random variable with zero mean and variance equal to $\delta\,\Delta_{spk}$ for a non-negative real number δ.

Fig. 13-A illustrates that PSP V_{peak} and Γ_V filters discussed above persist in response to the jittered-periodic presynaptic spike trains. The solid curves correspond to the mean value for each attribute (V_{peak}, V_{trough}, S_{peak} and Γ_V) and the dashed-gray curves correspond to the classical, unperturbed filters. Fig. 13-A illustrates that these two quantities almost coincide. This also occurs for the X_{peak}, Z_{peak} and ΔS_{peak} filters (Fig. S16). The variability of the filters is larger for V_{peak} and V_{trough} than for the other filters, and is frequency-dependent (compare the shadow regions for each filter across frequencies) and STP-dependent (compare the shadow regions for each input frequency across values of τ_{dep} and τ_{fac}).

3.11.2 PSP V_{peak} and Γ_V BPFs persist in response to Poisson-distributed spike trains and are modulated by them

We use Poisson-distributed spike trains with stationary mean firing rates ($< f_{spk} >$) within the same range as the spiking input frequencies used above. For comparison with the previously discussed cases, we identify the mean firing rate with the spiking frequency f_{spk} from which it originates.

Fig. 14-A illustrates that PSP V_{peak} and Γ_V filters persists in response to Poisson-distributed presynaptic inputs, but the perturbations from the classical filters (in response to periodic inputs) are more prominent than in the case discussed above (the solid and dashed curves do not coincide and they are significantly further apart). As expected, the response variability to Poisson inputs is larger than for jittered-periodic inputs (compare the shadow regiones in Figs. 13-A and 14-A and Figs. S16-A and S17-A). Similarly to the filters discussed above, the variability is larger for the V_{peak} and V_{trough} filters than for the other filters, is frequency-dependent (compare the shadow regions for each filter across frequencies), and STP-dependent (compare the shadow regiones for each input frequency across values of τ_{dep} and τ_{fac}.

3.12 STP controls the variability PSP V_{peak} and Γ_V BPFs in response to randomly-distributed spike trains

A salient feature of the frequency filters presented in Figs. 13-A and 14-A is the dependence of the response variability (shadow regions), not only with the mean input frequency (or rate), but also with the time constants controlling the short-term depression and facilitation processes (for the same input frequencies).

We quantified these dependencies in Figs. 13- and 14-B, -C and D for values of $\tau_{dep} = \tau_{fac}$ within a representative range for the V_{peak} and V_{trough} profiles. For each value of $\tau_{dep} = \tau_{fac}$ we computed the average variance for each profile (across input frequencies). We obtained similar results by using the maximal variance for each profile.

In all cases, the variability first increases as $\tau_{dep} = \tau_{fac}$ increase for relative small values of these parameters, and then it decreases as $\tau_{dep} = \tau_{fac}$ continues to increase. For each set of time constants (τ_{dec} and τ), there is a value

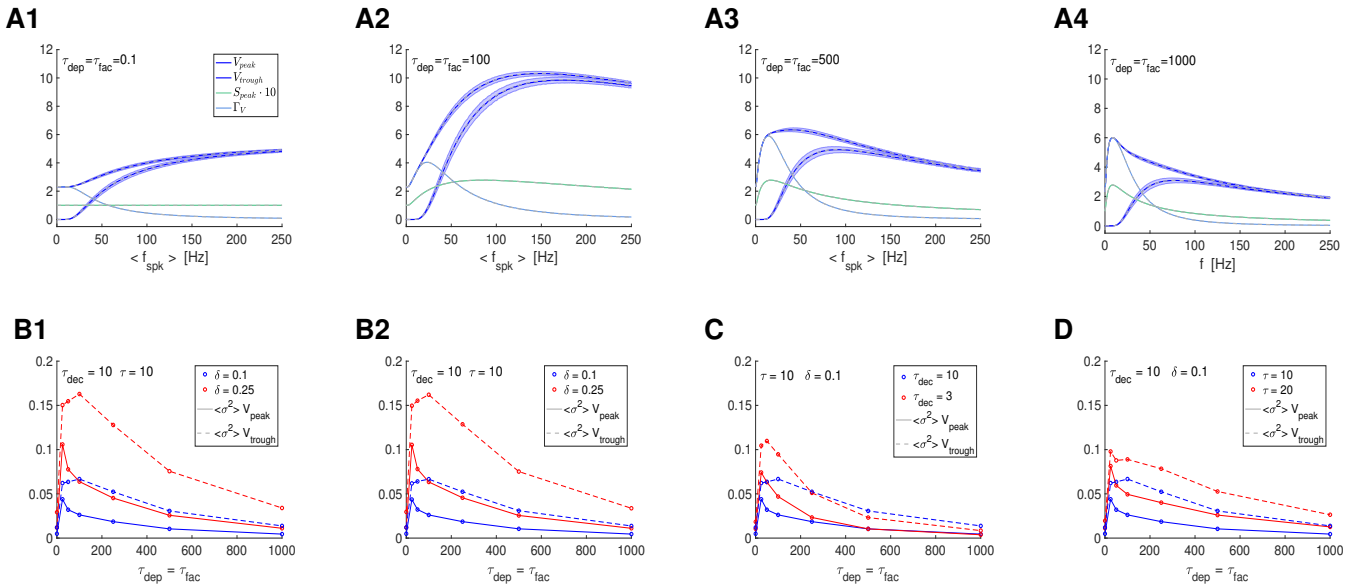

Figure 13: **Postsynaptic filters in response to jittered (randomly perturbed) periodic presynaptic inputs in the presence of STP: frequency- and STP-dependent variability.** For each value of the mean presynaptic input frequency $< f_{spk} >$, the ISI sequence $\{\Delta_{spk,n}\}$ $(n = 1, \ldots, N_{spk})$ has the form $\Delta_{spk,n} = \Delta_{spk} + \delta_{spk,n}$ where Δ_{spk} is the ISI corresponding to f_{spk} ($f_{spk} = 1000/\Delta_{spk}$) and the sequence $\{\delta_{spk,n}\}$ are drawn from a normal distribution with zero mean and variance equal to $\delta\,\Delta_{spk}$. **A.** Superimposed V_{peak}, V_{trough}, S_{peak} and Γ_V profiles for representative parameter values. We used $\tau_{dec} = 10$ and $\tau = 10$ in all panels. Solid curves correspond to the mean values for each attribute (V_{peak}, V_{trough}, S_{peak} and Γ_V). The shadow regions (V_{peak}, V_{trough} and S_{peak} correspond to one standard deviation from the mean. The dashed gray curves, almost coinciding with the solid curves, represent the corresponding deterministic profiles (response to periodic spike train inputs with frequency f_{spk}). **A1.** $\tau_{dep} = \tau_{fac} = 0.1$. **A2.** $\tau_{dep} = \tau_{fac} = 100$. **A3.** $\tau_{dep} = \tau_{fac} = 500$. **A4.** $\tau_{dep} = \tau_{fac} = 1000$. **B.** Averaged variances for the V_{peak} (solid) and V_{trough} (dashed) profiles as a function of $\tau_{dep} = \tau_{fac}$ for representative parameter values. The average variance for each profile was computed by averaging the corresponding response variances across all values of $< f_{spk} >$. **B.** Increasing the input variability (δ) increases the response variability. Panels B1 and B2 show two realizations for the same parameter values. We used $\tau = 10$ and $\tau_{dec} = 10$. **C.** Decreasing the synaptic decay time τ_{dec} causes an increase in the response variability. We used $\tau = 10$ and $\delta = 0.1$. **D.** Increasing the membrane potential time constant causes an increase in the response variability. We used $\tau_{dec} = 10$ and $\delta = 0.1$. We used the following additional parameter values: $C = 1$, $E_L = -60$, $I_{app} = 0$, $E_{syn} = 0$, $a_d = 0.1$, $a_f = 0.1$, $x_\infty = 1$, $z_\infty = 0$ and $T_{sw} = 1$.

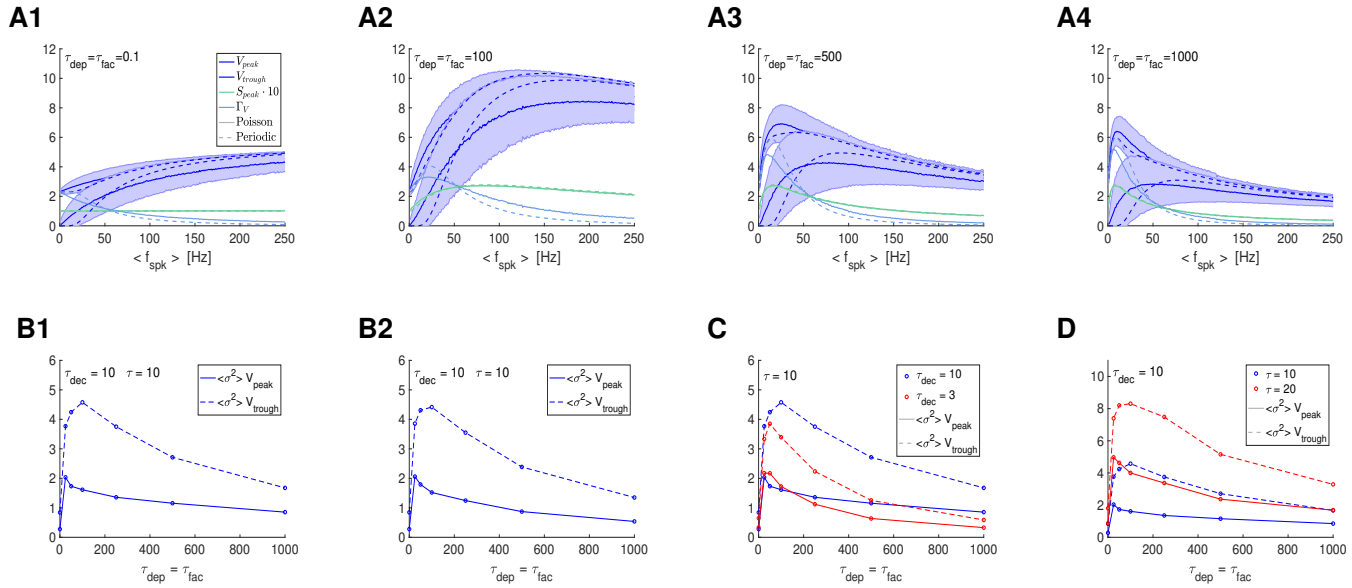

Figure 14: **Postsynaptic filters in response to Poisson-distributed presynaptic inputs in the presence of STP: frequency- and STP-dependent variability.** The mean rate of the Poisson distributed spike trains corresponds to $< f_{spk} >$. **A.** Superimposed V_{peak}, V_{trough}, S_{peak} and Γ_V profiles for representative parameter values. We used $\tau_{dec} = 10$ and $\tau = 10$ in all panels. Solid curves correspond to the mean values for each attribute (V_{peak}, V_{trough}, S_{peak} and Γ_V). The shadow regions (V_{peak}, V_{trough} and S_{peak} correspond to one standard deviation from the mean. The dashed curves represent the corresponding deterministic profiles (response to periodic spike train inputs with frequency f_{spk}). **A1.** $\tau_{dep} = \tau_{fac} = 0.1$. **A2.** $\tau_{dep} = \tau_{fac} = 100$. **A3.** $\tau_{dep} = \tau_{fac} = 500$. **A4.** $\tau_{dep} = \tau_{fac} = 1000$. **B.** Averaged variances for the V_{peak} (solid) and V_{trough} (dashed) profiles as a function of $\tau_{dep} = \tau_{fac}$ for representative parameter values. The average variance for each profile was computed by averaging the corresponding response variances across all values of $< f_{spk} >$. **B.** Two realizations for the same parameter values. We used $\tau = 10$ and $\tau_{dec} = 10$. **C.** Decreasing the synaptic decay time τ_{dec} causes a decrease in the response variability for large values of $< f_{spk} >$ and an increase in the response variability for (very) small values of f_{spk}. We used $\tau = 10$ and $\delta = 0.1$. **D.** Increasing the membrane potential time constant causes an increase in the response variability. We used $\tau_{dec} = 10$ and $\delta = 0.1$. We used the following additional parameter values: $C = 1$, $E_L = -60$, $I_{app} = 0$, $E_{syn} = 0$, $a_d = 0.1$, $a_f = 0.1$, $x_\infty = 1$, $z_\infty = 0$ and $T_{sw} = 1$.

of $\tau_{dep} = \tau_{fac}$ for which the variability is maximal. As expected, for the jittered periodic inputs the profiles' variability increases as the input variability increases (Figs. 13- B). The profiles' variability also increases as τ_{dec} decreases (Figs. 13- C) and τ increases (Figs. 13- D). For the Poisson-distributed inputs, in contrast, the profiles' variability decreases with decreasing values of τ_{dec} (Fig. 14-C), while it increases for increasing values of τ (Fig. 14-D).

Together, these results and the results of the previous section show that STP plays important roles not only in determining the patterns exhibit by networks, but also their robustness and accuracy of the information transmission.

4 Discussion

We set out to understand the dynamic mechanisms of generation of neuronal PSP filters, particularly how they are shaped by the time scales associated with the participating building blocks: the synaptic raise and decay dynamics (τ_{rse} and τ_{dec}), the synaptic STP time constants (τ_{dep} and τ_{fac}), and the intrinsic time constant (τ) of the postsynaptic cells (Fig. 1). To this end, we conducted a systematic study of the steady-state PSP response to (i) periodic presynaptic inputs over a range of frequencies $f_{spk} = 1000/\Delta_{spk}$ (Fig. 1, left), (ii) jittered periodic inputs with mean frequency $f_{spk} = 1000/\Delta_{spk}$, and (iii) Poisson-distributed presynaptic inputs with mean rate $r_{spk} = 1000/ < \Delta_{spk} >$ (Fig. 1, right). We used mathematical modeling, analytical calculations and numerical simulations. The use of periodic presynaptic spikes allowed us to systematically understand how frequency-filters are shaped by the time scales of the participating building blocks and how the filtering properties are communicated across levels of neuronal organization and modified along the process biophysical properties of the network component. The use of Poisson-distributed presynaptic spikes trains allowed us to validate some of the ideas developed for periodic presynaptic spike-trains by using more realistic inputs, to understand the similarities and differences between the more realistic responses and the responses the "clean" frequency-filters, and to understand how the variability of the filtering properties is controlled by the biophysical properties of the participating building blocks, primarily STP. The jittered inputs were used as an intermediate step to link between the purely deterministic and stochastic spike-train inputs.

We developed an analytical approximation of the membrane potential response of passive cells to presynaptic spike trains in the presence of STP. This allowed us to compute the peak (V_{peak}) and peak-to-trough amplitude (Γ_V) filters in terms of the participating time constants and other model parameters. The goal of this approach was to have an analytical expression to better understand the dependence of the PSP filters on the model parameters. This came at the expense of some simplifying assumptions that transform the multiplicative synaptic input to the passive membrane equation into an additive input. The resulting expressions make the contribution of the time constants and other parameters to the PSP filters's shape apparent. Because the passive membrane equation is linear, it is analytically solvable by other tools (e.g., Laplace transforms). However, the exact analytical solution provides little analytical clarity on how the model parameters shape the PSP filters. In fact, eqs. (21)-(23) can stand as a model of their own [99]. This approach can be extended to more complex scenarios. For example, it can be extended to networks where the presynaptic or postsynaptic cells are described by more complex linearized models involving additional ionic currents and weakly nonlinear models [100].

The role of STP on information filtering and related phenomena has been investigated before by many authors [3, 8–10, 16, 22, 24, 26–43, 46–51]. However, previous studies have not focused on the mechanisms of generation of postsynaptic frequency-filters and how they are shaped by the participating time scales. Previous work has also ignored the mechanisms governing the variability of the response to realistic presynaptic spike-train inputs. Because the synaptic response S is not directly measurable, a common simplifying assumption has been made by some authors [28,46,47,49]: that the voltage response of the postsynaptic cell is a scaled version of the synaptic response. While this assumption might be justified in many cases, our results indicate that it is by no mean universally expected, and there could be significant qualitative differences between the synaptic and postsynaptic frequency-filters. This was also highlighted in previous work on temporal filters in the presence of STP [44].

To address these issues, we divided our study in three steps, by investigating the response profiles (frequency-filters) of (i) synaptic update ΔS to the presynaptic spike trains, (ii) the synaptic variable S to ΔS, and (iii) the postsynaptic membrane potential V to S. We characterized the frequency-filters by using the (stationary) peak profiles (for $\bar{\Delta S}$, $\bar{S}$ and $\bar{V}$) and the (stationary) peak-to-trough amplitude profiles (for $\bar{S}$ and $\bar{V}$). By design, the effects of STP are present at the ΔS level giving rise to the synaptic update sequences $\Delta S_n = X_n Z_n$, which depend on

the time constants τ_{dep} and τ_{fac}. These are the target of the synaptic variables S during the raise phase immediately after the arrival of each presynaptic spike. The S frequency-filters are shaped by $\Delta S_n = X_n Z_n$ and the synaptic time constantes τ_{rse} and τ_{dec}. In turn, the synaptic variable S is the input to the current-balance equation describing the dynamics of the passive cell. The postsynaptic (V-) frequency-filters result from the interaction between S and the biophysical properties of the postsynaptic passive cell, particularly the time constant $\tau = C/G_L$.

Consistently with previous work, [3,21,28,46,47,49], $\bar{\Delta}S$ BPFs are generated by the interplay of low-pass (depression) and high-pass (facilitation) filters for the appropriate balances between the two processes. They are amplified by increasing values of τ_{fac} and the $\bar{\Delta}S$ resonant frequency decreases as τ_{fac} increases. The $\bar{X}$, $\bar{Z}$ and $\bar{\Delta}S$ profiles develop in response to multiple events, each controlled by the time constants τ_{dep} and τ_{fac}. We described the (global in time) filter properties in terms of the characteristic frequencies σ_{dep} ($\bar{X}$), σ_{fac} ($\bar{Z}$), and the characteristic frequency difference $\Delta_{kappa} = \kappa_{rse}$ and κ_{dec} ($\bar{\Delta S}$). These depend on τ_{dep} and τ_{fac} in a nonlinear manner. Increasing values of τ_{fac} and τ_{dep} cause σ_{fac} and σ_{dep}, respectively, to decrease (sharpen the $\bar{X}$, $\bar{Z}$ filters, respectively). Increasing values of τ_{fac} cause the $\bar{\Delta}S$ resonant frequency to decrease, the $\bar{\Delta}S$ peak to increase and the $\bar{\Delta}S$ BPF to become sharper. Increasing values of τ_{dep} cause the $\bar{\Delta}S$ resonant frequency to decrease and the $\bar{\Delta}S$ BPF to become sharper, but cause the the $\bar{\Delta}S$ peak to decrease.

For the to-$\bar{\Delta S}$ update model with instantaneous S raise, the peak envelope profiles $\bar{S}$ are identical to the $\bar{\Delta S}$ profiles. The Γ_S BPFs can be inherited from $\bar{\Delta S}$ ones or can be created by the interplay of a $\bar{\Delta S}$ HPF and Q_A (a LPF). In all cases, they become sharper and less peakier as τ_{dec} increases. For the to-$\bar{\Delta S}$ update model with non instantaneous S raise, the $\bar{S}$ profiles are attenuated as τ_{rse} increases and the Γ_S profiles are also attenuated as τ_{rse} increases.

For the by-$\bar{\Delta S}$ update model with instantaneous S raise, in contrast to the to-$\bar{\Delta S}$ model, the Γ_S profiles are inherited from the $\bar{\Delta S}$ profiles. The $\bar{S}$ profiles transition from LPFs or BPFs to HPFs as τ_{dec} increases, which may be bounded or unbounded (if they are HPFs, they remain so). These models lack a biophysical mechanism that balances the summation effects and created realistically saturated profiles. For the by-$\bar{\Delta S}$ update model with non-instantaneous S raise, the $\bar{S}$ profiles are attenuated as τ_{rse} increases and the Γ_S profiles are also attenuated as τ_{rse} increases.

Passive cells generate LPFs in response to sinusoidal input currents. In response to periodic presynaptic inputs, in the absence of STP, they produce Γ_V LPFs , but V_{peak} HPFs due to the effects of the summation phenomenon. These filters are modulated by the synaptic time constant τ_{dec} and the postsynaptic time constant τ. In the presence of STP, V_{peak} and Γ_V BPFs are possible under certain conditions. We found two qualitatively different mechanisms. The V_{peak} and Γ_V BPFs can be either inherited from the synaptic level, subject to the appropriate modifications, or generated across levels. Specifically, a V_{peak} BPF can be either result of an S_{peak} BPF generated as the result of synaptic depression and facilitation or the result of a S_{peak} LPF generated by the interplay of synaptic depression and PSP summation. Similarly, a Γ_V BPF can be the result of the interplay of synaptic facilitation and PSP summation. These types of BPFs persist in response to jitter periodic spike trains and Poisson-distributed spike trains with a frequency-dependent variability. Importantly, the variability properties of these BPFs are controlled by STP in a non-monotonic manner.

The feedforward network we studied (Fig. 1) is the simplest synaptic processing unit that can produce PSP BPFs involving STP. This allow us to systematically investigate the qualitatively different types of mechanisms of generation of PSP BPFs according to whether they are inherited from the synaptic level and generated across levels of organization. The same class of mechanisms could be present in feedforward networks exhibiting presynaptic BPFs in the absence of STP. Further research is needed to understand these mechanisms. Additional research is needed to understand how the various mechanisms interact and what new mechanisms are present in more complex networks including presynaptic BPFs, postsynaptic BPFs, STP, and possibly feedback connections. Finally, future work should focus on more complex, biophysically realistic models of STP where STP is determined by the combined effect of both pre- and post-synaptic factors [101] (see also [45, 46, 102]). As such, our study is the first step in the systematic understanding of the mechanisms of generation of neuronal filters in networks and contributes to the systematic understanding of information processing via neuronal filters.

Acknowledgments

HGR acknowledges support from the National Science Foundation grants DMS-1608077 and IOS-2002863. YM acknowledges support from the National Science Foundation Graduate Research Fellowship. The authors are grateful to Allen Tannenbaum for useful comments and support, and to Farzan Nadim, Dirk Bucher, Nelly Daur, Antoni Guillamon, Gema Huguet and Tomas Lázaro for useful comments and discussions. HGR is a Corresponding Investigator in CONICET, Argentina and a Graduate Faculty Member in the Behavioral Neurosciences Program at Rutgers University. HGR is also Visiting Researcher/Academic in the Neurosciences Institute and the Courant Institute of Mathematical Sciences at New York University.

Conflicts of Interest

The authors declare that they have no conflict of interest.

References

[1] B. Hutcheon and Y. Yarom. Resonance, oscillations and the intrinsic frequency preferences in neurons. *Trends Neurosci.*, 23:216–222, 2000.

[2] M. Tsodyks, A. Uziel, and H. Markram. Synchrony generation in recurrent networks with frequency-dependent synapses. *J. Neurosci.*, 20:1–5, 2000.

[3] E. M. Izhikevich, N. S. Desai, E. C. Walcott, and F. C. Hoppensteadt. Bursts as a unit of neural information: Selective communication via resonance. *Trends Neurosci.*, 26:161–167, 2003.

[4] E. Stark, A. Levi, and H. G. Rotstein. Neuronal resonance can be generated independently at distinct levels of organization. *PLoS Comp. Biol.*, 18:e1010364, 2022.

[5] J. Laudansky, B. Torben-Nielsen, I. Segev, and S. Shama. Spatially distributed dendritic resonance selectively filters synaptic input. *PLoS Comp. Biol.*, 8:e1003775, 2014.

[6] W. Maass. Searching for principles of brain computation. *Curr. Opin. Neurobiol.*, 11:81–92, 2016.

[7] M. Beiran and S. Ostojic. Contrasting the effects of adaptation and synaptic filtering on the timescales of dynamics in recurrent networks. *PLoS Comp. Biol.*, 15:e1006893, 2019.

[8] E. Fortune and G. Rose. Short-term plasticity as a temporal filter. *Trends Neurosci.*, 24:381–385, 2001.

[9] V. A. Klyachko and C. F. Stevens. Excitatory and feed-forward inhibitory hippocampal synapses work synergistically as an adaptive filter of natural spike trains. *PLoS Comp. Biol.*, 4:e207, 2006.

[10] A. Thomson. Presynaptic frequency- and pattern-dependent filtering. *J. Comp. Neurosci.*, 15:159–202, 2003.

[11] T. E. Akam and D. M. Kullmann. Oscillations and filtering networks support flexible routing of information. *Neuron*, 67:308–320, 2010.

[12] S. Blankenburg, W. Wu, B. Lindner, and S. Schreiber. Information filtering in resonant neurons. *J. Comp. Neurosci.*, 39:349–370, 2015.

[13] R. Rosenbaum, J. Rubin, and B. Doiron. Short term synaptic depression imposes a frequency dependent filter on synaptic information transfer. *PLoS Comp. Biol.*, 8:e1002557, 2012.

[14] N. Brunel, F. S. Chance, N. Fourcaud, and L. F. Abbott. Effects of synaptic noise and filtering on the frequency response of spiking neurons. *Phys. Rev. Lett.*, 86:2186–2189, 2001.

[15] D. Buonomano and W. Maass. State-dependent computations: spatiotemporal processing in cortical networks. *Nat. Rev. Neurosci.*, 10:113–125, 2009.

[16] J. E. Lisman. Bursts as a unit of neural information: making unreliable synapses reliable. *Trends Neurosci.*, 20:38–43, 1997.

[17] J. S. Sherfey, S. Ardid, J. Hass, M. E. Hasselmo, and N. J. Kopell. Flexible resonance in prefrontal networks with strong feedback inhibition. *PLoS Comp. Biol.*, 14:e1006357, 2018.

[18] E. Puil, B. Gimbarzevsky, and R. M. Miura. Quantification of membrane properties of trigeminal root ganglions in guinea pigs. *J. Neurophysiol.*, 55:995–1016, 1986.

[19] E. Puil, B. Gimbarzevsky, and R. M. Miura. Voltage dependence of membrane properties of trigeminal root ganglion neurons. *J. Neurophysiol.*, 58:66–86, 1987.

[20] R. Moreno-Bote and N. Parga. Role of synaptic filtering on the firing response of simple model neurons. *Phys. Rev. Lett.*, 92:028102, 2004.

[21] J. D. Drover, V. Tohidi, A. Bose, and F. Nadim. Combining synaptic and cellular resonance in a feedforward neuronal network. *Neurocomputing*, 70:2041–2045, 2007.

[22] A. A. George, A. M. Lyons-Warren, X. Ma, and B. A. Carlson. A diversity of synaptic filters are created by temporal summation of excitation and inhibition. *J. Neurosci.*, 31:14721–14734, 2011.

[23] R. S. Zucker. Short-term synaptic plasticity. *Annu. Rev. Neurosci.*, 12:13–31, 1989.

[24] R. S. Zucker and W. G. Regehr. Short-term synaptic plasticity. *Annu. Rev. Physiol.*, 64:355–405, 2002.

[25] C. Stevens and Y. Wang. Facilitation and depression at single central synapses. *Neuron*, 14:795–802, 1995.

[26] J. S. Dittman, A. C. Kreitzer, and W. G. Regehr. Interplay between facilitation, depression, and residual calcium at three presynaptic terminals. *J. Neurosci.*, 20:1374–1385, 2000.

[27] G. Silberberg, C. Wu, and H. Markram. Synaptic dynamics control the timing of neuronal excitation in the activated neocortical microcircuit. *J. Physiol.*, 556:19–27, 2004.

[28] H. Markram, A. Gupta, A. Uziel, Y. Wang, and M. Tsodyks. Information processing with frequency-dependent synaptic connections. *Neurobiology of Learning and Memory*, 70:101–112, 1998.

[29] E. Fortune and G. Rose. Short-term synaptic plasticity contributes to the temporal filtering of electrosensory information. *J. Neurosci.*, 20:7122–7130, 2000.

[30] E. Fortune and G. Rose. Passive and active membrane properties contribute to the temporal filtering properties of midbrain neurons in vivo. *J. Neurosci.*, 17:3815–3825, 1997.

[31] E. Fortune and G. Rose. Temporal filtering properties of ampullary electrosensory neurons in the torus semicircularis of eigenmannia: evolutionary and computational implications. *Brain Behav Evol*, 49:312–323, 1997.

[32] E. Fortune and G. Rose. Roles of short-term plasticity in behavior. *J Physiol Paris*, 96:539–545, 2002.

[33] M. S. Goldman, P. Maldonado, and L. F. Abbott. Redundancy reduction and sustained firing with stochastic depressing synapses. *J. Neurosci.*, 22:584–591, 2002.

[34] J. F. Mejias and J. J. Torres. The role of synaptic facilitation in spike coincidence detection. *J. Comp. Neurosci.*, 24:222–234, 2008.

[35] M. A. Bourjaily and P. Miller. Dynamic afferent synapses to decision-making networks improve performance in tasks requiring stimulus associations and discriminations. *J. Neurophysiol.*, 108:513–527, 2012.

[36] J. E. Lewis and L. Maler. Dynamics of electrosensory feedback: short-term plasticity and inhibition in a parallel fiber pathway. *J. Neurophysiol.*, 88:1695–1702, 2002.

[37] U. Kandaswamy, P.-Y. Deng, C. Stevens, and V. A. Klyachko. The role of presynaptic dynamics in processing of natural spike trains in hippocampal synapses. *J. Neurosci.*, 30:15904–15914, 2010.

[38] J. A. Varela, K. Sen, J. Gibson, J. Fost, L. F. Abbott, and S. B. Nelson. A quantitative description of short-term plasticity at excitatory synapses in layer 2/3 of rat primary visual cortex. *J. Neurosci.*, 17:7926–7940, 1997.

[39] F. S. Chance, S. B. Nelson, and L. F. Abbott. Synaptic depression and the temporal response characteristics of V1 cells. *J. Neurosci.*, 18:4785–4799, 1998.

[40] A. Zador and L. Dobrunz. Dynamic synapses in the cortex. *Neuron*, 19:1–4, 1997.

[41] D. V. Buonomano. Decoding temporal information: A model based on short-term synaptic plasticity. *J. Neurosci.*, 20:1129–1141, 2000.

[42] F. Pouille and M. Scanziani. Routing of spike series by dynamic circuits in the hippocampus. *Nature*, 429:717–723, 2004.

[43] L. abernet, S. P. Jadhav, D. E. Feldman, M. Carandini, and M. Scanziani. Somatosensory integration controlled by thalamocortical feed-forward inhibition. *Neuron*, 48:315–327, 2005.

[44] Y. Mondal, R. F. O. Pena, and H. G. Rotsten. Temporal filters in response to presynaptic spike trains: Interplay of cellular, synaptic and short-term plasticity time scales. *J. Comp. Neurosci.*, 50:395–429, 2022.

[45] A. Reyes, R. Lujan, A. Rozov, N. Burnashev, P. Somogyi, and B. Sakmann. Target-cell specific facilitation and depression in neocortical circuits. *Nature Neurosci.*, 1:279–285, 1998.

[46] H. Markram, Y. Wang, and M. Tsodyks. Differential signaling via the same axon of neocortical pyramidal neurons. *Proc. Natl. Acad. Sci. USA*, 95:5323–5328, 1998.

[47] M. Tsodyks, K. Pawelzik, and H. Markram. Neural networks with dynamic synapses. *Neural Comput.*, 10:821–835, 1998.

[48] M. Tsodyks and H. Markram. Plasticity of neocortical synapses enables transitions between rate and temporal coding. *Lect. Notes Comput. Sci*, 1112:445–450, 1996.

[49] M. Tsodyks and H. Markram. The neural code between neocortical pyramidal neurons depends on neurotransmitter release probability. *Proc. Natl. Acad. Sci. USA*, 94:719–723, 1997.

[50] Z. Rotman, P.-Y. Deng, and V. A. Klyachko. Short-term plasticity optimizes synaptic information transmission. *J. Neurosci.*, 31:14800–14809, 2011.

[51] Luiz Tauffer and Arvind Kumar. Short-term synaptic plasticity makes neurons sensitive to the distribution of presynaptic population firing rates. *Eneuro*, 8(2), 2021.

[52] G. Fuhrmann, I. Segev, and H. Markram. Coding of temporal information by activity-dependent synapses. *J. Physiol.*, 556:19–27, 2004.

[53] A. Maass, W. Zador. Dynamic stochastic synapses as computational units. *Neural Comput.*, 11:903–917, 1999.

[54] L. F. Abbott, J. A. Varela, K. Sen, and S. B. Nelson. Synaptic depression and cortical gain control. *Science*, 275:220–224, 1997.

[55] M. Tsodyks and S. Wu. Short-term synaptic plasticity. *Scholarpedia*, 8:3153, 2013.

[56] L. Abbott and W. G. Regehr. Synaptic computation. *Nature*, 431:796–803, 2004.

[57] A. Loebel and M. Tsodyks. Computation by ensemble synchronization in recurrent networks with synaptic depression. *J. Comp. Neurosci.*, 13:111–124, 2002.

[58] O. Barak and M. Tsodyks. Persistent activity in neural networks with dynamic synapses. *PLoS Comp. Biol.*, 3:e35, 2007.

[59] U. R. Karmarkar and D. V. Buonomano. Timing in the absence of clocks: Encoding time in neural network states. *Neuron*, 53:427–438, 2007.

[60] G. Mongillo, O. Barak, and M. Tsodyks. Synaptic theory of working memory. *Science*, 319:1543–1546, 2015.

[61] S. Carver, E. Roth, N. J. Cowan, and E. S. Fortune. Synaptic plasticity can produce and enhance direction selectivity. *PLoS Comp. Biol.*, 4:e32, 2008.

[62] W. Yuan, O. Dimigen, W. Sommer, and C. Zhou. A model of microsaccade-related neural responses induced by short-term depression in thalamocortical synapses. *Front. Comp. Neurosci.*, 7:47, 2013.

[63] D. L. Cook, P. C. Schwindt, L. A. Grande, and W. J. Spain. Synaptic depression in the localization of sound. *Nature*, 421:66–70, 2003.

[64] M. H. Hennig, M. Postlethwaite, I. D. Forsythe, and B. P. Graham. Interactions between multiple sources of short-term plasticity during evoked and spontaneous activity at the rat calyx of held. *J. Physiol.*, 586:3129–3146, 2008.

[65] David Holcman and Misha Tsodyks. The emergence of up and down states in cortical networks. *PLoS computational biology*, 2(3):e23, 2006.

[66] S.-I. Amari. Dynamics of pattern formation in lateral-inhibition type neural fields. *Biol. Cybern.*, 27:77–87, 1977.

[67] O. Barak, M. Tsodyks, and R. Romo. Neuronal population coding of parametric working memory. *J. Neurosci.*, 319:1543–1546, 2008.

[68] G. Deco, E. Rolls, and R. Romo. Synaptic dynamics and decision making. *Proc. Natl. Acad. Sci. USA*, 107:7547–7549, 2010.

[69] A. Destexhe and E. Marder. Plasticity in single neuron and circuit computations. *Nature*, 431:785–795, 2004.

[70] J. F. Mejias and J. J. Torres. Maximum memory capacity on neural networks with short-term synaptic depression and facilitation. *Neural Comput.*, 21:851–871, 2009.

[71] P.-Y. Deng and A. Klyachko. The diverse functions of short-term plasticity components in synaptic computations. *Commun. Integr. Biol.*, 4:543–548, 2011.

[72] X. J. Wang. Neurophysiological and computational principles of cortical rhythms in cognition. *Physiol. Rev.*, 90:1195–1268, 2010.

[73] F. G. Pike, R. S. Goddard, J. M. Suckling, P. Ganter, N. Kasthuri, and O. Paulsen. Distinct frequency preferences of different types of rat hippocampal neurons in response to oscillatory input currents. *J. Physiol.*, 529:205–213, 2000.

[74] R. Zemankovics, S. Káli, O. Paulsen, T. F. Freund, and N. Hájos. Differences in subthreshold resonance of hippocampal pyramidal cells and interneurons: The role of h-current and passive membrane characteristics. *J. Physiol.*, 588:2109–2132, 2010.

[75] M. J. E. Richardson, N. Brunel, and V. Hakim. From subthreshold to firing-rate resonance. *J. Neurophysiol.*, 89:2538–2554, 2003.

[76] H. G. Rotstein and F. Nadim. Frequency preference in two-dimensional neural models: a linear analysis of the interaction between resonant and amplifying currents. *J. Comp. Neurosci.*, 37:9–28, 2014.

[77] H. G. Rotstein. Subthreshold amplitude and phase resonance in models of quadratic type: nonlinear effects generated by the interplay of resonant and amplifying currents. *J. Comp. Neurosci.*, 38:325–354, 2015.

[78] H. G. Rotstein. Spiking resonances in models with the same slow resonant and fast amplifying currents but different subthreshold dynamic properties. *J. Comp. Neurosci.*, 43:243–271, 2017.

[79] K. Kang, M. Shelley, J. A. Henrie, and R. Shapley. LFP spectral peaks in V1 cortex: network resonance and cortico-cortical feedback. *J. Comp. Neurosci.*, 29:495–507, 2010.

[80] D. Vierling-Claassen, J. A. Cardin, C. I. Moore, and S. R. Jones. Computational modeling of distinct neocortical oscillations driven by cell-type selective optogenetic drive: separable resonant circuits controlled by low-threshold spiking and fast-spiking interneurons. *Front. Hum. Neurosci.*, 4:00198, 2010.

[81] E. Ledoux and Brunel N. Dynamics of networks of excitatory and inhibitory neurons in response to time-dependent inputs. *Front. Comp. Neurosci.*, 5:1–17, 2011.

[82] R. Veltz and T. J. Sejnowski. Periodic forcing of stabilized E-I networks: Nonlinear resonance curves and dynamics. *Neural Comput.*, 27:2477–2509, 2015.

[83] E. Stark, R. Eichler, L. Roux, S. Fujisawa, H. G. Rotstein, and G. Buzsáki. Inhibition-induced theta resonance in cortical circuits. *Neuron*, 80:1263–1276, 2013.

[84] C. Borgers, G. Talei Franzesi, Fiona E. N. LeBeau, E. S. Boyden, and N. J. Kopell. Minimal size of cell assemblies coordinated by gamma oscillations. *PLoS Comp. Biol.*, 8:e1002362, 2012.

[85] P. Dayan and L. F. Abbott. *Theoretical Neuroscience*. The MIT Press, Cambridge, Massachusetts, 2001.

[86] G. B. Ermentrout and D. Terman. *Mathematical Foundations of Neuroscience*. Springer, 2010.

[87] P. Miller. *An introductory course in computational neuroscience*. MIT Press, Cambridge, MA, 2018.

[88] H. G. Rotstein and E. G. Tabak. Analysis of spike-driven processes through attributable components. *Communications in Mathematical Sciences*, 17:1177–1192, 2019.

[89] K. L. Magleby and J. E. Zengel. A quantitative description of stimulation-induced changes in transmitter release at the frog neuromuscular junction. *J. Gen. Physiol.*, 80:613–638, 1982.

[90] M. H. Hennig. Theoretical models of synaptic short term plasticity. *Front. Comp. Neurosci.*, 7:45, 2013.

[91] H. Markram and M. Tsodyks. Redistribution of synaptic efficacy between neocortical pyramidal neurons. *Nature*, 382:807–810, 1996.

[92] H. Markram, D. Pikus, A. Gupta, and M. Tsodyks. Potential for multiple mechanisms, phenomena and algorithms for synaptic plasticity at single synapses. *Neuropharmacology*, 37:489–500, 1998.

[93] R. Fernandez and J. A. White. Artificial synaptic conductances reduce subthreshold oscillations and periodic firing in stellate cells of the entorhinal cortex. *J. Neurosci.*, 28:3790–3803, 2008.

[94] R. F. O. Pena and H. G. Rotstein. The voltage and spiking responses of subthreshold resonant neurons to structured and fluctuating inputs: emergence and loss of resonance and variability. *Biol. Cybern.*, 116:163–190, 2022.

[95] R. L. Burden and J. D. Faires. *Numerical analysis*. PWS Publishing Company - Boston, 1980.

[96] A. G. R. Turnquist and H. G. Rotstein. Quadratization: From conductance-based models to caricature models with parabolic nonlinearities. *In: Jaeger D., Jung R. (Ed.) Encyclop edia of Computational Neuroscience. Springer-Verlag, New York*, 2018.

[97] R. F. O. Pena, V. Lima, R. O. Shimoura, C. C. Ceballos, H. G. Rotstein, and A. C. Roque. Asymmetrical voltage response in resonant neurons shaped by nonlinearities. *Chaos*, 29:103135, 2019.

[98] W. Gerstner, W. M. Kistler, R. Naud, and L. Paninski. *Neuronal dynamics: From single neurons to networks and models of cognition*. Cambridge University Press, 2014.

[99] D. Levenstein, V. A. Alvarez, A Amarasingham, H. Azab, R. C. Gerkin, A. Hasenstaub, R. Iyer, R. Jolivet, S. Marzen, J. D. Monaco, A. Prinz, S. Quarishi, F. Santamaría, S. Shivkumar, M. F. Singh, D. B. Stockton, R. Traub, H. G. Rotstein, F. Nadim, and D. Redish. On the role of theory and modeling in neuroscience. *J. Neurosci. (in press)*, 43:1074–1088, 2023.

[100] U. Chialva, V. Gonzalez Bosca, and H. G. Rotstein. Low-dimensional models of single neurons: A review. *Biol. Cybern.*, 117:163 – 183, 2023.

[101] A. Losonczy, L. Zhang, R. Shigemoto, P. Somogyi, and Z. Nusser. Cell type dependence and variability in the short-term plasticity of EPSCs in identified mouse hippocampal interneurones. *J. Physiol.*, 542:193–210, 2002.

[102] A. Gupta, Y. Wang, and H. Markram. Organizing principles for a diversity of GABAergic interneurons and synapses in the neocortex. *Science*, 287:273–278, 2000.

A Approximate analytical solution to the passive postsynaptic cell receiving presynaptic spike inputs

Here we compute an analytical approximate solution to the model (1)-(4), describing the dynamics of a postsynaptic passive cell receiving presynaptic spike inputs at time $t_1, t_2, \ldots, t_N$.

A.1 Approximate solution to the synaptic variable

We first compute the approximate solution to the synaptic variable S whose dynamics are described by eq. (3) with $S(0) = 0$, under the assumption of instantaneous raise to a value ΔS_n ($n = 1, \ldots, N$) at the arrival of each presynaptic spike. The assumption $S(0) = 0$ implies that $S(t) = 0$ for $0 \leq t \leq t_1$. For the duration of a presynaptic spike ($t_n < t < t_n + T_{sw}$), we approximate $S(t)$ by the synaptic update value ΔS_n (constant). For the remainder of the presynaptic interspike interval ($t_n + T_{sw} \leq t < t_{n+1}$), $S(t)$ decreases according to the second term in (3). The approximate solution is given by

$$S_a(t) = \begin{cases} \Delta S_n & t_n < t < t_n + T_{sw} \\ \\ \Delta S_n \, e^{-(t-t_n-T_{sw})/\tau_{dec}} & t_n + T_{sw} \leq t < t_{n+1} \end{cases} \tag{75}$$

for $n = 1, \ldots, N$.

From eq. (76) for $S_a(t)$, the larger the duration T_{sw} of the presynaptic spike ($T_{sw} < \Delta_{spk}$) or the larger the synaptic decay time τ_{dec}, the larger $S_a(t)$ during the presynaptic ISI. In that sense, increasing τ_{dec} or T_{sw} has a similar overall effect on the PSP response as increasing G_{syn}. However, changes in the former two have stronger dynamic effects (e.g., cause changes in the voltage response peak) than changes in G_{syn} (Fig. 7).

A.2 Approximate solution to the postsynaptic membrane potential: Postsynaptic passive cell

We first approximate eq. (1) as follows

$$\tau \frac{dV}{dt} = -V + \alpha_n S_a(t) \tag{76}$$

for $n = 1, \ldots, N$ where

$$\tau = \frac{C}{G_L}, \qquad \alpha = \frac{G_{syn}\,(E_{syn} - E_L)}{G_L} \qquad \text{and} \qquad \alpha_n = \alpha\,(1 - \sigma_n). \tag{77}$$

The variable V in eq. (77) represents $V - E_L - I_{app}/G_L$ in eq. (1). The third term in eq. (77) is a current input approximation to the conductance input in the synaptic current (1). To account for this, we introduce a correction factor $1 - \sigma_n$ where σ_n is updated at the beginning of each ISI and $\sigma_1 = 0$.

Prior to the arrival of the first presynaptic spike ($t \le t_1$), $V(t) = 0$. For the duration of a presynaptic spike ($t_n < t < t_n + T_{sw}$),

$$\tau \frac{dV}{dt} = -V + \alpha_n \Delta S_n, \qquad V(t_n) = V_{0,n}, \tag{78}$$

where $V_{0,n}$ is the value of V at the end of the previous cycle. The solution to (79) is given by

$$V_I(t) = \alpha_n \Delta S_n + (V_{o,n} - \alpha_n \Delta S_n)\, e^{-(t-t_n)/\tau}. \tag{79}$$

We define

$$\beta_n = V_I(t_n + T_{sw}) = \alpha_n \Delta S_n + (V_{o,n} - \alpha_n \Delta S_n)\, e^{-T_{sw}/\tau}. \tag{80}$$

For the remainder of the presynaptic interspike interval ($t_n + T_{sw} < t < t_{n+1}$),

$$\tau \frac{dV}{dt} = -V + \alpha_n \Delta S_n\, e^{-(t-t_n-T_{sw})/\tau} \qquad V(t_n + T_{sw}) = \beta_n, \tag{81}$$

For $\tau_{dec} \neq \tau$, the solution to (82) is given by

$$V_{II}(t) = \frac{\alpha_n\, \tau_{dec}\, \Delta S_n}{\tau_{dec} - \tau}\, e^{Tsw/\tau_{dec}}\, e^{-(t-t_n)/\tau_{dec}} + \left[\beta_n - \frac{\alpha_n\, \tau_{dec}\, \Delta S_n}{\tau_{dec} - \tau}\right] e^{T_{sw}/\tau}\, e^{-(t-t_n)/\tau}. \tag{82}$$

We define

$$V_{0,n+1} = V_{II}(t_{n+1}) = \frac{\alpha_n\, \tau_{dec}\, \Delta S_n}{\tau_{dec} - \tau}\, e^{T_{sw}/\tau_{dec}}\, e^{-(t_{n+1}-t_n)/\tau_{dec}} + \left[\beta_n - \frac{\alpha_n\, \tau_{dec}\, \Delta S_n}{\tau_{dec} - \tau}\right] e^{T_{sw}/\tau}\, e^{-(t_{n+1}-t_n)/\tau} =$$

$$= \frac{\alpha_n\, \tau_{dec}\, \Delta S_n}{\tau_{dec} - \tau}\, e^{T_{sw}/\tau_{dec}}\, e^{-\Delta_{spk,n}/\tau_{dec}} + \left[\beta_n - \frac{\alpha_n\, \tau_{dec}\, \Delta S_n}{\tau_{dec} - \tau}\right] e^{T_{sw}/\tau}\, e^{-\Delta_{spk,n}/\tau}. \tag{83}$$

For the duration of the presynaptic spike, $V(t) = V_I(t)$ is an increasing function. $V(t) = V_{II}(t)$ continues to be an increasing function after the presynaptic spike is off until the two exponential terms balance out and $V_{II}(t)$ decreases. Therefore, within some frequency range, $V(t)$ peaks after the presynaptic spike is off. The peak time for $V_{II}(t)$ in eq. (83) is given

$$t_{peak,n} = t_n + \frac{\tau_{dec}\, \tau}{\tau_{dec} - \tau}\, \ln\left(-\frac{b_n\, \tau_{dec}}{a_n\, \tau}\right) \tag{84}$$

where

$$a_n = \frac{\alpha_n \, \tau_{dec} \, \Delta S_n}{\tau_{dec} - \tau} \, e^{T_{sw}/\tau_{dec}} \qquad \text{and} \qquad b_n = \left[\beta_n - \frac{\alpha_n \, \tau_{dec} \, \Delta S_n}{\tau_{dec} - \tau} \right] \, e^{T_{sw}/\tau}. \tag{85}$$

The peak value of $V(t)$ is given by

$$V_{peak,n} = V_{II}(t_{peak,n}). \tag{86}$$

We define σ_{n+1} as

$$\sigma_{n+1} = \frac{\eta \, V_{peak,n} + (1-\eta) \, V_{0,n+1}}{(E_{syn} - E_L)}. \tag{87}$$

or

$$\sigma_{n+1} = \frac{\eta \, V_{peak,n}}{(E_{syn} - E_L)}. \tag{88}$$

For $\tau_{dec} = \tau$, the solution to (82) is given by

$$V_{II}(t) = \frac{\alpha_n \, \Delta S_n}{\tau} \, e^{T_{sw}/\tau} \, t \, e^{-(t-t_n)/\tau} + \left[\beta_n - \frac{\alpha_n \, \Delta S_n}{\tau} \, (t_n + T_{sw}) \right] \, e^{T_{sw}/\tau} \, e^{-(t-t_n)/\tau}. \tag{89}$$

The peak time for $V_{II}(t)$ in eq. (90) is given

$$t_{peak,n} = t_n + \tau - \frac{b_n}{a_n} \tag{90}$$

where

$$a_n = \frac{\alpha_n \, \Delta S_n}{\tau} \, e^{T_{sw}/\tau_{dec}} \qquad \text{and} \qquad b_n = \left[\beta_n - \frac{\alpha_n \, \Delta S_n}{\tau} \, T_{sw} \right] \, e^{T_{sw}/\tau_{dec}}. \tag{91}$$

The peak values of $V(t)$ is given by (87) with β_n given by (81) and $V_{0,n+1} = V_{II}(t_{n+1})$

Supplementary Material

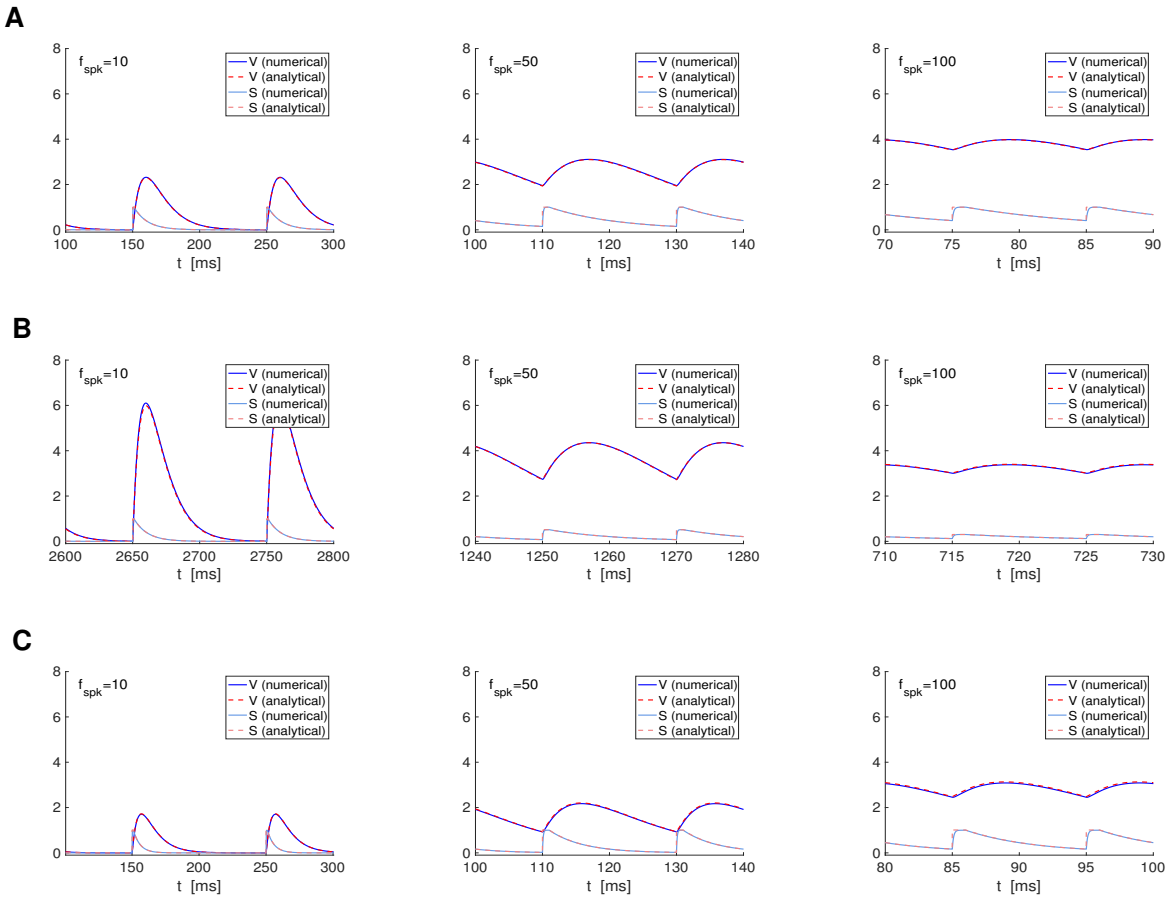

Figure S1: **Analytical approximation of the membrane potential response of passive cells to presynaptic spikes: Representative examples I.** For the numerical approximations we used the model for a passive cell receiving presynaptic spike-train input (1)-(4). For STP we use the DA model (7)-(9). For the analytical approximations we used eqs. (21)-(23) together with eqs. (80) and (83) in the Appendix A. **A.** $G_L = 0.1$ ($\tau = 10$), $\tau_{dec} = 10$, $\tau_{dep} = \tau_{fac} = 0.1$. **B.** $G_L = 0.1$ ($\tau = 10$), $\tau_{dec} = 10$, $\tau_{dep} = \tau_{fac} = 1000$. **C.** $G_L = 0.1$ ($\tau = 10$), $\tau_{dec} = 5$, $\tau_{dep} = \tau_{fac} = 0.1$. We used the following additional parameter values: $a_d = 0.1$, $a_f = 0.1$, $x_\infty = 1$, $z_\infty = 0$, $\tau_{rse} = 0.1$, $C = 1$, $E_L = -60$, $I_{app} = 0$, $G_{syn} = 0.1$, $E_{syn} = -60$.

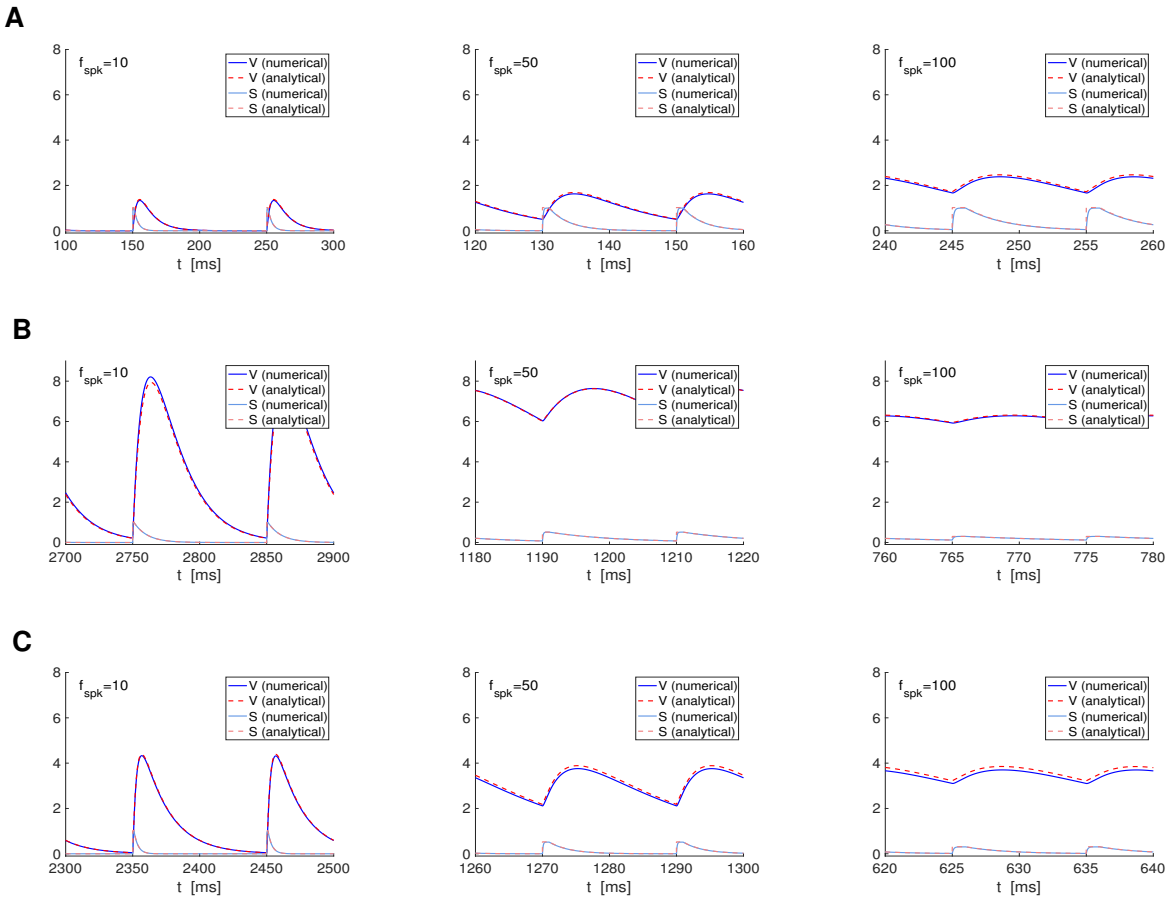

Figure S2: **Analytical approximation of the membrane potential response of passive cells to presynaptic spikes: Representative examples II.** For the numerical approximations we used the model for a passive cell receiving presynaptic spike-train input (1)-(4). For STP we used the DA model (7)-(9). For the analytical approximations we used eqs. (21)-(23) together with eqs. (80) and (83) in the Appendix A. **A.** $G_L = 0.1$ ($\tau = 10$), $\tau_{dec} = 3$, $\tau_{dep} = \tau_{fac} = 0.1$. **B.** $G_L = 0.05$ ($\tau = 20$), $\tau_{dec} = 10$, $\tau_{dep} = \tau_{fac} = 1000$. **C.** $G_L = 0.05$ ($\tau = 20$), $\tau_{dec} = 5$, $\tau_{dep} = \tau_{fac} = 1000$. We used the following additional parameter values: $a_d = 0.1$, $a_f = 0.1$, $x_\infty = 1$, $z_\infty = 0$, $\tau_{rse} = 0.1$, $C = 1$, $E_L = -60$, $I_{app} = 0$, $G_{syn} = 0.1$, $E_{syn} = -60$.

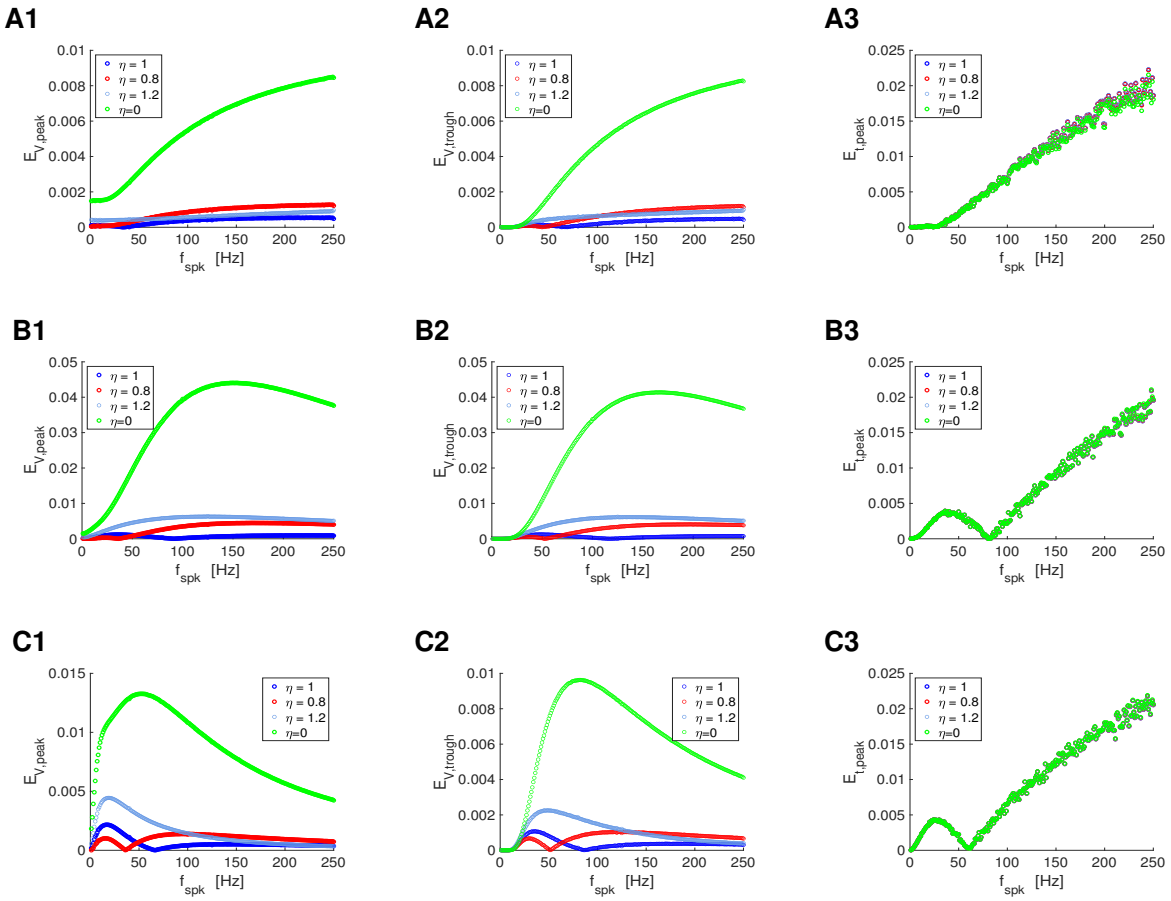

Figure S3: **Error between the numerical and analytical approximations for the stationary peaks (V_{peak}), troughs (V_{trough}), and peak times (t_{peak}) of the membrane potential responses of passive cells to presynaptic spikes: Representative examples I.** For the numerical (num) approximations we used the model for a passive cell receiving presynaptic spike-train input (1)-(4). For STP we used the DA model (7)-(9). For the analytical approximations we used eqs. (21)-(23) together with eqs. (80) and (83) in the Appendix A. For the computations of the analytical (anl) approximations to V_{peak}, V_{trough} and t_{peak} we used eqs. (24)-(31). Simulations were carried out until the difference between two consecutive numerical peaks were below a tolerance value equal to 0.001. The last values of V_{peak}, V_{trough} and t_{peak} in the resulting sequences were taken as an approximation to the corresponding stationary values. **Left column.** Relative error for V_{peak} defined as $\mid V_{peak,num} - 60 - V_{peak,anl} \mid / \mid V_{peak,num} \mid$. **Middle column.** Relative error for V_{trough} defined as $\mid V_{trough,num} - 60 - V_{trough,anl} \mid / \mid V_{trough,num} \mid$. **Right column.** Relative error for t_{peak} defined as $\mid t_{peak,num} - t_{peak,anl} \mid / \mid \Delta_{spk} \mid$. **A.** $G_L = 0.1$ ($\tau = 10$), $\tau_{dec} = 10$, $\tau_{dep} = \tau_{fac} = 0.01$. **B.** $G_L = 0.1$ ($\tau = 10$), $\tau_{dec} = 5$, $\tau_{dep} = \tau_{fac} = 100$. **C.** $G_L = 0.1$ ($\tau = 10$), $\tau_{dec} = 10$, $\tau_{dep} = \tau_{fac} = 500$. We used the following additional parameter values: $a_d = 0.1$, $a_f = 0.1$, $x_\infty = 1$, $z_\infty = 0$, $\tau_{rse} = 0.1$, $C = 1$, $E_L = -60$, $I_{app} = 0$, $G_{syn} = 0.1$, $E_{syn} = -60$, $\Delta t = 0.01$.

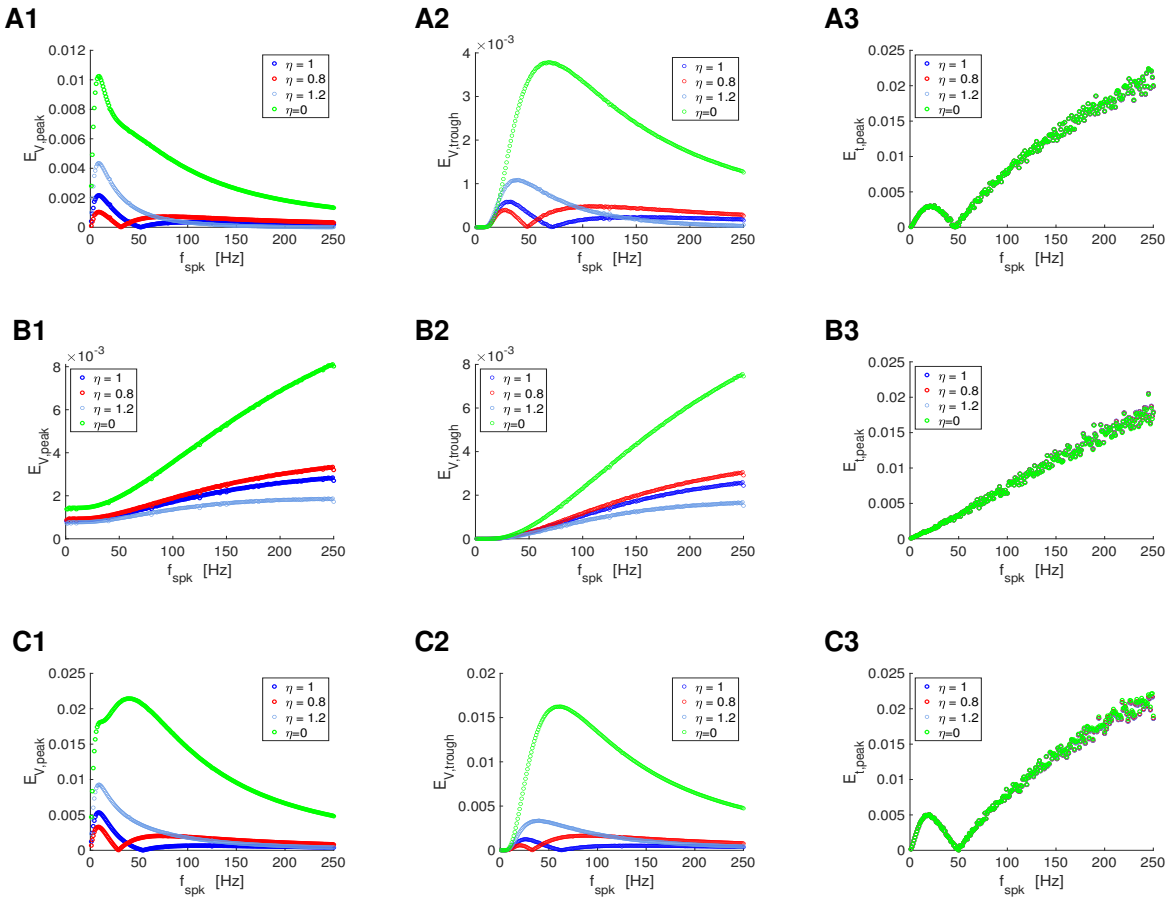

Figure S4: **Error between the numerical and analytical approximations for the stationary peaks ($\mathbf{V}_{peak}$), troughs ($\mathbf{V}_{trough}$), and peak times ($\mathbf{t}_{peak}$) of the membrane potential responses of passive cells to presynaptic spikes: Representative examples II.** For the numerical (num) approximations we used the model for a passive cell receiving presynaptic spike-train input (1)-(4). For STP we used the DA model (7)-(9). For the analytical approximations we used eqs. (21)-(23) together with eqs. (80) and (83) in the Appendix A. For the computations of the analytical (anl) approximations to V_{peak}, V_{trough} and t_{peak} we used eqs. (24)-(31). Simulations were carried out until the difference between two consecutive numerical peaks were below a tolerance value equal to 0.001. The last values of V_{peak}, V_{trough} and t_{peak} in the resulting sequences were taken as an approximation to the corresponding stationary values. **Left column.** Relative error for V_{peak} defined as $|\, V_{peak,num} - 60 - V_{peak,anl}\,|/|\, V_{peak,num}\,|$. **Middle column.** Relative error for V_{trough} defined as $|\, V_{trough,num} - 60 - V_{trough,anl}\,|/|\, V_{trough,num}\,|$. **Right column.** Relative error for t_{peak} defined as $|\, t_{peak,num} - t_{peak,anl}\,|/|\, \Delta_{spk}\,|$. **A.** $G_L = 0.1$ ($\tau = 10$), $\tau_{dec} = 10$, $\tau_{dep} = \tau_{fac} = 1000$. **B.** $G_L = 0.1$ ($\tau = 10$), $\tau_{dec} = 3$, $\tau_{dep} = \tau_{fac} = 0.01$. **C.** $G_L = 0.05$ ($\tau = 20$), $\tau_{dec} = 10$, $\tau_{dep} = \tau_{fac} = 1000$. We used the following additional parameter values: $a_d = 0.1$, $a_f = 0.1$, $x_\infty = 1$, $z_\infty = 0$, $\tau_{rse} = 0.1$, $C = 1$, $E_L = -60$, $I_{app} = 0$, $G_{syn} = 0.1$, $E_{syn} = -60$, $\Delta t = 0.01$.

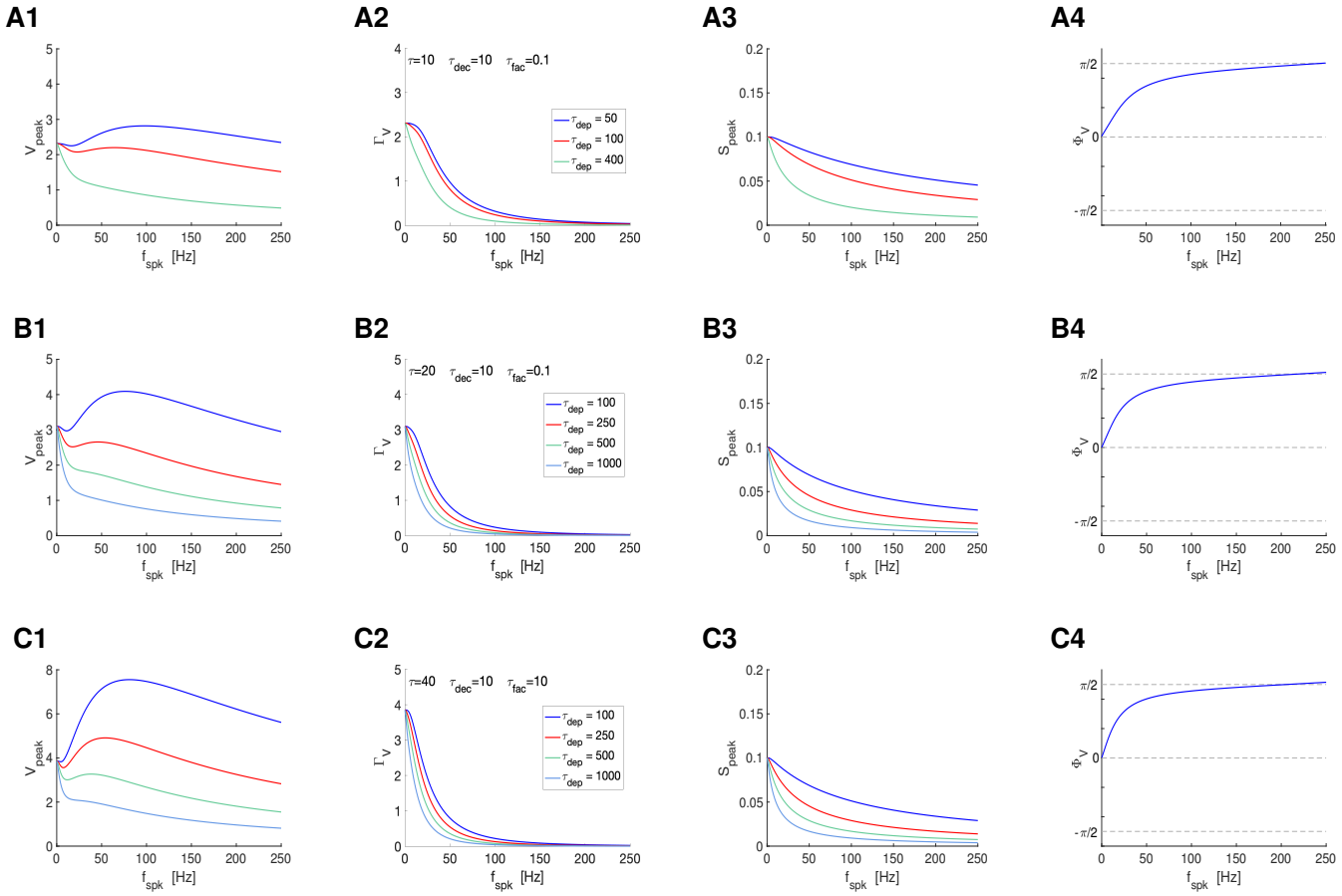

Figure S5: **Postsynaptic filters in response to periodic presynaptic spike inputs emerging from the interplay of short-term depression and postsynaptic summation.** Superimposed filters for representative values of the short-term depression time constant τ_{dep}. **A.** $\tau = 10$. **B.** $\tau = 20$. **C.** $\tau = 40$. **A, B, C.** $\tau_{dec} = 10$ and $\tau_{fac} = 0.1$. **Left column.** V peak profiles. **Middle-left column.** V peak-to-trough amplitude profiles. **Middle-right column.** S peak profiles. **Right column.** V phase profiles. We used eq. (64) for the PSP V with I_{syn} described by eqs. (2)-(4) appropriately adapted to account for the translation of V to the equilibrium point, and STP described by eqs. (12) and (13) (DA model). The impedance amplitude (Z) and phase (Φ_Z) were computed using eqs. (36) and (37). The analytical approximations for the PSP peak sequence response of passive cells to presynaptic inputs are described in Section2.2 (see also Appendix A). The approximation of $V_{peak,n}$, $V_{trough,n}$ and $t_{V,peak}$ were computed as described in Section 3.4. The PSP amplitude Γ_V was computed by using eq. (65) and the PSP phase Φ_V was computed using eq. (66). The synaptic (S) peak (S_{peak}) and phase (Φ_S) profiles were computed similarly to these for V. We used the following additional parameter values: $C = 1$, $E_L = -60$, $I_{app} = 0$, $G_{syn} = 0.1$, $E_{syn} = 0$, $a_d = 0.1$, $a_f = 0.1$, $x_\infty = 1$, $z_\infty = 0$ and $T_{sw} = 1$.

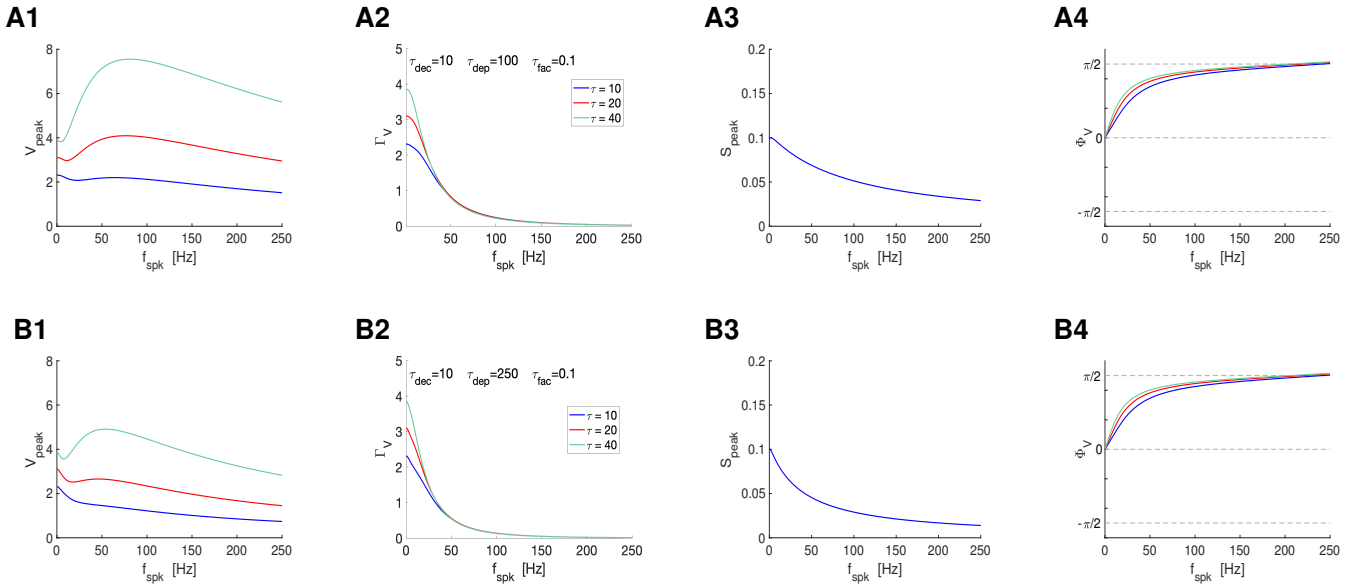

Figure S6: **Postsynaptic filters in response to periodic presynaptic spike inputs emerging from the interplay of short-term depression and postsynaptic summation.** Superimposed filters for representative values of the membrane time constant τ. **A.** $\tau_{dep} = 100$. **B.** $\tau_{dep} = 250$. **A, B** $\tau_{dec} = 10$ and $\tau_{fac} = 0.1$. **Left column.** V peak profiles. **Middle-left column.** V peak-to-trough amplitude profiles. **Middle-right column.** S peak profiles. They are independent of τ. **Right column.** V phase profiles. We used eq. (64) for the PSP V with I_{syn} described by eqs. (2)-(4) appropriately adapted to account for the translation of V to the equilibrium point, and STP described by eqs. (12) and (13) (DA model). The impedance amplitude (Z) and phase (Φ_Z) were computed using eqs. (36) and (37). The analytical approximations for the PSP peak sequence response of passive cells to presynaptic inputs are described in Section2.2 (see also Appendix A). The approximation of $V_{peak,n}$, $V_{trough,n}$ and $t_{V,peak}$ were computed as described in Section 3.4. The PSP amplitude Γ_V was computed by using eq. (65) and the PSP phase Φ_V was computed using eq. (66). The synaptic (S) peak (S_{peak}) and phase (Φ_S) profiles were computed similarly to these for V. We used the following additional parameter values: $C = 1$, $E_L = -60$, $I_{app} = 0$, $G_{syn} = 0.1$, $E_{syn} = 0$, $a_d = 0.1$, $a_f = 0.1$, $x_\infty = 1$, $z_\infty = 0$ and $T_{sw} = 1$.

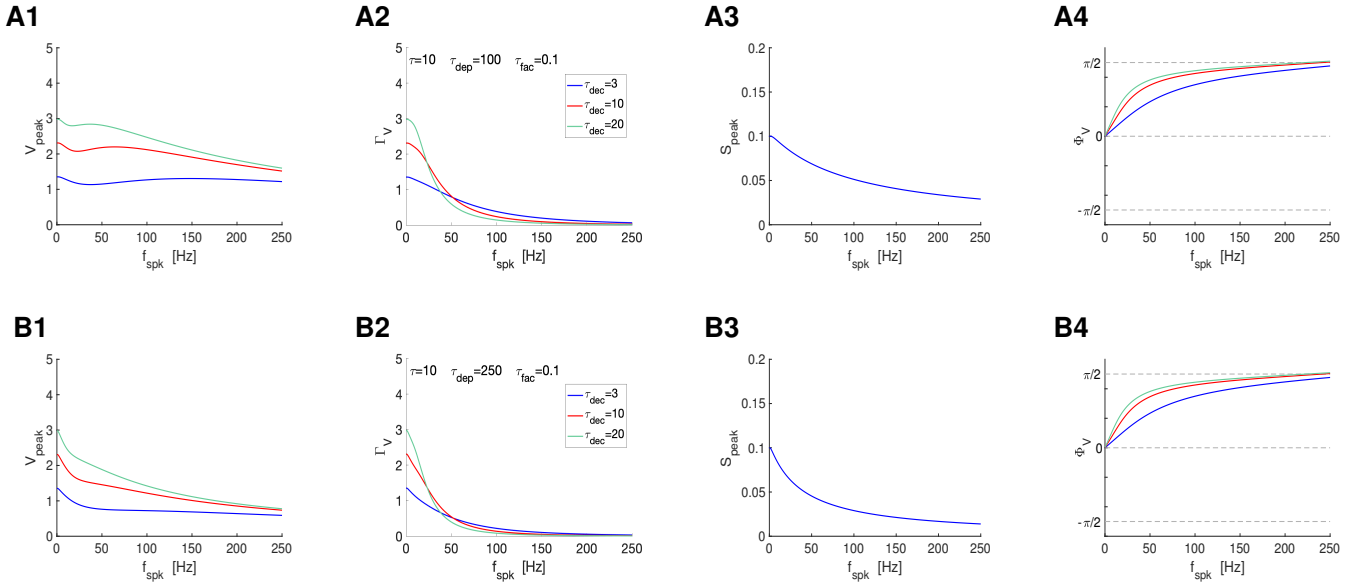

Figure S7: **Postsynaptic filters in response to periodic presynaptic spike inputs emerging from the interplay of short-term depression and postsynaptic summation.** Superimposed filters for representative values of the synaptic decay time constant τ_{dec}. **A.** $\tau_{dep} = 100$. **B.** $\tau_{dep} = 150$. **A, B.** $\tau = 10$ and $\tau_{fac} = 0.1$. **Left column.** V peak profiles. **Middle-left column.** V peak-to-trough amplitude profiles. **Middle-right column.** S peak profiles. They are independent of τ_{dec}. **Right column.** V phase profiles. We used eq. (64) for the PSP V with I_{syn} described by eqs. (2)-(4) appropriately adapted to account for the translation of V to the equilibrium point, and STP described by eqs. (12) and (13) (DA model). The impedance amplitude (Z) and phase (Φ_Z) were computed using eqs. (36) and (37). The analytical approximations for the PSP peak sequence response of passive cells to presynaptic inputs are described in Section2.2 (see also Appendix A). The approximation of $V_{peak,n}$, $V_{trough,n}$ and $t_{V,peak}$ were computed as described in Section 3.4. The PSP amplitude Γ_V was computed by using eq. (65) and the PSP phase Φ_V was computed using eq. (66). The synaptic (S) peak (S_{peak}) and phase (Φ_S) profiles were computed similarly to these for V. We used the following additional parameter values: $C = 1$, $E_L = -60$, $I_{app} = 0$, $G_{syn} = 0.1$, $E_{syn} = 0$, $a_d = 0.1$, $a_f = 0.1$, $x_\infty = 1$, $z_\infty = 0$ and $T_{sw} = 1$.

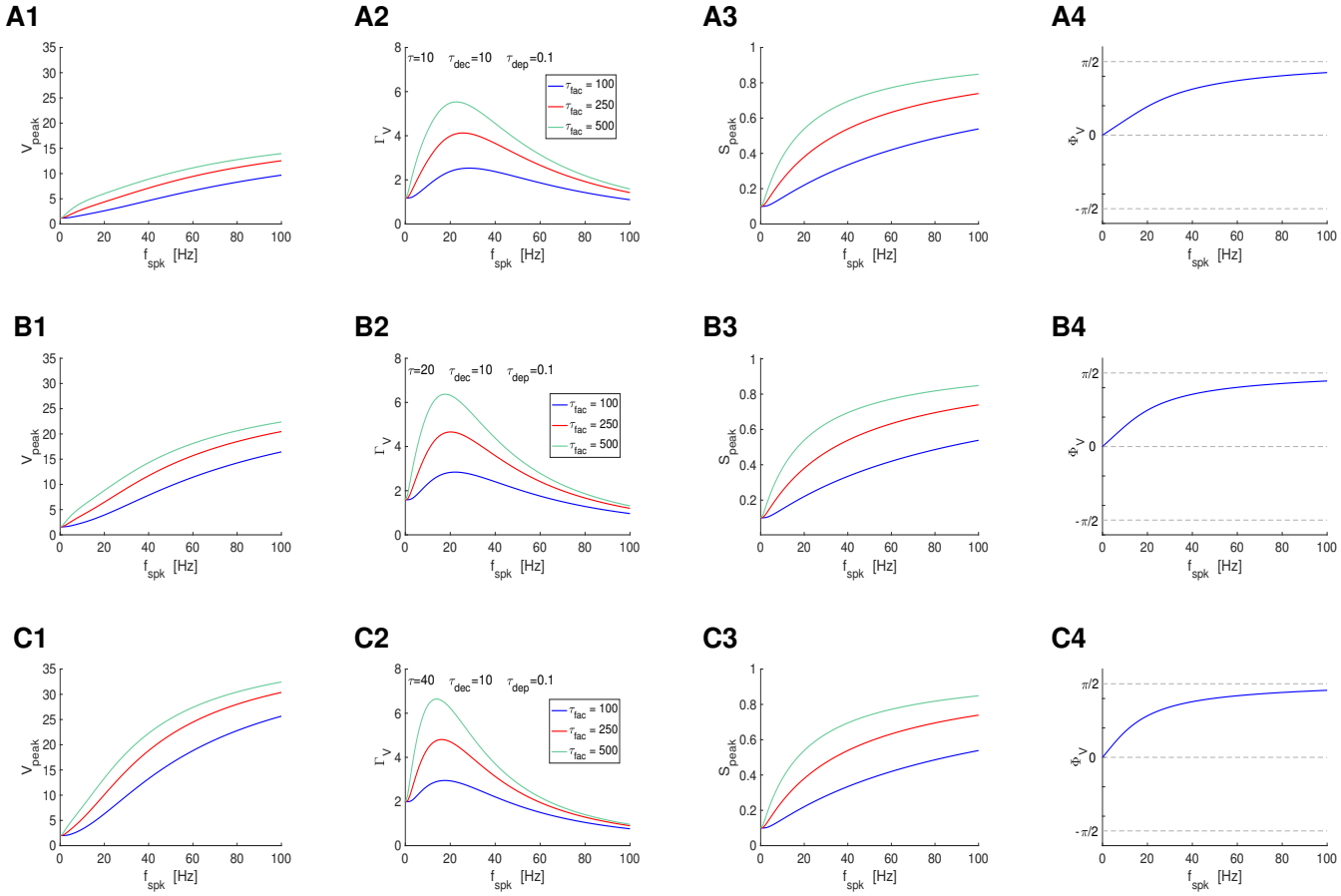

Figure S8: **Postsynaptic filters in response to periodic presynaptic spike inputs emerging from the interplay of short-term facilitation and postsynaptic summation.** Superimposed filters for representative values of the short-term facilitation time constant τ_{fac}. **A.** $\tau = 10$. **B.** $\tau = 20$. **C.** $\tau = 40$. **A, B, C.** $\tau_{dec} = 10$ and $\tau_{dep} = 0.1$. **Left column.** V peak profiles. **Middle-left column.** V peak-to-trough amplitude profiles. **Middle-right column.** S peak profiles. **Right column.** V phase profiles. We used eq. (64) for the PSP V with I_{syn} described by eqs. (2)-(4) appropriately adapted to account for the translation of V to the equilibrium point, and STP described by eqs. (12) and (13) (DA model). The impedance amplitude (Z) and phase (Φ_Z) were computed using eqs. (36) and (37). The analytical approximations for the PSP peak sequence response of passive cells to presynaptic inputs are described in Section2.2 (see also Appendix A). The approximation of $V_{peak,n}$, $V_{trough,n}$ and $t_{V,peak}$ were computed as described in Section 3.4. The PSP amplitude Γ_V was computed by using eq. (65) and the PSP phase Φ_V was computed using eq. (66). The synaptic (S) peak (S_{peak}) and phase (Φ_S) profiles were computed similarly to these for V. We used the following additional parameter values: $C = 1$, $E_L = -60$, $I_{app} = 0$, $G_{syn} = 0.05$, $E_{syn} = 0$, $a_d = 0.1$, $a_f = 0.1$, $x_\infty = 1$, $z_\infty = 0$ and $T_{sw} = 1$.

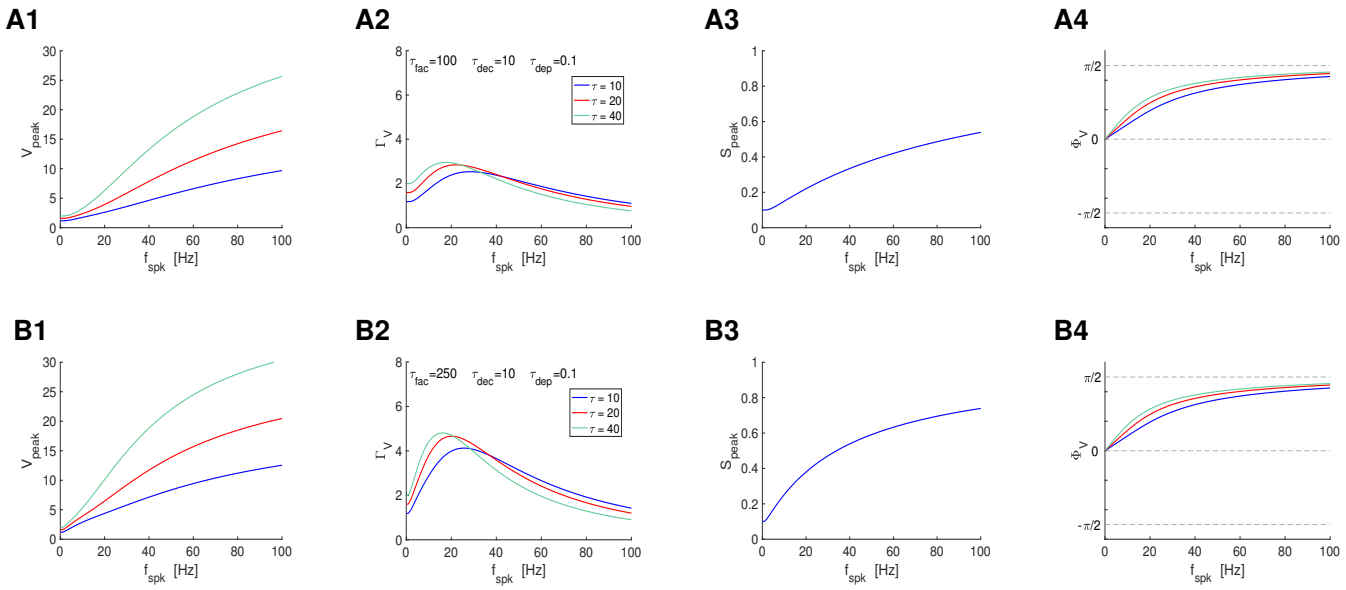

Figure S9: **Postsynaptic filters in response to periodic presynaptic spike inputs emerging from the interplay of short-term facilitation and postsynaptic summation.** Superimposed filters for various values of the membrane time constant τ. **A.** $\tau_{fac} = 100$. **B.** $\tau_{fac} = 250$. **A, B, C.** $\tau_{dec} = 10$ and $\tau_{dep} = 0.1$. **Middle-left column.** V peak-to-trough amplitude profiles. **Middle-right column.** S peak profiles. **Right column.** V phase profiles. We used eq. (64) for the PSP V with I_{syn} described by eqs. (2)-(4) appropriately adapted to account for the translation of V to the equilibrium point, and STP described by eqs. (12) and (13) (DA model). The impedance amplitude (Z) and phase (Φ_Z) were computed using eqs. (36) and (37). The analytical approximations for the PSP peak sequence response of passive cells to presynaptic inputs are described in Section2.2 (see also Appendix A). The approximation of $V_{peak,n}$, $V_{trough,n}$ and $t_{V,peak}$ were computed as described in Section 3.4. The PSP amplitude Γ_V was computed by using eq. (65) and the PSP phase Φ_V was computed using eq. (66). The synaptic (S) peak (S_{peak}) and phase (Φ_S) profiles were computed similarly to these for V. We used the following additional parameter values: $C = 1$, $E_L = -60$, $I_{app} = 0$, $G_{syn} = 0.1$, $E_{syn} = 0$, $a_d = 0.1$, $a_f = 0.1$, $x_\infty = 1$, $z_\infty = 0$ and $T_{sw} = 1$.

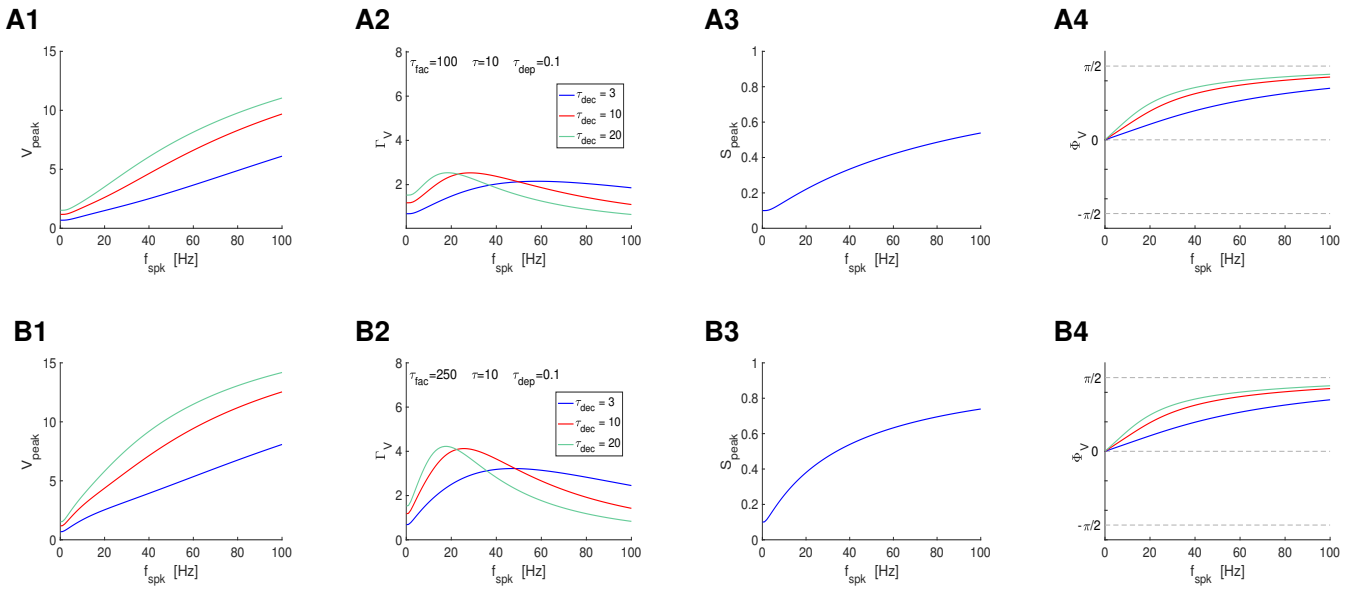

Figure S10: **Postsynaptic filters in response to periodic presynaptic spike inputs emerging from the interplay of short-term depression and postsynaptic summation.** Superimposed filters for representative values of the synaptic decay time constant τ_{dec}. **A.** $\tau_{dep} = 100$. **B.** $\tau_{dep} = 150$. **A, B.** $\tau = 10$ and $\tau_{fac} = 0.1$. **Left column.** V peak profiles. **Middle-left column.** V peak-to-trough amplitude profiles. **Middle-right column.** S peak profiles. They are independent of τ_{dec}. **Right column.** V phase profiles. We used eq. (64) for the PSP V with I_{syn} described by eqs. (2)-(4) appropriately adapted to account for the translation of V to the equilibrium point, and STP described by eqs. (12) and (13) (DA model). The impedance amplitude (Z) and phase (Φ_Z) were computed using eqs. (36) and (37). The analytical approximations for the PSP peak sequence response of passive cells to presynaptic inputs are described in Section2.2 (see also Appendix A). The approximation of $V_{peak,n}$, $V_{trough,n}$ and $t_{V,peak}$ were computed as described in Section 3.4. The PSP amplitude Γ_V was computed by using eq. (65) and the PSP phase Φ_V was computed using eq. (66). The synaptic (S) peak (S_{peak}) and phase (Φ_S) profiles were computed similarly to these for V. We used the following additional parameter values: $C = 1$, $E_L = -60$, $I_{app} = 0$, $G_{syn} = 0.1$, $E_{syn} = 0$, $a_d = 0.1$, $a_f = 0.1$, $x_\infty = 1$, $z_\infty = 0$ and $T_{sw} = 1$.

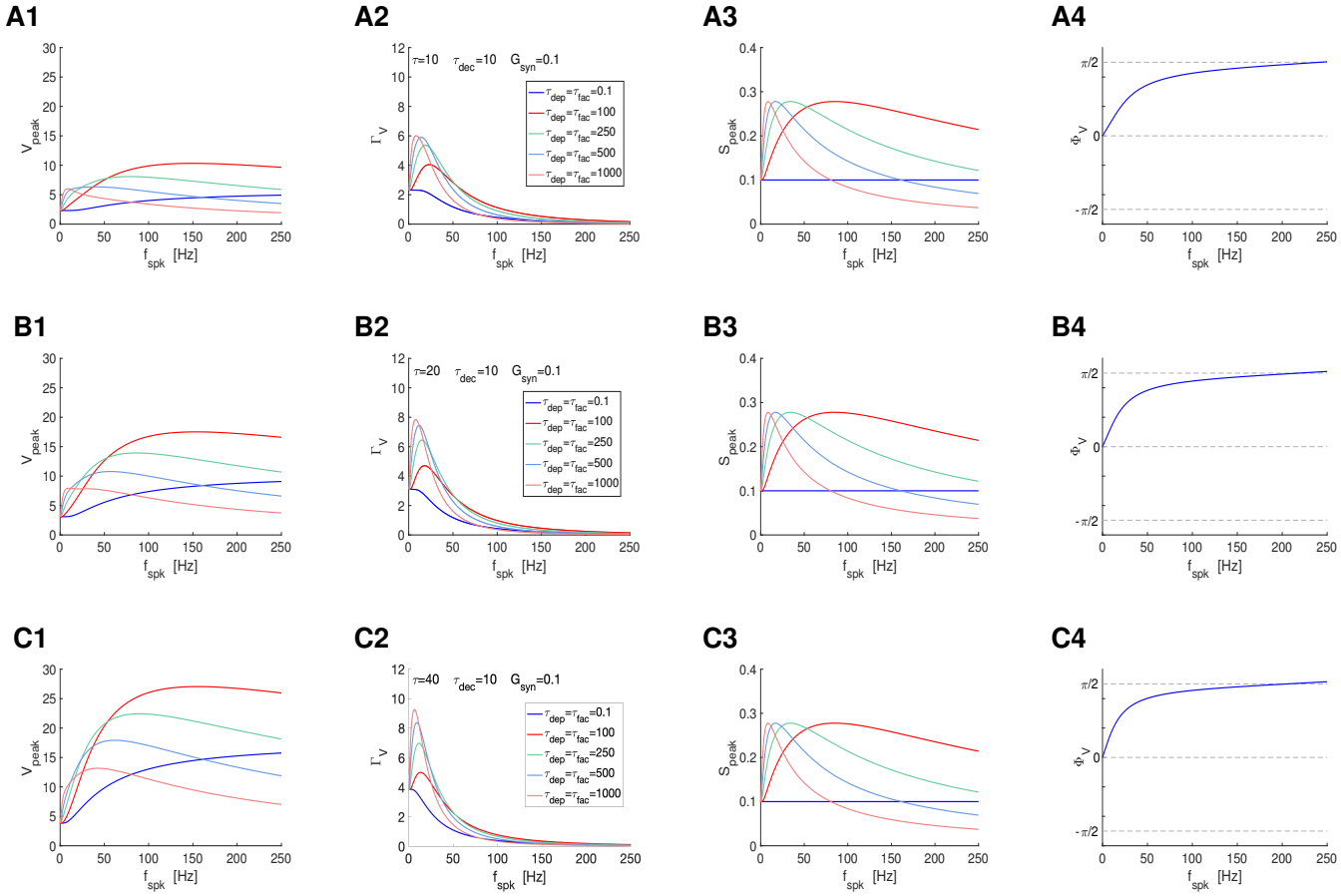

Figure S11: **Postsynaptic filters in response to periodic presynaptic spike inputs emerging from the interplay of short-term depression, facilitation and postsynaptic summation.** Superimposed filters for representative values of the depression and facilitation time constants τ_{dep} and τ_{fac}, respectively. **A.** $\tau = 10$. **B.** $\tau = 20$. **C.** $\tau = 40$. **A, B, C.** $\tau_{dec} = 10$ and $G_{syn} = 0.1$. **Left column.** V peak profiles. **Middle-left column.** V peak-to-trough amplitude profiles. **Middle-right column.** S peak profiles. **Right column.** V phase profiles. We used eq. (64) for the PSP V with I_{syn} described by eqs. (2)-(4) appropriately adapted to account for the translation of V to the equilibrium point, and STP described by eqs. (12) and (13) (DA model). The impedance amplitude (Z) and phase (Φ_Z) were computed using eqs. (36) and (37). The analytical approximations for the PSP peak sequence response of passive cells to presynaptic inputs are described in Section2.2 (see also Appendix A). The approximation of $V_{peak,n}$, $V_{trough,n}$ and $t_{V,peak}$ were computed as described in Section 3.4. The PSP amplitude Γ_V was computed by using eq. (65) and the PSP phase Φ_V was computed using eq. (66). The synaptic (S) peak (S_{peak}) and phase (Φ_S) profiles were computed similarly to these for V. We used the following additional parameter values: $C = 1$, $E_L = -60$, $I_{app} = 0$, $G_{syn} = 0.05$, $E_{syn} = 0$, $a_d = 0.1$, $a_f = 0.1$, $x_\infty = 1$, $z_\infty = 0$ and $T_{sw} = 1$.

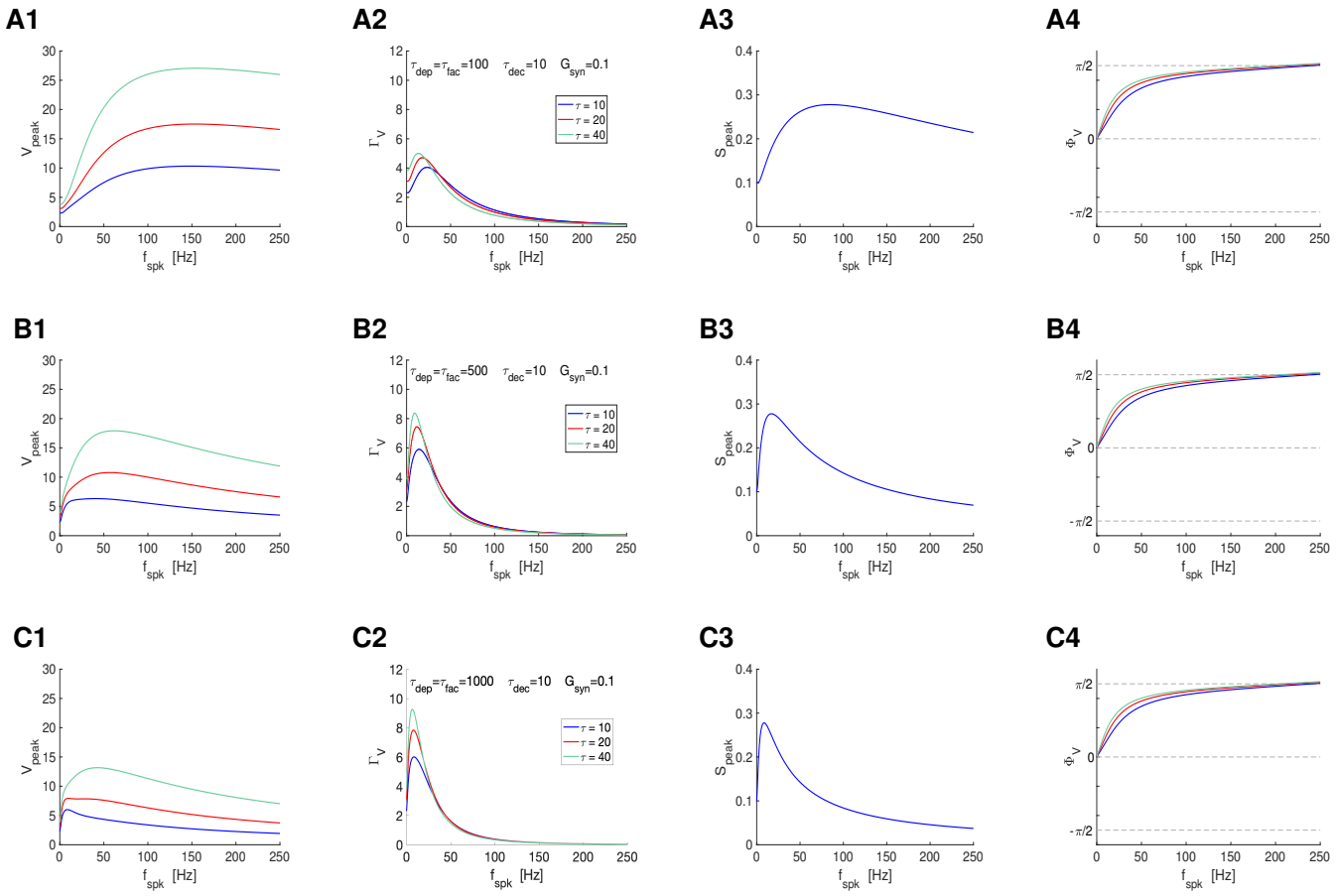

Figure S12: **Postsynaptic filters in response to periodic presynaptic spike inputs emerging from the interplay of short-term depression, facilitation and postsynaptic summation.** Superimposed filters for representative values of the membrane time constant τ. **A.** $\tau_{dep} = \tau_{fac} = 100$. **B.** $\tau_{dep} = \tau_{fac} = 500$. **C.** $\tau_{dep} = \tau_{fac} = 1000$. **A, B, C.** $\tau_{dec} = 10$ and $G_{syn} = 0.1$. **Left column.** V peak profiles. **Middle-left column.** V peak-to-trough amplitude profiles. **Middle-right column.** S peak profiles. **Right column.** V phase profiles. We used eq. (64) for the PSP V with I_{syn} described by eqs. (2)-(4) appropriately adapted to account for the translation of V to the equilibrium point, and STP described by eqs. (12) and (13) (DA model). The impedance amplitude (Z) and phase (Φ_Z) were computed using eqs. (36) and (37). The analytical approximations for the PSP peak sequence response of passive cells to presynaptic inputs are described in Section2.2 (see also Appendix A). The approximation of $V_{peak,n}$, $V_{trough,n}$ and $t_{V,peak}$ were computed as described in Section 3.4. The PSP amplitude Γ_V was computed by using eq. (65) and the PSP phase Φ_V was computed using eq. (66). The synaptic (S) peak (S_{peak}) and phase (Φ_S) profiles were computed similarly to these for V. We used the following additional parameter values: $C = 1$, $E_L = -60$, $I_{app} = 0$, $G_{syn} = 0.05$, $E_{syn} = 0$, $a_d = 0.1$, $a_f = 0.1$, $x_\infty = 1$, $z_\infty = 0$ and $T_{sw} = 1$.

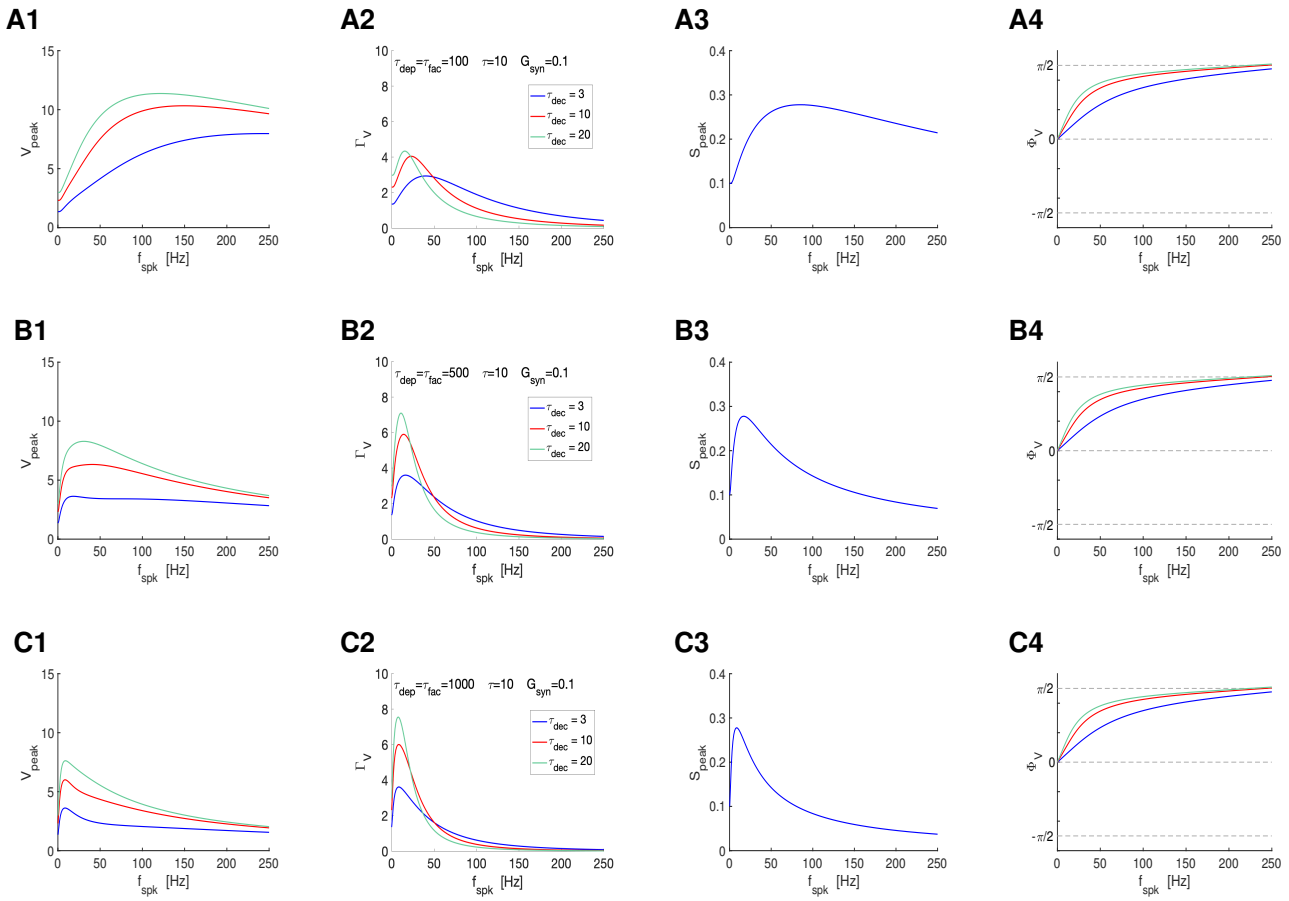

Figure S13: **Postsynaptic filters in response to periodic presynaptic spike inputs emerging from the interplay of short-term depression, facilitation and postsynaptic summation.** Superimposed filters for representative values of the depression synaptic decay time τ_{dec}. **A.** $\tau_{dep} = \tau_{fac} = 100$. **B.** $\tau_{dep} = \tau_{fac} = 500$. **C.** $\tau_{dep} = \tau_{fac} = 1000$. **A, B, C.** $\tau = 10$ and $G_{syn} = 0.1$. **Left column.** V peak profiles. **Middle-left column.** V peak-to-trough amplitude profiles. **Middle-right column.** S peak profiles. **Right column.** V phase profiles. We used eq. (64) for the PSP V with I_{syn} described by eqs. (2)-(4) appropriately adapted to account for the translation of V to the equilibrium point, and STP described by eqs. (12) and (13) (DA model). The impedance amplitude (Z) and phase (Φ_Z) were computed using eqs. (36) and (37). The analytical approximations for the PSP peak sequence response of passive cells to presynaptic inputs are described in Section2.2 (see also Appendix A). The approximation of $V_{peak,n}$, $V_{trough,n}$ and $t_{V,peak}$ were computed as described in Section 3.4. The PSP amplitude Γ_V was computed by using eq. (65) and the PSP phase Φ_V was computed using eq. (66). The synaptic (S) peak (S_{peak}) and phase (Φ_S) profiles were computed similarly to these for V. We used the following additional parameter values: $C = 1$, $E_L = -60$, $I_{app} = 0$, $G_{syn} = 0.05$, $E_{syn} = 0$, $a_d = 0.1$, $a_f = 0.1$, $x_\infty = 1$, $z_\infty = 0$ and $T_{sw} = 1$.

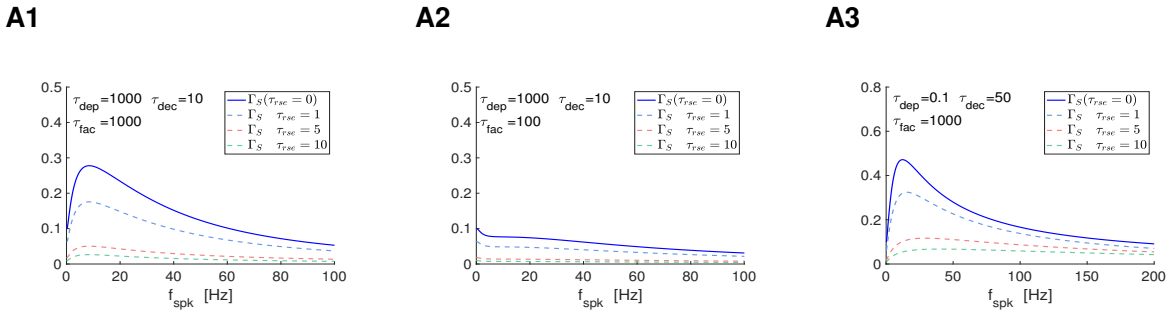

Figure S14: Γ_S **filters in response to periodic presynaptic spike inputs (frequency f_{spk}) for the to-ΔS update models with non-instantaneous update: representative examples.** We used eqs. (12) and (13) (DA model) for $\bar{\Delta S}$ **A.** To-ΔS model (synaptic update to ΔS). Effects of τ_{rse}. The S and Γ_S filters were computed using eqs. (50) and (51), respectively. **A1.** Γ_S band-pass filters attenuated by increasing values of τ_{rse}. **A2.** Γ_S low-pass filters attenuated by increasing values of τ_{rse}. **A3.** The Γ_S band-pass filter generated by the interplay of a ΔS high-pass filter and a Q_A (a low-pass filter) (Fig. 5-A6) is attenuated by increasing values of τ_{rse} and transitions to a high-pass filter. We used the following additional parameter values: $a_d = 0.1$, $a_f = 0.1$, $x_\infty = 1$, $z_\infty = 0$ and $T_{sw} = 1$.

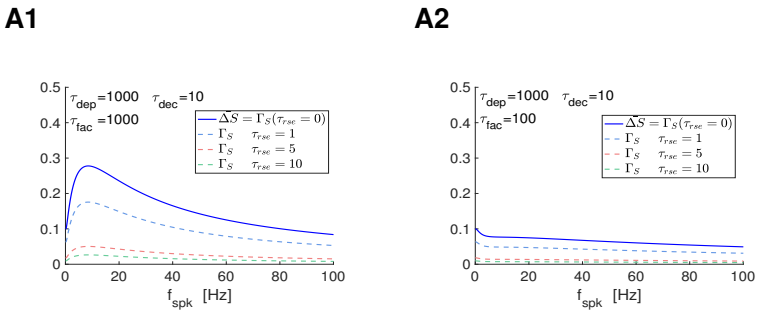

Figure S15: Γ_S **filters in response to periodic presynaptic spike inputs (frequency f_{spk}) for the by-ΔS update models with non-instantaneous update: representative examples.** We used eqs. (12) and (13) (DA model) for $\bar{\Delta S}$ **A.** By-ΔS model (synaptic update to ΔS). Effects of τ_{rse}. The S and Γ_S filters were computed using eqs. (61) and (62), respectively. **A1.** Γ_S band-pass filters attenuated by increasing values of τ_{rse}. **A2.** Γ_S low-pass filters attenuated by increasing values of τ_{rse}. We used the following additional parameter values: $a_d = 0.1$, $a_f = 0.1$, $x_\infty = 1$, $z_\infty = 0$ and $T_{sw} = 1$.

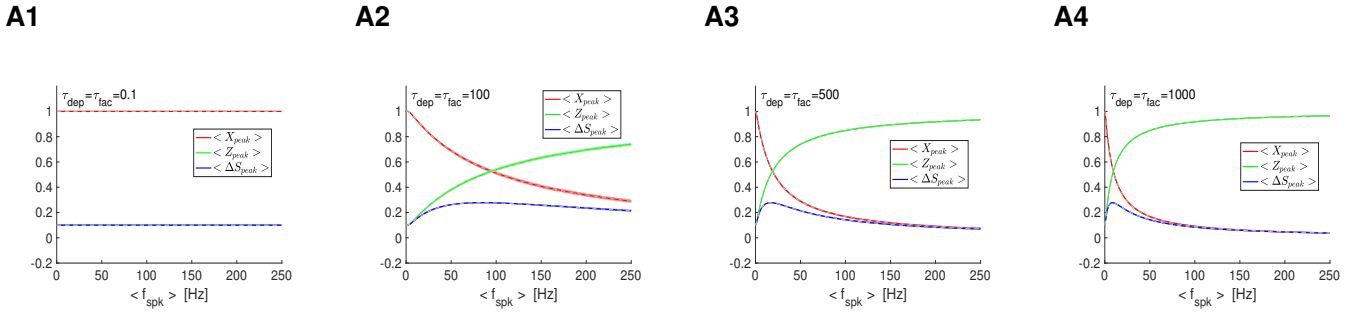

Figure S16: X, Z **and** ΔS **filters in response to jittered (randomly perturbed) periodic presynaptic inputs in the presence of STP: frequency- and STP-dependent variability.** For each value of the mean presynaptic input frequency $< f_{spk} >$, the ISI sequence $\{\Delta_{spk,n}\}$ $(n = 1, \ldots, N_{spk})$ has the form $\Delta_{spk,n} = \Delta_{spk} + \delta_{spk,n}$ where Δ_{spk} is the ISI corresponding to f_{spk} $(f_{spk} = 1000/\Delta_{spk})$ and the sequence $\{\delta_{spk,n}\}$ are drawn from a normal distribution with zero mean and variance equal to $\delta\,\Delta_{spk}$. **A.** Superimposed X_{peak}, Z_{peak} and ΔS_{peak} profiles for representative parameter values. We used $\tau_{dec} = 10$ and $\tau = 10$ in all panels. Solid curves correspond to the mean values for each attribute (X_{peak}, Z_{peak} and ΔS_{peak}). The shadow regions correspond to one standard deviation from the mean. The dashed gray curves, almost coinciding with the solid curves, represent the corresponding deterministic profiles (response to periodic spike train inputs with frequency f_{spk}). **A1.** $\tau_{dep} = \tau_{fac} = 0.1$. **A2.** $\tau_{dep} = \tau_{fac} = 100$. **A3.** $\tau_{dep} = \tau_{fac} = 500$. **A4.** $\tau_{dep} = \tau_{fac} = 1000$. We used the following additional parameter values: $C = 1$, $E_L = -60$, $I_{app} = 0$, $E_{syn} = 0$, $a_d = 0.1$, $a_f = 0.1$, $x_\infty = 1$, $z_\infty = 0$ and $T_{sw} = 1$.

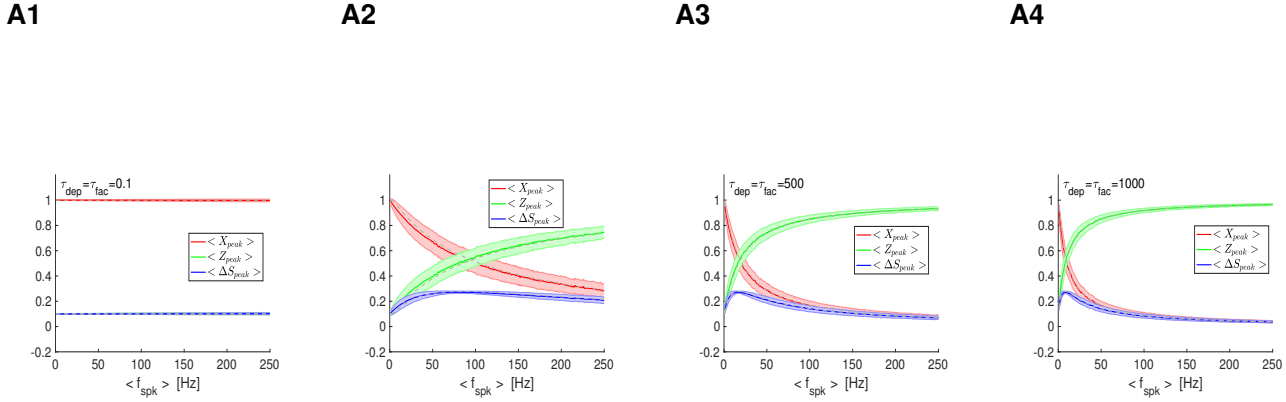

Figure S17: X, Z **and** ΔS **filters in response to Poisson-distributed presynaptic inputs in the presence of STP: frequency- and STP-dependent variability.** The mean rate of the Poisson distributed spike trains corresponds to $< f_{spk} >$. Superimposed X_{peak}, Z_{peak} and ΔS_{peak} profiles for representative parameter values. We used $\tau_{dec} = 10$ and $\tau = 10$ in all panels. Solid curves correspond to the mean values for each attribute (X_{peak}, Z_{peak} and ΔS_{peak}). The shadow regions correspond to one standard deviation from the mean. The dashed curves represent the corresponding deterministic profiles (response to periodic spike train inputs with frequency f_{spk}). **A1.** $\tau_{dep} = \tau_{fac} = 0.1$. **A2.** $\tau_{dep} = \tau_{fac} = 100$. **A3.** $\tau_{dep} = \tau_{fac} = 500$. **A4.** $\tau_{dep} = \tau_{fac} = 1000$. We used the following additional parameter values: $C = 1$, $E_L = -60$, $I_{app} = 0$, $E_{syn} = 0$, $a_d = 0.1$, $a_f = 0.1$, $x_\infty = 1$, $z_\infty = 0$ and $T_{sw} = 1$.